UNIVERSITAT POLITÈCNICA DE CATALUNYA
BARCELONATECH
Escola d'Enginyeria de Barcelona Est

TREBALL FI DE MÀSTER

Màster en Ciència i Enginyeria dels Materials

SYSTEMATIC CHARACTERIZATION OF THE MICROMECHANICAL BEHAVIOUR OF INORGANIC MATRIX COMPOSITES:

From microstructural analysis to finite element simulation

Memòria

Autor: Víctor Lamelas Cubero

Director: Joan Josep Roa Rovira

Convocatòria: Octubre 2017

"Un muro es duro, pero más duro es un nitruro"

Anónimo

Resum

El nitrur de bor cúbic (cBN) policristal·lí és un material ceràmic compost que pertany a la família dels materials súper durs. La informació sobre el comportament mecànic a escales micromètriques d'aquests materials és normalment escassa. En aquest sentit, la present investigació desenvolupa un estudi sistemàtic de les propietats micro mecàniques d'un material compost de cBN amb matriu ceràmica de nitrur de titani (TiN).

L'estudi complert es divideix entres lots de caracterització ben interrelacionats entre ells:

1. **Anàlisis composicional i microstructural**. S'han desenvolupat anàlisis de composicions químiques mitjançant EDS i EMPA. A més s'ha realitzat l'estudi microstructural mitjançant tres metodologies diferents i s'han comparat els resultat i la precisió reportada per cadascuna d'elles.
2. **Assaig micromecànic**. S'ha implementat la metodologia de nanoindentació massiva, aconseguint extreure les propietats intrínseques de cadascuna de les fases del material a més del seu comportament com a material compost. Les dureses que s'han obtingut han estat de 32,82 i 55 GPa per a el TiN, cBN i el material compost respectivament.
3. Anàlisi per **elements finits** d'un volum representatiu de material extret mitjançant la reconstrucció d'una tomografia realitzada amb la tècnica de Canó d'ions focalitzat (FIB).

Per últim també s'han mecanitzat pilars de mida micromètrica fi de poder comparar la resposta mecànica del material compost predita per la simulació amb la resposta física d'un pilar de material compost en ser comprimit.

Resumen

El nitruro de boro cúbico (cBN) poli cristalino es un material cerámico compuesto que perteneciente a la familia de los materiales *súper duros*. Como en el caso de los demás materiales *súper duros*, la información sobre su comportamiento mecánico a escala micrométrica es escasa. En este sentido, la presente investigación desarrolla un estudio sistemático de las propiedades micro mecánicas de un material compuesto de cBN con matriz nitruro de titanio (TiN).

El estudio completo se puede dividir en tres lotes de caracterización bien interrelacionados entre ellos:

1. **Análisis composicional y microestructural**. Se han desarrollado análisis de composición química mediante EDS y EMPA. Además se ha desarrollado un estudio microestructural mediante tres metodologías distintas y se han comparado los resultados y precisión obtenidos porcada una de ellas.
2. **Ensayo micromecánico**. Se ha implementado la metodología de Nanoindentación masiva, consiguiendo extraer las propiedades intrínsecas de cada una de las fases del material además de su comportamiento como material compuesto. Las durezas obtenidas para el TiN, cBN y PcBN como material compuesto han sido respectivamente 32, 82 y 55 GPa.
3. Análisis por **elementos finitos** de un volumen representativo de material extraído mediante la reconstrucción de una tomografía realizada con la técnica de cañón de haz de iones focalizado (FIB).

Por último también se han mecanizado pilares micrométricos a fin de poder comparar la respuesta mecánica predicha por la simulación con la respuesta física de un pilar de material compuesto al ser comprimido.

Abstract

Polycrystalline cubic boron nitride (PCBN) is a super-hard material with a multiphase composite character. As it is the case for other super hard materials, information on the small-scale response of PCBN is rather scarce. In this sense, the present work conducts a systematic micro-mechanical study of the mechanical integrity of a cBN embedded in TiN as a binder.

The whole study is divided in three well-connected testing batches:

1. **Chemical and microstructural analysis**. EMPA and EDS analysis are performed and three microstructural analysis methodologies are developed and compared.
2. **Micromechanical testing**. Massive nanoindentation technique is implemented and corresponding deformation/damage mechanisms are also investigated. Main hardness for TiN, cBN and PcBN have been directly obtained from Ulm and Constantinides (1) method and their values are 32, 82 and 55 GPa respectively.
3. **Finite element analysis (FEA)** for a representative volume element of PcBN material, extracted by means of Focused Ion Beam (FIB) tomography, is held and its mechanical results are discussed.

Finally, composite micrometric pillars have been machined with the aim of comparing FEA results with the physical response of the material in micro-pillar compression tests.

Acknowledgements

Special thanks for the constant help and support received from Professor Joan Josep Roa, whose love for research is contagious. Thanks a lot to Luis Llanes for his big trust on young students and the big opportunities of personal growth.

Many thanks to Joël Cougnoni who, selflessly, introduced me into ABAQUS and generic knowledge of FE simulations of materials microstructures. Thanks to Fernando Garcia for the familiar contact with all the students and big coordination duties that he manages. Finally thanks to Trifon Trifonov for the big patience and support in FIB hours and long sessions.

Glossary

BN	Boron Nitride
hBN	Hexagonal Boron Nitride
cBN	Cubic Boron nitride
HPHT	High Pressure High Temperature
LIM	Linear Intercept Method
$\bar{d}_{cBN}$	cBN particle mean size
C_{cBN}	cBN contiguity
λ_{TiN}	Mean free path
ROI	Region of interest
ISE	Indentation Size effect
V^*	Activation volume
OPAN	Colloidal sub-micrometric Alumina
FIB	Focused Ion Beam
FE-SEM	Field Emission-Scanning Electron Microscopy
ITT	Instrumented indentation technique
RVE	Representative Volume Element
VOI	Volume of Interest
CDF	Cumulative Distribution Function
PDF	Probability Density Function
dV	Volume differential
ARR	Atom Removal Rate
FEA	Finite Element Analysis
BC	Boundary Conditions
σ_{yC} **(MPa)**	Yield Compressive Strength
$\sigma_{10\%\ Placticity}$	Compressive strength at 10% plasticity
UX, UY, UZ	Displacement in X,YZ axis
URX, URY, URZ	Rotation around X, Y, Z axis

Table of Contents

Introduction

Polycrystalline cubic boron nitride (PCBN) is a super-hard material with a multiphase composite character. The synergic combination of properties associated with its constitutive phases has made them a preeminent material choice for extremely demanding applications, where improved and consistent performance together with high reliability are required. Classically, only two materials in engineering have met the highly demanding hardness standards to be considered from Super Hard materials family, they have been cBN and diamond. Both of the materials were firstly produced synthetically in the mid 50's and from that moment have had a very important role in cutting, conforming, machining, eroding and many other wear applications.

In the specific case of this master thesis all the investigation will be held on a PcBN material composite, formed by a titanium nitride (TiN) ceramic matrix and cBN ceramic particles. Although some hardness is lost when using composite materials, many other mechanical properties are enhanced and engineering performance of the components is improved. In addition, the usage of PcBN composite materials allows optimizing each material for very different applications by tailoring several parameters as matrix nature, content, additives, coatings, grain size, grain size distributions etc.

Up to this time, research in mechanical properties of cBN-based materials have been mainly focused from two very clear points of view:

A. **Films and thin films research**. Because of being isoelectric with diamond, cBN is getting a lot of attention from electronics industry (2). Its high rigidity makes the material very interesting for MEMS applications (3). In addition, its high hardness (only surpassed by diamond) makes cBN a very interesting material for wear resistant coatings [(4), (5), (6)].

   All of these three applications use cBN in form of films. In this way of using cBN, micromechanical testing has been used for years to characterize mechanical behaviour [(7), (8)], but anyways thin films stress solicitations and states are very specific and not always comparable to the behaviour that the material should have in any other application.

B. **Coarse industrial research on working elements performance**. Mostly the tool life of several components while working in service conditions is studied [(9), (10), (11)]. Most of the cBN research nowadays is based in evaluating different PcBN grades, with several modifications in their microstructure, composition, coating etc implemented in different commercial products and evaluate their performance in

terms of productivity, tool life, surface quality etc. indifferent industrial operations with high wear demanding solicitations like stir welding, turning, milling etc.
This type of research is very useful for industry but sometimes it may lack the precision to detect some of the information needed to go further in new materials development.

The far mechanical solicitation of thin films and the coarse characterization of PcBN tool performance makes necessary the mechanical characterization of PcBN materials as a composite in the micrometric scale. Both of the existing phases in PcBN materials are within the micrometric scale, and therefore out of range of most of the traditional mechanical testing techniques.

The study and comprehension of the local properties is important in order to understand the mechanisms that will lead the material to the final failure. PcBN composites present a brittle fracture where the interaction between phases, the loading transference and the locations of fracture determines completely the performance of the PcBN components. In this sense, the correct measure of the individual components toughness or/and elasto-plastic properties, may lead to the introduction of real mechanical properties values into meso-mechanic models that differentiate within phases.

Is important to highlight how the properties of the composite are very different to the properties of the grains of cBN individually or of the bonding matrix. That is why is necessary to characterize micromechanically all of the present phases and their interactions individually in order to include these factors in bigger models that can be closer to physical reality. It is here where the biggest added value that this type of fundamental research projects can be noticed. All the knowledge developed for these types of materials can be latter a big improvement in their applicability. A good example could be the gradual substitution of hard metals by PcBN based materials in high cost operating tunnelling machines; a better material comprehension could optimize and decrease the substitution of tunnelling inserts saving big amounts of money.

Then once the interest of this research has been highlighted, is important to notice that the way all in which the different tests and characterisation have been developed is as important as the relationship and sequence that they follow. **Figure 1** shows which are the logics that rule the whole master thesis, the main idea is: to process a specific material for a specific application, characterize its core behaviour and finally build proper models that could improve materials performance in current applications or create new applications through the better understanding of materials.

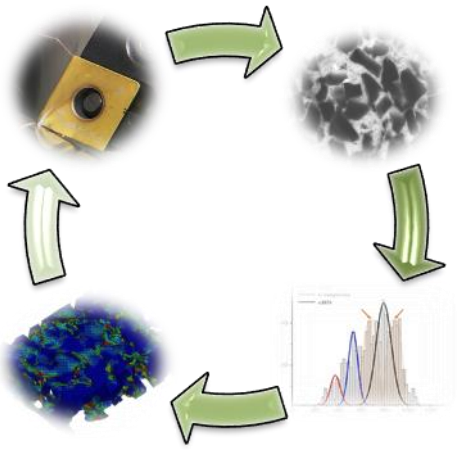

Figure 1 - Workflow and proceeding logics for the whole research.

Project objectives

The main objective of the current master thesis is:

- To perform a global systematic characterisation study of a sample of PcBN material that allows going from physical analysis to Finite Element modelling.

To do so, some other intermediate objectives have to be achieved. These are:

- Precisely analyse the material microstructure and morphology. With an special emphasis on:
    - Binder geometry and interaction with reinforcement particles
    - Reinforcement shape and size
- Characterize mechanically each of the single phases present in PcBN separately through the implementation of Massive Nanoindentation technique.
- Characterize the composite mechanical behaviour through the data analysis of:
    - Deep nanoindentation tests
    - FIB machined PcBN micro-pillar compression
- Obtain and simulate a representative volume element of TiN+cBN material through FIB tomography, image processing and mesh creation

Theoretical Frame

Materials

Cubic Boron Nitride - cBN

Cubic boron nitride (cBN), is a ceramic material, which the second hardest material only after diamond, and it belongs to the super-hard materials family (over 40GPa on hardness at the micrometric length scale by using the Vickers scale). This characteristic makes c-BN one of the most important materials for industrial applications as turning, cutting, drilling, grinding etc. Regarding technological progress, c-BN tools represent a big advance in terms of tool life and operation performance in front of its competitors and previous solutions as WC/Co tools or even diamond tools (9). Table 1 shows a comparison between the basic properties and characteristic of cBN and other typical abrasive materials can be seen:

Table 1- Properties of abrasive materials **(12)**

Material	Density ($g \cdot cm^{-3}$)	Vickers Hardness (GPa)	Compressive strength (GPa)	Thermal conductivity (W/m·K)	Thermal expansion ($10^{-6} \cdot K^{-1}$)
cBN	3.45	50	5.3	740	1.2
Diamond	3.51	110	8.7	2000	4.8
WC	14.7	20	4.5	100	5.4
SiC	3.20	28	3.9	120	4.0

At first sight cBN is not even a competitor to diamond tools or materials when it works at room temperature, while this material is widely employed at temperatures higher than 450ºC due to it is stable and hard compared to diamond (13). Diamond shows twice the hardness of cBN, much higher compressive strength and the best thermal conductivity within all materials. In addition diamond is a material with which industry is much more used to work with. Diamond is better characterized than cBN, its industrial synthesis is much more controlled and optimized (the catalysis needed for its production give higher productivities) and since both materials where accomplished synthetically in the mid 50`s much more development efforts have been dedicated to diamond.

However, cBN has found its application and importance within industry. This is principally due to two main reasons:

1. Thermal stability. When talking of diamond working temperatures are very limited because its oxidation starts at 400ºC and its conversion to graphite takes place above 900ºC. This range of temperatures are easily achieved in applications of high contact and strong friction as machining or drilling.

   In the other hand cBN structure is stable at atmospheric pressure up to 2000ºC in inert atmosphere and it doesn't oxidize up to 700ºC a, making this material a very interesting one (13). Moreover, the hardness reduction in diamond is accentuated beyond 500ºC becoming inferior to the hardness shown by cBN at 800ºC or above.
2. Chemical inertness. Diamond in contact with ferrous alloys or Nickel superalloys tend to lose its integrity due to the formation of carbides, the application of diamond tools is limited to non-metallic materials (geological materials for drilling in oil and gas industry) and some non-ferrous alloys. Being steel the most widely used material in industry, this is a big drawback and that is why hard metal tools and cBN are getting such a big interest during the last years.

   cBN also shows high chemical stability in presence of strong acids and highly oxidizing conditions, due to the formation of a passivation layer of born oxide.

From the classical point of view of materials science structure, processing and properties have to be well characterized in order to understand the roots and origin of the cBN described advantages and good performance (14). The whole comprehension of the material nature from its fundamental nature to its processing will give the required base in order to improve its performance.

Structure:

cBN is a synthetic allotrope of boron nitride (BN) with a three dimensional network of short and strong covalent bonds, which is critical for its properties. The common and natural way to find BN in nature (atmospheric conditions) is in a hexagonal lattice (analogous to graphite in diamond). The hexagonal lattice shown in **Figure 2** consists of a stacking arrangement along c axis of planar layers of hexagonal rings where boron (B) and nitrogen (N) occupy the edges. The layer sequence is ABAB… with B and N atoms also altering along the *c-axis*. The interlayer B-N bonds are strongly covalent (sp2) whereas the interlayer bonds are based on Van der Walls forces.

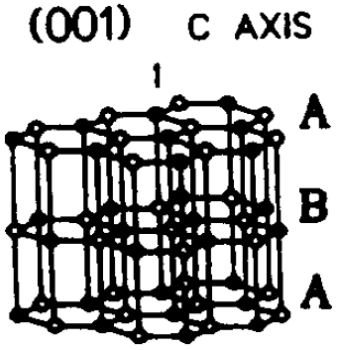

Figure 2-Crystal structure of hexagonal-BN **(16)**

In order to change BN from its natural allotropic phase into one with a much higher added value, high temperature and high pressure (HPHT) must be applied to the material. **Figure 3** shows the pressure (P)-temperature (T) diagram for BN and sets the regions at which hBN and cBN are thermodynamically stable. Typically, the processing values of P and T are around 6 GPa and 1350ºC, respectively

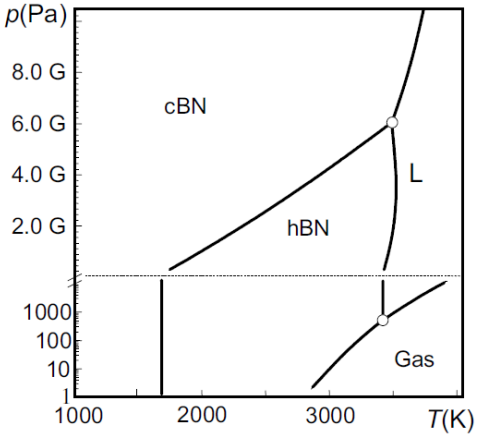

Figure 3- Pressure vs Temperature diagram for BN **(15)**

The formation of cBN occurs via a destructive-reconstructive diffusion like process; the high pressure applied reduces the interplanar spacing of the hBN and produces a deformation of the hexagons that leads into hybridization change from sp2 to sp3. Each planar layer of the lattice splits into two planes: one containing B atoms, and the other N atoms along the c-axis and there are alternate layers of B and N. Because of the three-dimensional (3D) order change, the change requires breakage and change in the nature of chemical bonds (16). This process ends in a cubic closest-packed lattice (see **Figure 4**) where B and N have sp3 coordination.

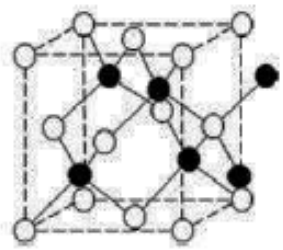

Figure 4- Crystal structure of cBN

The resulting crystallography can be assumed as an Face Centered Cubic (FCC) structure with six (1 1 0) cleavage planes.

Processing:

There are two main industrial ways to process cBN materials, both of them involve high pressures and temperature but include its particularities. The two main processing routes are:

a. Direct conversion from h- to cBN: This is the primary method that was developed in which just P and T are applied. In this process parameters as starting hBN particle size

and crystallinity are very important factors for the resulting cBN grains. This is the rawest way of obtaining cBN, and in this sense the transition from h- to cBN is done in a small volumes.

b. hBN→ cBN conversion using a catalyzed process: This is the method that has tended to be the best industrial option to produce cBN materials. The main reason for using catalyzers is in order to enhance the kinetics of the transformation in order to boost the production rates. The most typical catalysts are selected nitrides of alkali or alkaline earth metals. Liquid assisted sintering process consolidates cBN much faster at lower P and promotes superior properties. This is because not only the diffusion mechanisms are more effective when using a binder but also because of the process of filling the pores as well as the binder/crystal interaction results in a better final polycrystalline cBN (PcBN).

Both processing methods, led to develop different cBN microstructures by controlling the main processing parameters, like the P and T. The different cBN grades in terms of grain size will condition later the optimal engineering application and affect the particle strength, hardness and fracture characteristics among other properties.

. The crystal structure of cBN is cubic with {1 1 1} planes arranged in a three layer stacking sequence (FCC). This is why the produced grains of cBN may vary their geometry from a perfect cube to an octahedron, including the other intermediate geometries. By varying the processing conditions, (like T, P, catalyst, etc.) is possible to change the growth rates of the {100} or {111} crystal directions and therefor modify grains shape (17). The detailed atomic growth mechanisms on the different planes are different, hence the different response to P, T or driving force (DF) variations as it is depicted in **Figure 5.**

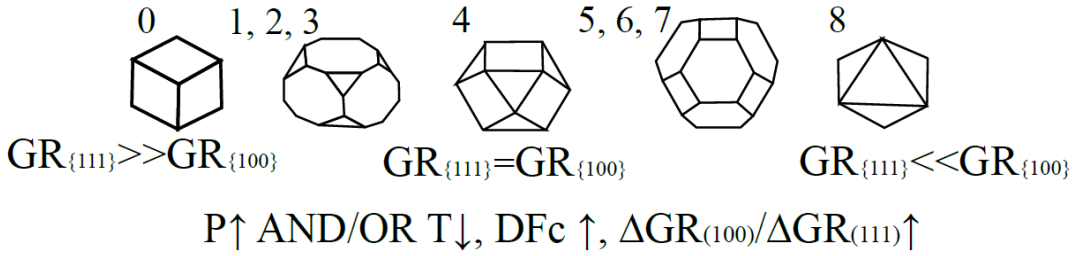

Figure 5- The effect of HPHT synthesis conditions on cBN grain morphology (DFc is driving force for crystallisation). **(17)**

Generally it can be said that cubic-octahedral crystals with an equal mix of (111) and (100) facets will be the best grains for abrasive applications (18). However a fully controlled growth of cBN crystals during HPHT system as the one achieved with diamond materials is still not possible, and cBN will preferably show a tetrahedral or octahedral morphology.

PcBN Inorganic matrix composites

Once all cBN advantages are highlighted its technological importance gets obvious. However, cBN as most ceramic tool materials suffers from low fracture toughness and may fail prematurely due to brittle nature, resulting in low reliability and scattered working life. In order to minimize this embrittlement, is necessary a correct understanding of the material land in order to optimize and design a new cBN microstructure with enhanced properties from the view point of materials science.

The most commonly used solution in order to take profit of cBN advantages and minimize its drawbacks is the use of inorganic ceramic-ceramic composite materials. Although sacrificing some hardness and wear resistance, cBN is normally used in a two-phase polycrystalline structure consisting of micron sized grains of cBN held together by a ceramic binder material as it is depicted in **Figure 6.**

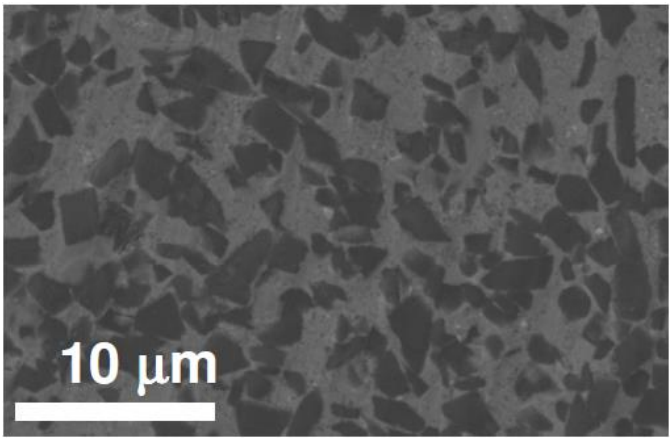

Figure 6- Typical microstructure shown by PcBN composites, where dark particles correspond to cBN reinforcement and light material to ceramic binder matrix**.**

A number of factors are known to affect the mechanical properties and performance of inorganic matrix composites, including:

1. Binder material and %Vol.: Different binder phases are used in different applications where abrasive and chemical erosion can often occur. In this way, PcBN is available in metallic matrix systems, ceramic matrix, low and high cBN content, coated systems etc.

   The use of a metal and/or a ceramic matrix is a compromise between toughness and hardness, respectively. For the cases in which the material is going to work against hard counter faces and highly demanding wear requirements (e.g. machining tools case) ceramic matrixes are preferred. Within this context, PcBN/ceramic binder, although being submitted to some vibrations or discontinuous forces, it is mainly

optimized for wear applications. Therefore, only the cases of ceramic matrixes are going to be discussed below.

- **Low cBN content materials (40-60% Vol. cBN)** have generally a titanium based ceramic binder agent and tend to be more resistant to chemical wear mechanisms found for continuous machining operations. However, this material is less tough.
- **High cBN content materials (>70% Vol. cBN)** have generally aluminum or titanium based ceramic matrix and tend to be used in applications where abrasion wear (see **Figure 7**) is dominant and thermal dissipation is critical. For example in the machining of super alloys process, cast irons or martensites.

When machining hardened samples with interrupted surfaces (a very common situation in industry), the cutting tool toughness becomes a critical parameter, since the interruption applies on samples impact loads that may cause brittle fracture. The general designing consideration is to enhance cBN volume % as higher is the interruption of the machining. When the cBN content increases, the resulting composite material presents a higher toughness value as reported in Ref. (19). This phenomenon may be related that the resulting material presents a higher crack path roughness and a higher failure load

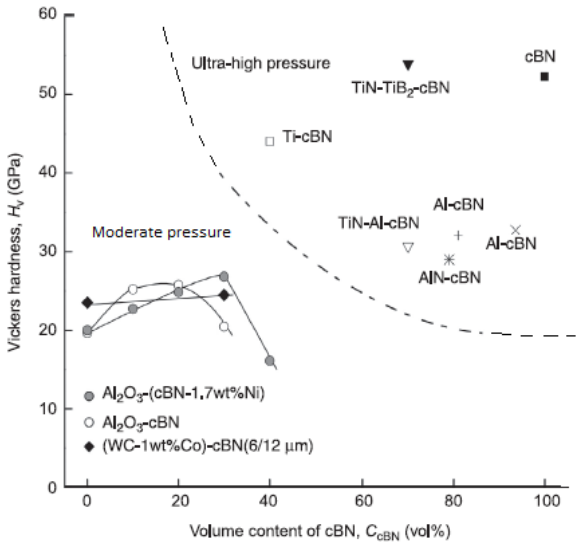

Figure 7 - Comparison of the hardness of several cBN composites as a function of cBN volume content. **(19)**

2. Grain size ($\bar{d}_{cBN}$) and grain size distribution: the size of the reinforcement particles in any composite material is known to modify the microstructural and mechanical properties as well as their final application. That is why an exhaustive microstructural

characterization even of size and/or distribution are important to predict mechanical properties of these materials.

In the case of PcBN materials, cBN are considered hard reinforcing particles. There are 2D and 3D methodologies in order to characterize particle size:

- In the 2D methodologies the most common methodology are the *linear intercept method* (LIM) and the *planimetric* method.

  The first one consists in drawing a series of horizontal parallel lines onto a microscopy image and then measuring the length of the carbides crossed by every line. Using the following equation grain size is obtained:

$$\bar{d}_{cBN} = \frac{v_{cBN}}{2N_{cBN/cBN} + N_{cBN/TiN}} \qquad \textbf{Equation 1}$$

  Where $N_{cBN/cBN}$ and $N_{cBN/TiN}$ are the number of intercepts per unit length of boron nitride-boron nitride and boron nitride-binder boundary respectively, and υ_{cBN} corresponds to the volumetric fraction of boron nitride.

  On the other hand, planimetric analysis is carried out by number of grains per unit area because of being a two-dimensional measurement is expected to be more precise than the previous one.

- *3D analyses* are mostly based in the digital reconstruction of a representative volume element of the studied material. Following, a correct thresholding and labeling of the different material phases and finally volume data analysis.

  3D analyses are expected to be the best approximation to real microstructural parameters, and moreover, they do not need approximations as particle shape. However, mainly in all of the different microstructures, a lot of time consuming are required to reconstruct a real 3D microstructure. Furthermore, this methodology is

As a general consideration having finer reinforcing particles and better dispersed ones will give better mechanical properties to the inorganic composite ceramic/ceramic material. However, this cannot be taken as a determining factor since load transfer conditions between matrix and reinforcement has to be complied and other mechanical properties factors as crack deflection or others can be decreased when decreasing grain size.

3. Other microstructural parameters:

3.1. Contiguity (C_{cBN}): Contiguity is described as the fraction of the interface area of a phase shared by particles of the same phase (20), and can be measured from the linear intercept method by:

$$C_{cBN} = \frac{2N_{cBN/cBN}}{2N_{cBN/cBN}+N_{cBN/TiN}} \qquad \textbf{Equation 2}$$

Its value goes from zero (completely unconnected particles to one (a single fully connected phase). Several models have been developed (Roebuck (21), Torres (22), Exner (23)) in order to relate and predict the relationship between contiguity, particle size and % vol. binder. Even so, all the models coincide in the fact that contiguity decreases when increasing binder content and/or reinforcement size.

3.2. Mean free path (λ_{TiN}): This parameter describes the average size of the binder phase. It can be measured by the linear intercept method as:

$$\lambda_{TiN} = \frac{2v_{TiN}}{N_{cBN/TiN}} \qquad \textbf{Equation 3}$$

The discussion and comprehension of all these microstructural parameters is of interest to further investigate how they contribute to the structural performance of PcBN pieces. This knowledge can then be used as a design tool to design and/or improve next generation materials with improved their mechanical properties like fracture toughness and hardness.

Techniques

FIB

Focused Ion Beam (FIB) equipment is being more used day by day in materials science laboratories. While in the beginning it only found applications in microelectronics nowadays its main uses are related to materials science in several practices as: preparation and direct observation of transversal cuts into the sample, transmission electron microscopy (TEM) and atom probe tomography (APT) sample preparation, 3D-tomography reconstruction and during the machining process of several geometries (24).

FIB microscope is based in the same principle as scanning electron microscopy SEM where it is possible scan an area with a beam of focused charged particles in order to obtain a magnified image of the area. In SEM technique, the electrons interact with the surface of the sample and depending on the way they are scattered different detectors can be used to detect them and led to transduce that information into topography. In the case of FIB instead of electrons the charged particles are ions they can be Xenon focused atoms or as in the case of the used FIB they are Ga^{+3} ions. In the case that these ions are operated at low beam currents the beam may be used for imaging (although being much more harmful to the sample than electrons); when high currents are used the target sample can be machined in the desired geometries.

Along this master's thesis, a Zeiss Neon40 is used to perform the 3D-tomographies as well as to mill some cBN micropillars. This equipment uses two different columns, one of electrons and one for Ga^{+} ions. Electrons column is situated perpendicular to the surface of interest while the ion column has a relative angle to the electron column of 54º as it is depicted in **Figure 8**. In both cases charged particles emitters are needed in order that these particles can be later focalized and emitted in a high vacuum chamber. In one hand electrons will be obtained from a tungsten filament electrode while Ga^{+} will come from a liquid-metal ion source (LMSI) with low melting temperature (35ºC), low partial pressure and high surface tension (25).

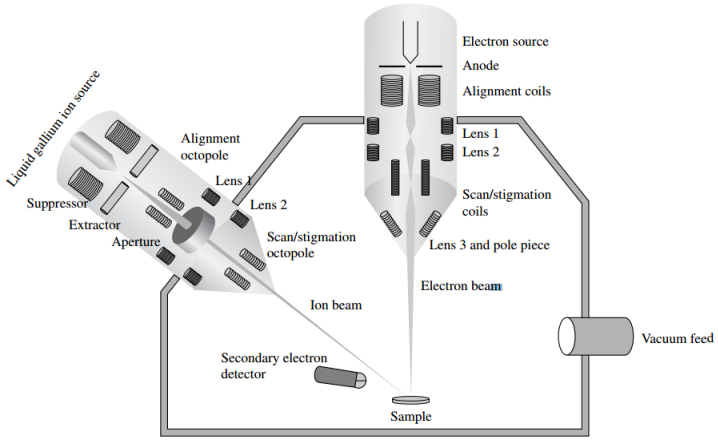

Figure 8 - Scheme of a FIB equipment (25)

Every one of the two columns has its own purpose:

- Electrons column will be mainly used to observe the surface topography of the sample.
- Ions column can be also used to observe topography (at less resolution), but mainly is used for the machining/controlled erosion of the sample.

  In the case of visualization by means of ions is important to take into account the fact that a continuous expose of the sample to the ions current may affect its physical nature by ions implantation or mechanical erosion.

Within all the different possibilities that FIB equipment offers, in this project only some of them were fully developed:

i) Micromechanical samples machining: when machining a material through a FIB there are several considerations that have to be taken into account. The reason of this multifactorial process is that several interactions occur when the energetic particles and the first layers of material are in touch. The interaction ion-material results are mainly:

a. **Sputtering of atoms from material (machining)**. The ratio of sputtered atoms from the substrate each Ga atom that collides the sample is called Atom Removal Rate (ARR).

   Materials with higher ratios are more easily machined, for the case of super-hard materials the atom removal is very limited due to their strong covalent and directional bonding. For example, during the experimental procedure of this master's thesis, it has been found that the removal rate of cBN material respect to standard material (Si) is nearly 6 times smaller; getting penetration depths of 3.5 µm in cBN for milling currents that may penetrate up to 20 µm in Si.

b. Backscattered ions that bounce from the sample

c. Generation of secondary electrons

d. Ion implantation or amorphization

Ga^{+3} ions are much more massive and larger in size than electrons, so theirs penetrations depth will be lower than the one for electrons. However, their momentum is much higher so when they collide against the sample atoms ions will cause sputtering of material. The characteristic of this sputter follows a strong relationship between operation times and quantity of "sputtered" material. In the case of high amount of material should be removed, large milling times will be needed. A way of decreasing a machining operation time may be increasing the ionic current, achieving a higher number of ionic impacts against the material per unit of time. One of the main problems when high milling time is required, special care has to be taken in order to avoid redeposition process of scattered atoms into the sample. During the milling process, the evaporated material redeposits in the opened whole and specially in the face of interest. The redeposited material is normally an amorphous phase rich in Ga^{+} that will make all the following characterisation techniques more difficult. That is why when high detail and precision are needed in the micromachined geometries; in order to avoid and/or reduce this effect, low currents are preferable.

Redeposition process will not be the only artefact and problem to face when we are trying to develop a correct use of FIB in materials science. Furthermore, another milling effects as "*curtain effect*" or also known as "*waterfall effect*". Mainly, the last FIB artefact is the main responsible to induce superficial grain growth; formation of gallium-material composites, among others.

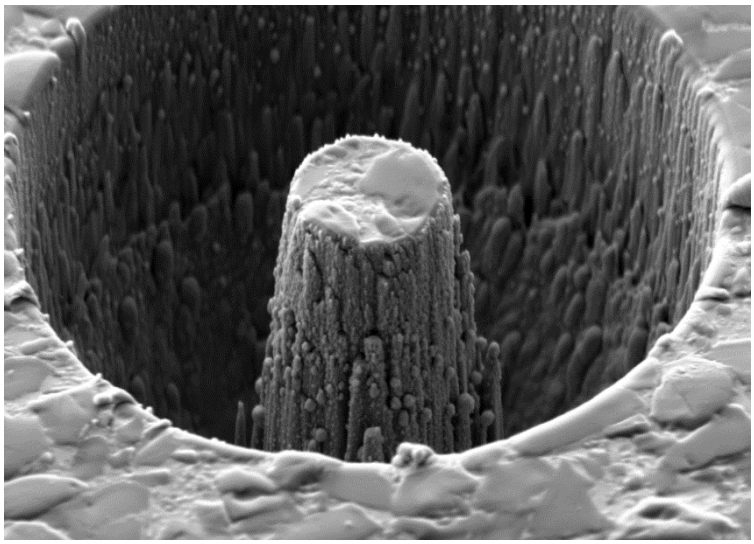

Figure 9- FIB micromachined pillar for the specific case of cBN, where artifacts like amorphisation, Ga implantation and tapering can be observed.

ii) *Deposition mode:* FIB equipment allows depositing some kind of protective layer of dielectric or conductive material with mainly two objectives. Firstly, protecting some parts of the sample surface in order to be damaged by the Ga^+ beam and secondly, decrease the redeposition phenomena when preparing the samples. This feature of FIB is especially important when high detailed sections are wanted to be obtained, or to keep structural stability in very thin sections.

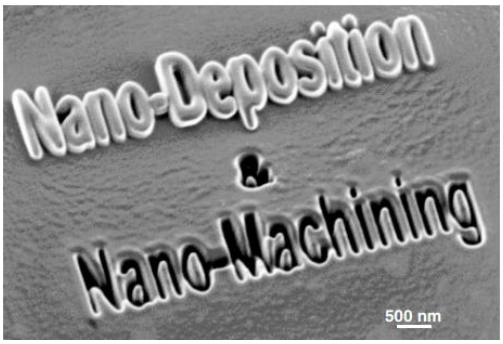

Figure 10 - SEM image showing the simultaneous milling and deposition capabilities of a FIB equipment.

iii*) Machining for tomographical analysis*: for achieving a 3D-tomographical reconstruction of a representative volume element (RVE) of a certain microstructure, the sectioning of the material is needed. In this sense, FIB equipment is the perfect choice for this image treatment technique. The material can be sectioned by means of focusing the ion beam against the sample and imaging the area of interest at the same time with the electron beam. The visualization of the slicing process may be held in-situ and the precision of FIB machining allows the sectioning to be done with a very little space between slice and slice.

Tomography – Section Based techniques

Tomography is a section based technique that is mainly focused in obtaining 3D information of the interior of a material/system through the reconstruction of a series of consecutive 2D parallel images known as tomograms, see **Figure 10**.

The origin of this technique comes from medicine, where multiple X-ray images are taken consecutively and 3D information of a specific part of the body is obtained in order to realise a better diagnose. In case of materials the information that is normally obtained from a tomography process is microstructural characteristics, crack morphology, interface geometries study, etc. In materials science there are several methods in order to obtain all the 2D images required to obtain the volume of study. Depending on the desired resolution non-destructive or destructive techniques may be considered. Within the destructive ones, there is the possibility of "slicing" the material in a controlled way by several methods like leaching, polishing, cutting, milling, etc.

In the specific case to perform a 3D-microstructural reconstruction like in this Master's thesis, the tomography process has been made by means of a destructive method, where the slicing of the material is physically done by erosion of the material with the ion beam of FIB/FESEM equipment. This tomography technique, the sample surface is oriented perpendicularly to the ion column and erodes the material with precisions determined by the ion beam, with a spot size down to the 5 nm approximately. With such a high precision, the distance between slices can be regulated to be in the range of the (10 nm) giving a high resolution in the reconstructed volumes (26).

Continuous imaging of all the slicing process is done by means of the SEM column that is oriented with 54º tilt respectively to the ion beam (see **Figure 11**).

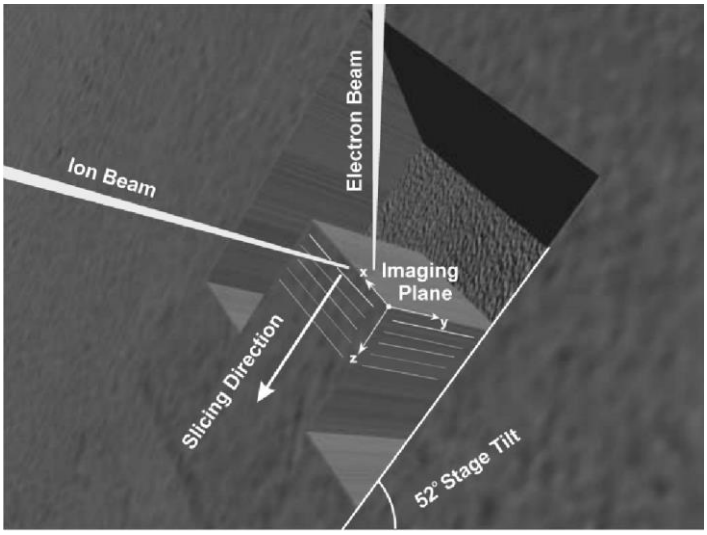

Figure 11 - Schematic representation of working principle of FIB/FE-SEM tomography technique**. (24)**

Despite all the advantages of FIB/FE-SEM tomography, this technique is limited to the analysis of small volumes of interest that will be within the micrometer range because of its low milling rate.

Micromechanical Testing

Nanoindentation

Nanoindentation is the most widely used micromechanical testing technique in materials science due to its simplicity and possibility of automation. It consists in the mechanical testing of materials through an indentation test where the load (P) and the penetration into the material (h) are recorded continuously, with precisions in the range of nN and nm respectively.

Originally instrumented indentation was developed in order to determine materials hardness (H) without need of imaging the residual imprint. Nowadays, an exhaustive analysis of a P vs. h curve reported by this technique is able to extract much more information of the material. A single nanoindentation test may bring light to several mechanical properties as elastic modulus (E), fracture toughness (K_Ic), time dependant properties, yield strength (σ_y), among other mechanical properties.

Instrumented indentation technique (ITT) always is held by equipment that consists in two well differentiated modules: control unit and nanoindentation unit.

- Control unit is the part that includes all the software control and the computing power of all the tests. Is through the control unit that all the testing conditions and parameters are set. All the testing parameters can be classified in two main groups:
    a) Test configuration parameters like indenter type, calibration, initial verifications etc.
    b) Testing variables like maximum applied load, time until reaching the highest load, time at highest load, unloading percentage, number of cycles etc.
- Nanoindentation unit: Is the actuator part, which this part applies force or displacement to the indenter tip in a controlled way. The applied forces are directly measured by means of the measurement of voltages or currents in the actuator. Other equipment's base their function in the combination of piezoelectric materials and load cells that offer direct force measurements. On the other hand, displacements are usually measured by the capacitive strain gauge and corrected and calibrated to take into account the compliance and other artefacts of the indentation column.

The typical configuration used in the nanoindentation unit in instrumented indentation equipments is shown in **Figure 12**.

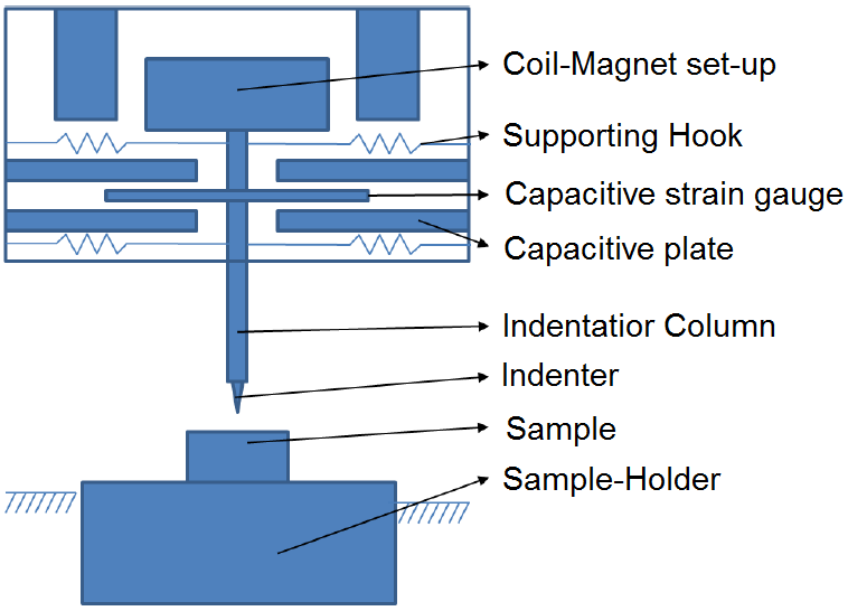

Figure 12 – Nanoindentation unit Scheme (27)

One of the most influencing parameters in the micromechanical testing of materials by instrumented nanoindentation is the geometry of the used indenter. Depending on their geometry different properties will be determined. There are mainly two different families of indenter tips:

a) Sharp tips, they present self-similar geometries with a stress singularity at the tip of their tip, theoretically in the tip the contact area is 0 and the stresses tends to infinite values (28). This fact assures always an elasto-plastic contact from the first moment of contact. Normally this type of indenters are the ones used for determining hardness, fracture toughness, yield strength etc.
b) Blunt tips, are indenters with geometries that enable elastic contact at the beginning of the loading. This fact makes possible the determination and study of the elastic modulus as well as extract the stress-strain curve. On the other hand as they do not have self-similar geometries there is difficulty in estimating contact area at larger depths.

In the case of this study, nanoindentation as raw technique was used to realize studies of indentation size effect (ISE) and to determine the mechanical properties of the composite material as a complex system.

Oliver and Pharr method (28) is the most employed method to determine mechanical properties as hardness and elastic modulus from the data supplied by instrumented indentation tests. This method analyses the load (P) vs penetration depth curves (h) obtained from the elastoplastic contact between an indenter tip and a substrate to determine not only hardness or young modulus

but also fracture toughness information, time dependant properties, yield stress among others (29).

Oliver and Pharr method is developed to use sharp indenters (Berkovich tip), due to the fact that they always produce an elasto-plastic deformations of the surface (ideally in the beginning the contact is punctual so the applied stress is infinite).

This method uses the P-h curve and approximations over the true projected contact area of the indentation to get all the mechanical behaviour information. In (28) is assumed that even if the loading is always elasto-plastic, the unloading is always elastic, then the total penetration depth will always have an elastic (h_s) + a plastic (h_c) contribution. See **Figure 13**, to observe how the elastic sink-in at maximum load (h_s) is not equal to the residual penetration depth. That is why a batch of mathematical equations have to be developed to go from the hard data to the mechanical properties of the material.

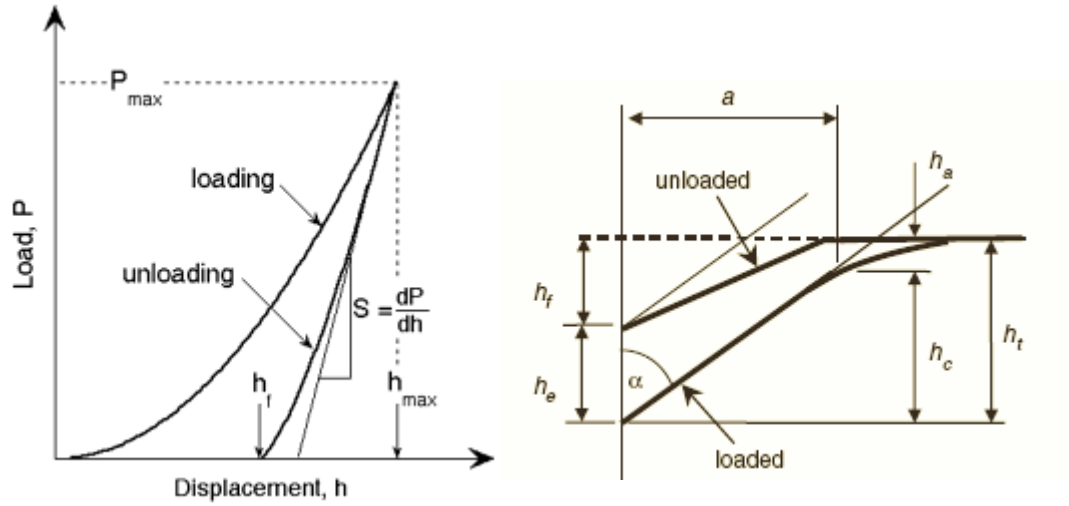

Figure 13 – Typical load-displacement curve obtained from an indentation with a Berkovich tip showing its important measured parameters. And **g**eometrical considerations about the contact between the indentation tip and the substrate **(30)**

The equations needed to relate load and displacement to effective stress and strain are the following:

$$h_c = h_{max} - \varepsilon \cdot \frac{P_{MAX}}{S} \qquad \textbf{Equation 4}$$

$$P_{max} = \alpha \cdot (h - h_r)^m \qquad \textbf{Equation 5}$$

Where h_c is the vertical distance along which contact is made, h_{max} is the maximum penetration depth of the tip into the substrate, ε is the strain ,*Pmax* maximum applied load against the surface,

S stress, , h_R and α and *m* are power law fittings. From them, even the hardness or the Young modulus can be extracted for a perfect Berkovich indenter as:

$$\boldsymbol{Hardness = \frac{P}{A(hc)}\ ; A(h_c) = 24.56 \cdot h_c{}^2} \qquad \textbf{Equation 6}$$

$$\boldsymbol{E_{eff} = \frac{1}{1.034} \cdot S \cdot \frac{\sqrt{\pi}}{2} \cdot \frac{1}{\sqrt{A}}} \qquad \textbf{Equation 7}$$

The determination of single phase properties have been done by means of a specific methodology of instrumented indentation called massive nanoindentation or grid indentation. In it, a big number of controlled indentations are done into the material under depth control mode and further statistical treatment of the acquired data by using the Ulm and Constantinides methodology (1) allows to determine deeper information of the material components.

Massive Nanoindentation

One of the most important advantages of nanoindentation is the fact that with the adequate equipment, indentations of few nanometres can be performed, allowing the study the local properties of composite materials like single grains with different crystallographic orientations, phases, thin films, surfaces, among others at the nanometric length scale. Making profit of this characteristic, massive nanoindentation tries to study the hardness and elastic modulus of individual phases included in much complex material systems like composite materials. This approach relies on a large array of indentation experiments at a specific scale of material observation defined by the indentation depth and the statistical analysis of the resulting data (1).

This technique was born as an extension of instrumented indentation for multi-scale composites. Under certain restrictions, it is able to provide quantitative and qualitative information about the morphology and mechanical properties of the constitutive phases comprising the composite material (1).

In nanoindentation testing we can find two different scenarios:

- The residual imprint and the elastic strain field are bigger in size than the inclusions or second microstructural phases. In this case, the obtained information will be related with the behaviour of the composite material at the micrometric length scale.

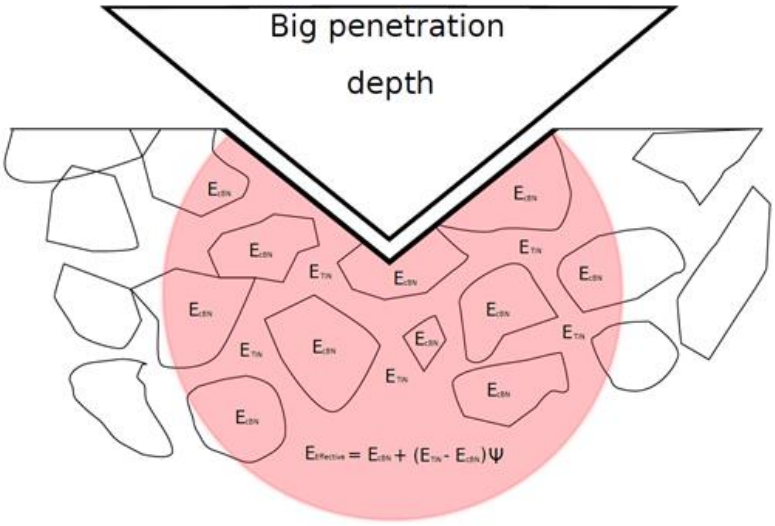

Figure 14 - Interaction between the elastic field caused by a deep indentation and the composite microstructure.

– The imprint and the elastic strain field are smaller than the microstructural characteristic elements. In this regard, there is the possibility of differentiating several mechanical properties from the different constitutive phases present in the composite material.

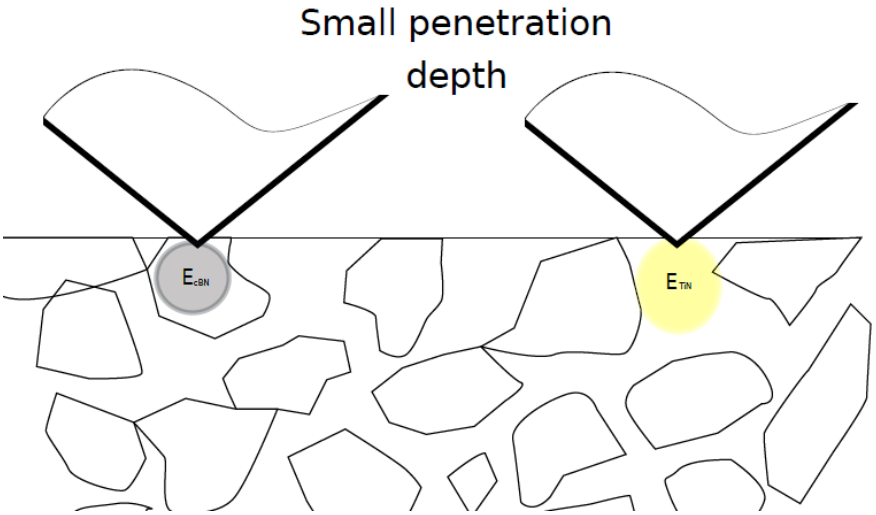

Figure 15 - Interaction between the elastic field caused by shallow indentations and the composite microstructure.

Massive nanoindentation technique implies the study of single-phase mechanical properties by performing a huge amount of shallow indentations and afterwards treat the mechanical properties obtained by using the Oliver and Pharr equations (28) by the statistical methodology proposed by Ulm and Constantinides (1). Within this context, it is necessary that the different phases in the complex material are significantly different in mechanical properties for the whole analysis to be useful. In order to apply continuum indentation analysis to heterogeneous systems, the indentation depth should be at most 1/10 of the characteristic size of the microstructure as

proposed by Buckle in Ref. (31). And even this rule is not restrictive enough when the mechanical properties of the two phases becomes too big $\frac{E_S}{E_f} \notin [0.2, 5]$.

The first step for the deconvolution technique is the generation of the experimental cumulative distribution function (CDF). For it, is necessary to sort the N indentations in increasing order of hardness or elastic modulus , depending on the property to be studied (32). In this way the CDF function for hardness will be defined by points like $D_x = (H_i, CDF_i)$ where H_1 will be the lowest hardness measured while H_N the highest. The N points of the experimental CDF are obtained by using the following equation:

$$\boldsymbol{D_x = \frac{i}{N} - \frac{1}{2N}} \quad \textbf{Equation 8}$$

Once the experimental CDF is obtained, it has to be assumed that the heterogeneous material is composed by j = 1, …, n material phases with significantly different mechanical properties. Each phase occupies a surface fraction f_j of the indented surface, and the mechanical properties distribution of each of the phases can be approximated by a Gaussian distribution. A Gaussian distribution for phase j can be defined for hardness property by its mean and standard deviation as $N_j^H = (\mu_j^H, \sigma_j^H)$ and for the elastic modulus as $N_j^M = (\mu_j^M, \sigma_j^M)$. (32)

$$\boldsymbol{p_j(x) = \frac{1}{\sqrt{2\pi {s_j}^2}} \cdot \exp(-\frac{(x-\mu_j)}{2{s_j}^2}} \quad \textbf{Equation 9}$$

Where x corresponds to the value of each measure (Modulus or Hardness); μ_j is the arithmetic mean of all the N_J values of each phase and s_j is the dispersion measure for the hardness/modulus values corresponding to each of the j phases.

In the case of having a pure or homogeneous material j = 1 and obviously the normal distribution would correspond to the mechanical properties of the material. But as a composite, each phase can be considered as an individual phase with its mechanical properties following a Gaussian distribution. If the mechanical properties of the material as a whole are wanted to be determined the approximation of "no mechanical interaction" between phases is needed. The overall frequency distribution of the mechanical properties for the composite material is obtained by the pondered addition of all the distributions of mechanical properties for each of the phases.

$$\boldsymbol{P(X) = \sum_{j=1}^{n} f_j \; p_j(x)} \quad \textbf{Equation 10}$$

where f_j is the volume fraction of the phase j subjected to the constraint:

$$\boldsymbol{\sum_{j=1}^{n} f_j = 1} \quad \textbf{Equation 11}$$

From the scope of CDF's (see **Figure 16** left) the fitting process consists in determining for each phase every (f_j,μ_j,σ_j) and the system of unknowns is solved by minimizing the difference between the experimental CDF and the weighted phases model:

$$\min \sum_{i=1}^{N} \left(\left(\sum_{j=1}^{n} f_j \, CDF_j \right) - CDF_{EXPERIMENTAL} \right)^2 \quad \textbf{Equation 12}$$

From the normal probability density functions (PDF) / histograms scope (see **Figure 16** right) all the unknowns are determined by minimizing the standard error between the observed value of the experimental frequency density (P^i) and the value of the theoretical probability density function.

$$min \sum_{i=1}^{m} \frac{\left(P^i - P(x_i) \right)^2}{m} \quad \textbf{Equation 13}$$

where *m* is the number of intervals (bins) chosen to construct the histogram.

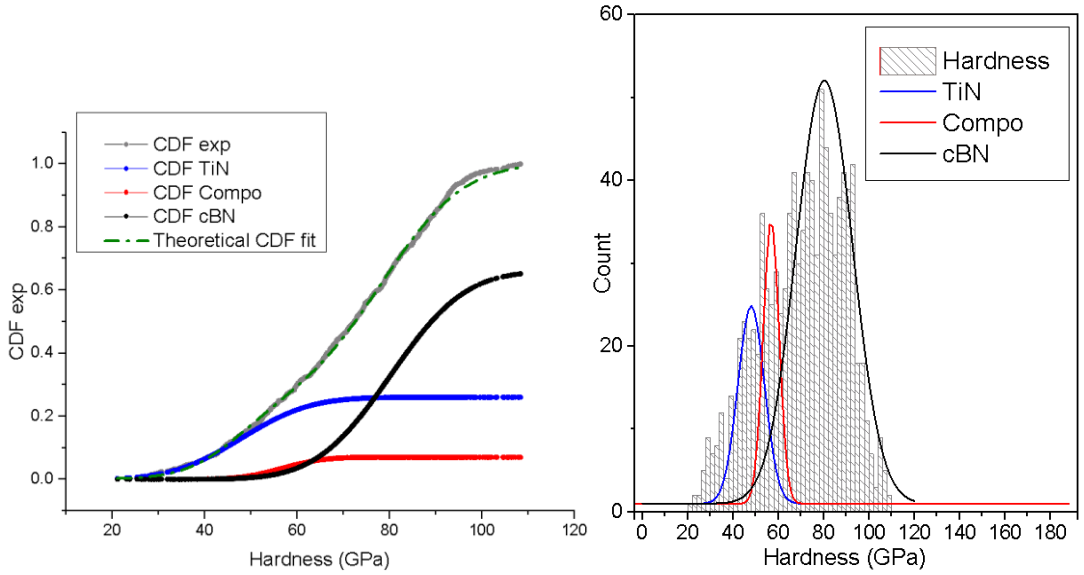

Figure 16 - Statistical indentation analysis of a composite material (TiN+cBN): Cumulative distribution function (CDF left) and probability density functions (PDF - right) if indentation Hardness (H). The experimental CDF is constructed by means of 1020 indentations and is deconvoluted in a series of three phase-specific CDF, which are assumed to be Gaussian and which are also displayed.

In order to obtain all the unknowns of each phase in a proper way ensuring that phases have sufficient contrast in properties, and thus to avoid the overlapping of two neighbouring Gaussians, the following restriction is also imposed:

$$\mu_j{}^H + \sigma_j{}^H \leq \mu_{j+1}{}^H + \sigma_{j+1}{}^H \quad \textbf{Equation 14}$$

The results of the study are estimates of the mean and standard deviation of indentation hardness ($\mu_j{}^H, \sigma_j{}^H$) and elastic modulus ($\mu_j{}^E, \sigma_j{}^E$) for each phase with mechanical differences, and the approximation of the surface fraction of each phase (f_j).

Micro-samples mechanical testing

With the continuous miniaturisation of all technical devices and the importance of nanotechnology in the present scientific research, the study of the behaviour of materials at the micro- and nanometric length scale has sparked the interest of the whole community. Up to which scale are the assumptions of continuum mechanics valid? When do the intrinsic microstructural lengths start to interfere with the deformation micro mechanisms? How do materials behave in micro sized components? How can the macroscopic behaviour and microscopic behaviour of materials be related?

Table 2 - Advantages and disadvantages that micromechanical testing can have from a materials science pointof view.

Micromechanical testing	
ADVANTAGES	**DISADVANTAGES**
✓ Extract the micromechanical properties of each constitutive phase	× ISE
✓ Leeds to predict the macroscopic behaviour and microdesign of new microstructures	× Scale effect (roughness problems)
✓ Necessary to stablish protocols	× Tip defect
	× Time consuming

One of the most important things to determine when performing micro mechanical testing is the relationship between the relevant size parameters and microstructural constrains to which the particular physical mechanisms are subjected.

In general, it is therefore the competition or coupling between two different size dependences that determines the properties of a material. We thus have to deal with the interaction of two length scales:

a) The dimension characteristic of the physical phenomenon involved, called the characteristic length.
b) Some microstructural dimension, denoted as the size parameter (33).

The correct understanding of this correlation will allow us to obtain useful information of macroscopic behaviour from micromechanical testing. While the results from the testing of micro-

samples will give direct information of the performance of materials in applications as thin films, MEMS, nanowires where physical phenomena will find size constrains.

With the appearance of lithography techniques, FIB and other nanofabrication processes, obtaining mechanical testing samples in the micrometric scale is no longer an impossible thing. Nowadays, is possible to obtain several geometries like: pillars, cantilevers, tensile samples (bone geometry), double cantilever beams… that allow us to test different properties in advanced materials (

Table 3).

Mechanical property	Sample geometry
Yield Strength	Pillar, Cantilever, bone
Mechanical property	**Sample geometry**
Yield Strength	Pillar, Cantilever, bone
Fracture Thoughness	Double Cantilever, notched cantilever

Table 3 - Different sample geometries test different mechanical properties.

In this Master's thesis two different types of micro machined samples have been milled and in a future will be in-situ tested in the Nanomechanical Inc company (Oak Ridge, EEUU) in order to extract the compression stress-strain curve (micropillar) as well as the fracture toughness (notched cantilever bending).

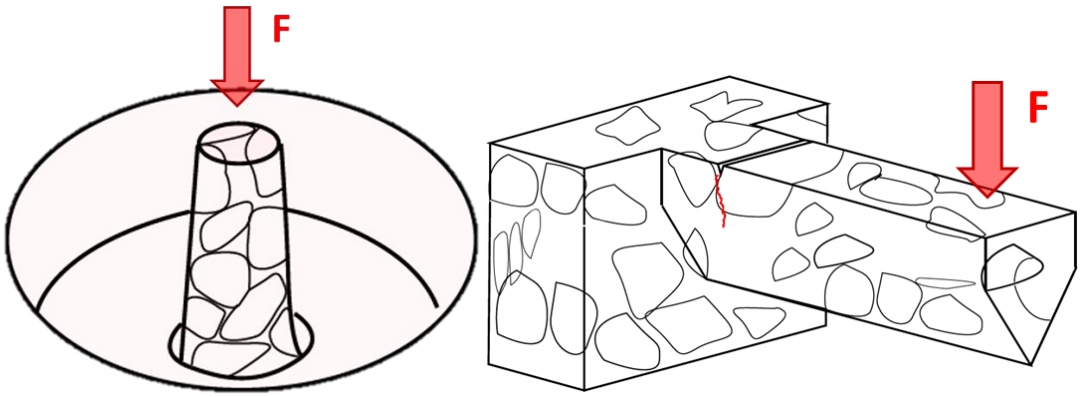

Figure 17 - Schematic representation of the mechanical tests done into microsized samples (Left: Micropillar compression/ Right: Notched cantilever bending.).

In one hand, pillar compression tests will be performed in order to determine the behaviour of the PcBN composite in the micro scale under monotonic compression loading. The objective of the testing was to obtain the stress-strain curves of the material for comparing them with the results given by the finite element analysis (FEA).

On the other hand, notched cantilever bending tests were done in order to try a novel qualitative characterisation technique to determine the adhesive energy between the PcBN

particles and the ceramic binder as well as in order to determine the fracture toughness. The obtained information could have been used as an input to improve FE simulations by introducing interfacial physical models instead of assuming a perfect adhesion between matrix and cBN grains. If the machining of samples and later testing could be performed the results could also show a qualitative evaluation of the fracture mechanisms occurring in the interface between cBN particles and TiN matrix.

Finite Element Simulations (ABAQUS Software)

Multi-scale modelling and homogenization has demonstrated to be promising methods for better understanding the deformation behaviour and mechanical strength of composite materials (34). On this basis, the present Master's thesis aims to understand the relation between microstructure and mechanical behaviour of PcBN composites by developing computational microstructure-based homogenization models that consider local properties of the material tested at the micrometric lengthscale and real microstructure models obtained by FIB 3D-tomography as inputs.

The followed flowchart for developing the whole simulation is depicted in **Figure 18**:

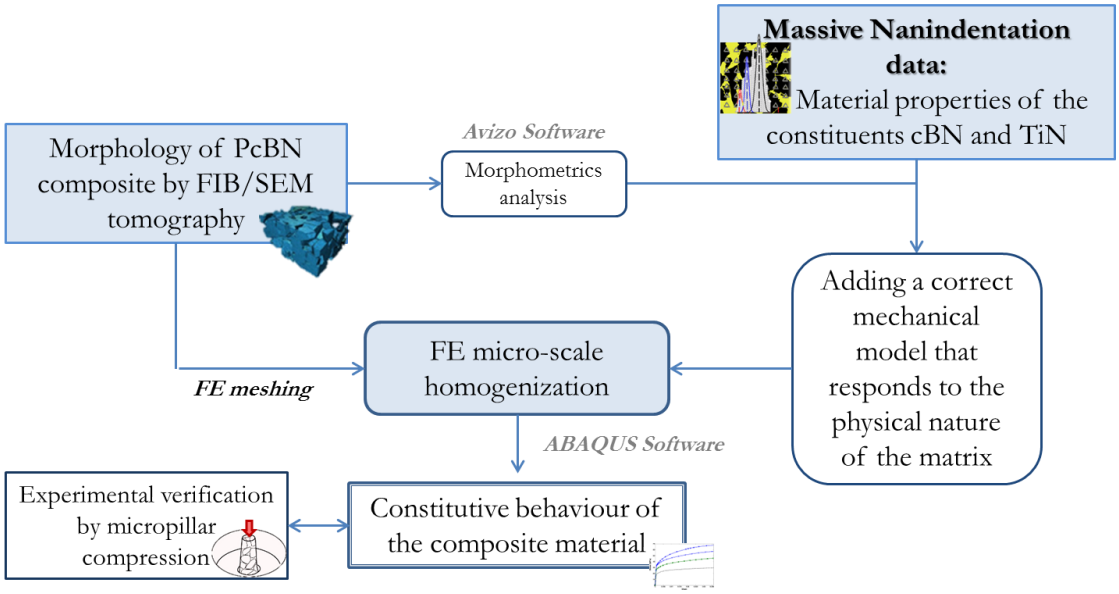

Figure 18 – Flowchart for the simulation analysis.

In the employed approach, the 3D configurations of the matrix and particles are obtained by FIB/SEM tomography and used to generate FE meshes of the real microstructure. The average constitutive behavior of the material as a composite is identified by adopting a classical direct transfer (matrix/reinforcement) micro-scale FE homogenization. The simulation method details

will be discussed in the following sections. Finally, the simulation obtained results are compared experimentally to micro-pillar compression tests.

Matrix simulation method

PcBN composites show a big contrast in mechanical properties between constituents and it can be considered as a particle-reinforced inorganic matrix material in which hard nitrides play the role of reinforcement and the TiN plays the role of elastic (and also brittle) matrix. In general, the higher strength of PCMC compared to the corresponding of pure ceramics is mainly attributed to the load transfer from softer matrixes to highly resistant particles. This principal hardening mechanism is known as direct strengthening effect and is not the only one who takes place in composite materials mechanical strengthening (indirect particle strengthening is normally also a very important one). The portion and contribution of each of the strengthening mechanisms in the overall composite behavior depends on several microstructural parameters like reinforcement size, shape, distribution, volume content, etc (35).

Indirect particle strengthening effect is related to the strengthening of the composite material due to the increase in the energy needed by the matrix dislocations to glide due to the introduction of second phase particles. For the case that we are studying, this mechanism is nearly negligible due to two main reasons:

- The deformation process of the TiN matrix is not substantially controlled by dislocation glide and dislocation strengthening. The best approximation for TiN mechanical behavior would be a linear elastic material with a brittle failure criterion (36). TiN because of the ionic and covalent atomic bonding highly oriented, dislocations have very high activation energy and plastic deformation is only observed at relatively high temperatures ranging between $0.4 \cdot Tm$ – $0.7 \cdot Tm$. This is a very important behavior to take into account when trying to simulate and homogenize as a continuum a composite material. Introducing brittle failure criterias instead of classical von Misses (J2 method) homogenization methods may be closer to reality when studying PCMC.

-High volumen content of reinforced particles: because of the big amount of hard particles that the composite material has, the small mechanical enhancements that could appear in the matrix due to indirect particle strengthening are not very relevant.

When the load-sharing matrix-particles mechanism is considered to be the dominant strengthening mechanism the dislocation strengthening is negligible. For these cases various continuum-based approaches including the unit-cell, modified shear-lag theory and other different FE models have been proposed. Lots of them are able to explain the deformation behavior or the

composite materials. However, most of the models make many assumptions in the input parameters (shape of the reinforcement/network) (37), and are further from reality, than the model proposed in this project.

FE micromechanical homogenization

In the framework of continuum mechanics, a FE homogenization method is used to derive the effective mechanical properties of the bulk material from its detailed microstructural definition, from a representative volume element (dV).

Even 2D or 3D homogenization strategies lay in the principle or representative volume element or unit-cell which, if submitted to periodic boundary conditions and considering periodicity of the microstructure, can provide a good estimation of the effective macroscopic response from only a meso or micro-scale volume test/simulation. Moreover, considering periodic boundary conditions reduces a lot computational cost and localization problems sensitivity.

So, in order to take profit of all of these advantages of the unit-cell mode of operation, is necessary to be sure that the microstructure of our PCMC really meets the assumptions taken by it. In the cases where microstructure is not periodic, is highly anisotropic and/or depends strongly in the spatial distribution of the reinforcements; the unit-cell models may not provide a reliable prediction of the homogenized behavior (38). Here relays the importance of finding the correct volume element (in size and location) that allows approximating from a microstructure-based homogenization the mean constitutive response of the material.

Representative volume element (RVE) definition

When developing a FE simulation is of high importance to establish perfectly which the RVE of the material is. RVE is defined in Ref. (39) as: “the smallest material volume element of the composite for which the usual spatially constant overall modulus macroscopic constitutive representation is a sufficiently accurate model to represent mean constitutive response”. This definition also implies that applied loads and boundary conditions vary are much larger than the microstructural length scale of the composite.

Several methods for determining RVE have been developed (39) and even some of them have been able to propose approximate quantitative analytical estimations of the minimum RVE size in two-phase linear elastic random composites, only by means of equations. Drugan and Willis use tensors of the non-local constitutive equations with strain fields that change with the position until the local and non-local terms are different enough to do not be considered as homogeneous response. Following this method, they proposed for a two-phase composite with isotropic matrix and spherical isotropic reinforcements a RVE of 4.5 times the characteristic reinforcement diameter, obtaining only a 1% of error when only mechanical response is being studied.

However, normally real composites are not reinforced by spheres and alternative methods have to be done to determine RVE with good precision. Analytical methods that rely only on mathematical models have not been developed for real composites, and if a precise determination of RVE is needed methods that rely on real microstructures modeling are the best ones.

The method followed in this project in order to determine precisely the RVE has been the one proposed by Galli and Cugnoni in Ref. (40). This method uses in its homogenization strategy the real 3D-microstructure of the material obtained by tomography in order to be closer to reality and reflect better the effects of particle-particle interactions, particle aspect ratio, particle clustering etc. In the other hand, this method needs high cost techniques like FIB/FESEM or X-ray synchrotron tomography to obtain the real microstructure as well as giving as a result larger RVE than the ones determined by other ways that imply higher computational costs.

The followed method answer the following question: Which is the minimum characteristic microstructure volume size that makes the average properties of the mixture to be representative of the mean constitutive response of the continuum? This question was answered by increasing and changing the position of the volume of interest within the material until obtaining the minimum volume required at which volume fraction of reinforcement and macroscopic effective response are stable. The steps to follow in order to determine the appropriate area are:

1. Cubes of various edge sizes "*a*" are extracted from different locations of the obtained tomographic volume.

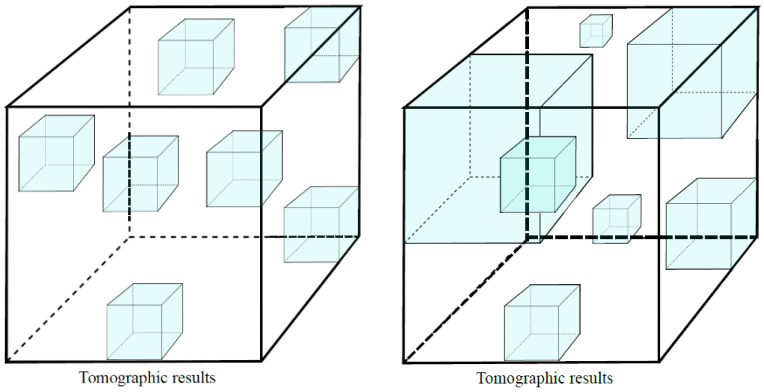

Figure 19 - Different volumes of the same size but different location extracted from the tomographic volume (left) different volumes of different sizes and locations extacted from the tomographic volume (right**)**

2. The volume fraction of each of the phases is calculated by means of any image processing software (Avizo 8.0 in this case), where the initial guess for the RVE size (a_{RVE}^{ini}) corresponds to the minimum cube size at which the volume fraction of constituents remains constant.

3. The following step is based in finding the convergence of macroscopic stress-strain behavior. Several cubes from different positions of the tomographic results of a > a_{RVE}^{ini} are meshed and simulated mechanically.

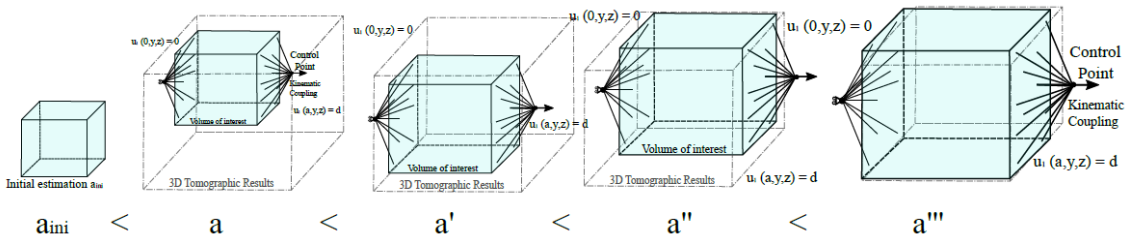

Figure 20 - Depiction of the mechanical simulation of different volume elements extracted from different locations of the tomographic reconstruction

4. Simulations for the different cube sizes are held until the minimum volume cube satisfies the following condition:

$$\forall\, a, a > a_{RVE}, \forall\, e, e < \bar{\varepsilon}: Err(e,a) = \frac{|\bar{\sigma}(e,a) - \bar{\sigma}(e,a_{rve})|}{\bar{\sigma}(e,a_{rve})} < 2\% \qquad \text{(X)}$$

Once the RVE size is determined, the mechanical analysis of the material can be held by means of the mechanical simulation of volumes that are, at least, as big as the RVE.

Finite element mechanical simulations and potential results

Continuum mechanics considers a sample divided in volume differentials (dV = V→0) and assumes that every one of the dV are in mechanical equilibrium and that inside a dV the gradient of stress state is 0. Continuum mechanics can be different *dV* with different mechanical/material properties, but the mechanical properties within a *dV* have to remain the same.

FE simulations make use of the basic principles of continuum mechanics to analyse any geometry under complex stress states and many other mechanical scenarios. In the case of FE modelling a digital computer aided design file (CAD) is subdivided in several *dV* called elements through the process called meshing. Following, the continuum mechanics mathematical models are implemented in every one of the FE under several contour conditions to obtain the simulation of a complex mechanical state.

FE calculations always yield approximations of the analytical result of the partial differential equations that should be solved to obtain the exact value. The approximation is optimized by the minimization of the associated error function. The precision of the FE approximations is influenced by multiple factors that affect the quality of the simulations. In the specific case of mechanical simulations the most important considerations to take into account before starting are the following:

- **Element type.** The obtained mesh uses tetrahedral elements of the type (C3D4), this means that there is only one integration point per side. In mechanical simulations is normally advised to use more complex elements like C3D10 where tetrahedrons have an additional integration point in every side of tetrahedrons, however as the calculations are easier to perform with C3D4 elements, this drawback could be countered by the addition of a higher number of elements into the model. While the typical simulated models with C3D10 elements count with around 50k elements, the simulated model counts with 800k. Making the computational complexity comparable.

  Most of the times the nature of the presented problem already establishes an element type that could fit's better the mathematical calculations needed for that specific physical condition (thermal transfer, mechanical loading, fluid dynamics etc.)
- **Mesh size and refinement.** In FES as finer is a mesh the higher resolution is achieved in the final simulation. An ideal simulation would have an infinite number of elements, as further a simulation is from this condition less accuracy will have. A compromise between mesh size and computation cost has to be achieved, and normally meshes are only specially refined in complex geometries where stress concentration or complex stress states can appear. In the case of microstructural simulations, the geometry of grains and especially of binder path makes necessary the use of refined meshes for nearly all the simulated volume.
- **Geometry simplifications and symmetry considerations.** Geometric simplifications or the use of symmetric planes (plus proper boundary conditions) to run simulations with a lower computational requirements are typical practices in science and engineering works.

  In the case of microstructural FES, the importance of a proper determination of the RVE lays in this approach. RVE is the smallest volume (less computationally demanding volume) that allows applying periodic boundary conditions and extrapolating meso and macro scale properties from micro-scale measurement.
- **Material modelling:** When simulating the physical properties that will rule the behaviour of all the elements are established by the user. All the resulting calculations will be conditioned by the similarities of the physical model to reality. That is why is highly recommendable to model the element properties as closer to reality as possible, and using experimental data as inputs for the simulation always that is possible.

  In the specific case of mechanical simulation, for example, using the real Stress-Strain curve of the material instead of modelling the plasticity of the material by theoretical models as J2, Lode, Ideal plasticity etc. will always present better results.

- **Boundary conditions**. A small deviation in the initial boundary conditions may result in a big difference in the final results. Is very important to imagine which are the testing conditions that would be carried in a physical testing and try to translate them into accurate boundary conditions in the simulation file. For the case of this master thesis, research most of the boundary conditions were imposed as if were mechanical testing machines that were applying loads and restricting movement.
- **Assemblies and part interactions**

When performed controlling all of these considerations, FE mechanical simulations can supply very useful information and valuable results. FE analysis may give approximations on energetic information that other ways could not be measured or supply direct data on the response of a very specific point contained in a much more complex system.

From the post processing of the resulting data in this Master's Thesis the main results that are expected to be obtained from FEA are:

- The analytical mechanical response of a RVE element of PcBN material under different applied strain conditions, reported as a stress strain curve for the material.
    - Because of the influence of the volume of the tested sample over the mechanical properties in ceramic materials and because of the small volumes in which PcBN composites are manufactured, the application of FES to obtain the stress-strain curves is especially interesting.
- The qualitative observation of how the stresses are distributed within the material as a composite and inside of each of the phases. And how the interface between both phases affect in the load transfer. This will be reported as colour maps of stress intensity.

Experimental process: Materials and Methods

Studied sample

The studied material is part of a machining chipbreaker tool from the commercial brand Sumitomo. In the commercial documents the studied material is considered to be the next cBN generation materials in which no impurities are found and tailored coatings are added to the machining tools to enhance its service performance (see Ref. (41) for more information). The working region is a small (1x1.7x2 mm approx.) insert embedded in a hard metal bigger WC-CO structure that gives to it the geometrical functionality, see **Figure 17**.

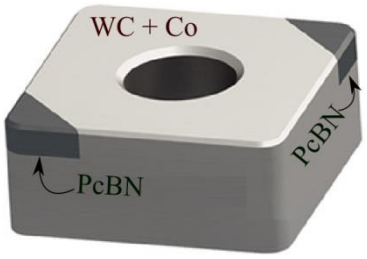

Figure 21- PcBN chipbreaker insert escheme.

The PcBN darkest region in **Figure 21** is the region of interest and it consists in a ceramic/ceramic composite obtained by catalysed conversion process where cBN is the reinforcement and TiN is the matrix.

Methodology

Chemical and microstructural characterisation:

The influence of several microstructural and compositional parameters over the PcBN composites properties have been already discussed in previous sections (see page 20). According to it, chemical composition (binder/reinforcement particles nature) and several microstructural parameters like ($\bar{d}_{cBN}$, C_{cBN}, λ_{TiN}) have to be the first things to characterise when trying to understand a material behaviour and nature.

The first step to be done was a common polishing, that enable all the following characterisation techniques to be implemented successfully. The sample was mirror polished following a series of polishing stages where diamond polishing pastes of decreasing particle size and a final stage with OPAN (sub-micrometric alumina suspension) were used. This methodology has given an irregular surface due to the difference of polishing rate between the ceramic reinforcement particles and ceramic matrix, being deeper in the TiN matrix than in the PcBN particles. However, the resulting surface quality is considered to be good enough to realize the microstructural and mechanical tests.

Once the sample was polished, the chemical composition of the binder material was studied. A semi-quantitative chemical composition analysis was done by means of Energy Dispersive X-

Ray spectroscopy (EDS) technique, in a Jeol JSM 6400 FE-SEM equipment. This technique is based in the principle of irradiation of the material by means of a highly energetic electron beam and the detection and analysis of the characteristic X-Ray wavelengths emmitedemisions.

Firstly, a general analysis of a 20x30 μm region of the material was done as a first approach for the material composition. Then, more precise EDS analysis were made on specific sites of the microstructure, where singularities were expected to appear, in order to study in more detail local compositions (see **Figure 22**).

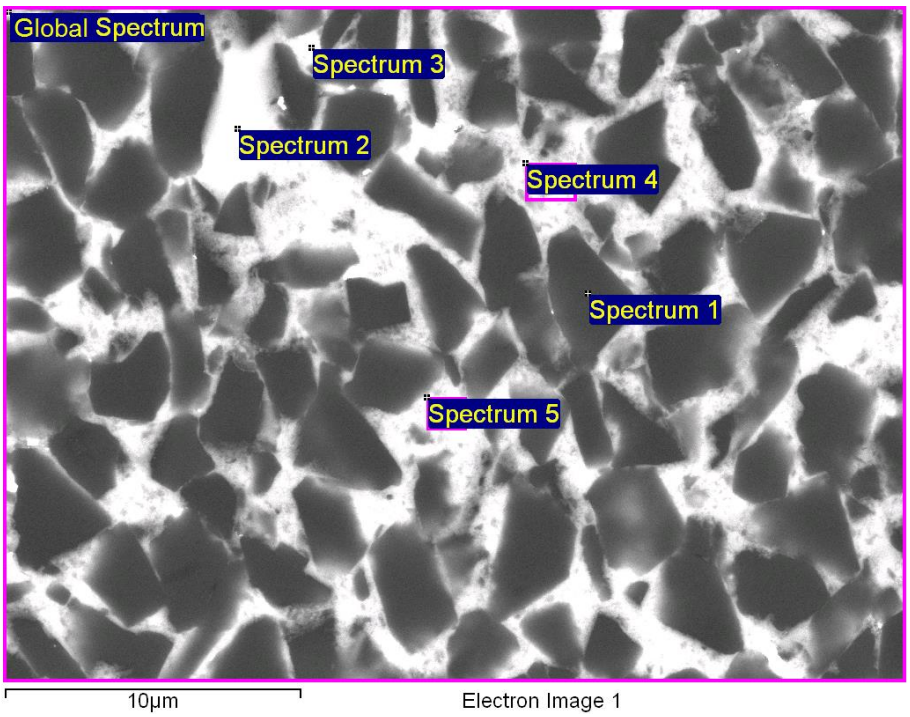

Figure 22. Map of the different spectra (spots represented in the image) taken into account when doing the EDS analysis of the material.

For Spectrum 1 a pure cBN particle wanted to be analysed, Spectrums 2,3 and 4 have as main objective the complete characterization of the TiN matrix due to the FESEM image exhibits different quality contrast. Finally, Spectrum 5 wants to distinguish the presence of specific species in the interface between the PcBN and TiN.

From the microstructural characterisation, mainly four microstructural parameters wanted to be determined: Binder Vol. %, cBN grain size, contiguity and mean free path. To achieve this, three different methods have been followed: linear intercept method, 2D particle image analysis and 3D-tomography analysis. Later results from different methodologies have been compared and discussed when possible.

- For linear intercept method six FESEM microstructure images were obtained by means of Jeol JSM 6400 FESEM equipment, at the same magnification of 2500 and 20 kV of imaging voltage. The image analysis was made using ImageJ software. Five lines in different directions were used for every micrograph resulting in a total number of 30 analysed lines per micrograph. All the microstructural parameters were determined by counting N_{TiN}, N_{cBN}, $N_{TiN\text{-}cBN}$ and $N_{cBN\text{-}cBN}$ for every line, and applying equations (1 to 3). Where N_{TiN} and N_{cBN} are the number of segments of every specie crossed by the line.

- 2D particle analysis method could only measure binder Vol. % and cBN grain size. The followed methodology for this aim was, smoothing filtering and binarization of the images using the ImageJ software and then direct measurement of:

- Binder Vol. % by dividing number of white pixels by total number of pixel in the binarized micrographs.

- $\boldsymbol{TiN\ Vol.}\% = \frac{\boldsymbol{Pixel\ N°_{White=TiN}}}{\boldsymbol{Pixel\ N°_{All}}}$ **Equation 15** cBN grain size by measuring (see Figure 23) and averaging the surface of 60 grains per micrograph (N=60·6= 360), and approximating its surface as if their geometry was a sphere.

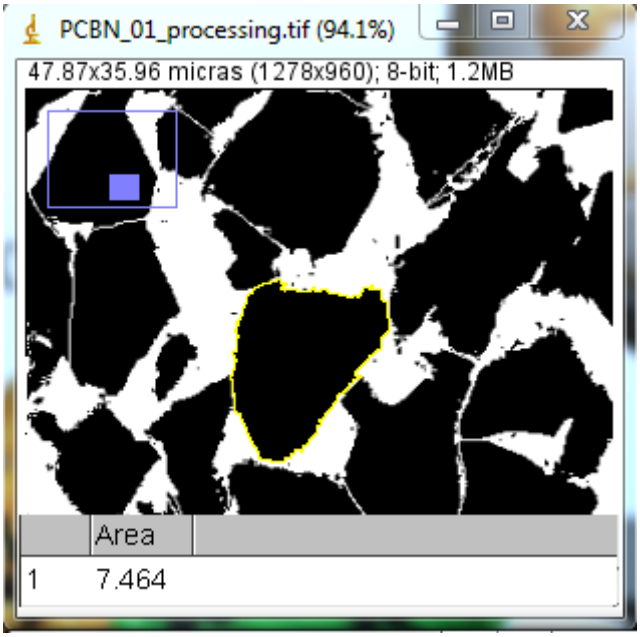

Figure 23 - Detail of a binarized micrograph where the particle area is being measured.

- 3D Tomography analysis is able to measure 4 of the microstructural parameters, and is the only method that does not need to do the Gurland assumption as reported in Ref. (42) of

spherical particles to realize all calculations. The used software for the study has been Avizo 9.0.

The first step when realizing a tomography in the deposition of a protective layer of platinum in order to flatten the surface, prevent the redeposition, reduce the erosion effect and diminish the curtain effect. Platinum gas was deposited at 30 kV and at different intensities depending the area to be covered. In this Master's thesis, the intensity was held constant and equals to 50 pA over a surface of 15µm x 15µm.

Once the protective layer was deposited, it was necessary to open a trench into the material so that the cross-section of the material and not the surface was visualized as it is depicted in **Figure 24**. This trench had to be big enough in order to visualize along the entire 3D-tomography the region of interest, within this context, the surrounding material may not interfere negatively in the visualization of the tomographic area of interest. Lateral and frontal trenches were machined at the highest milling current that still gave precise results (30kV 2nA).

Afterwards, a geometric shape was marked over the initial platinum layer by means of machining and dielectric deposition with the objective of mathematically determine the each slice thickness (see **Figure 20b**) and to correlate the slice number with its position in the Volume of Interest (VOI). Finally, before starting the slicing of the material it is necessary to re-polishing the frontal face at low machining currents (normally at 500 pA, which will be the current employed to conduct the 3D-tomography), achieving straight walls and very low redeposition.

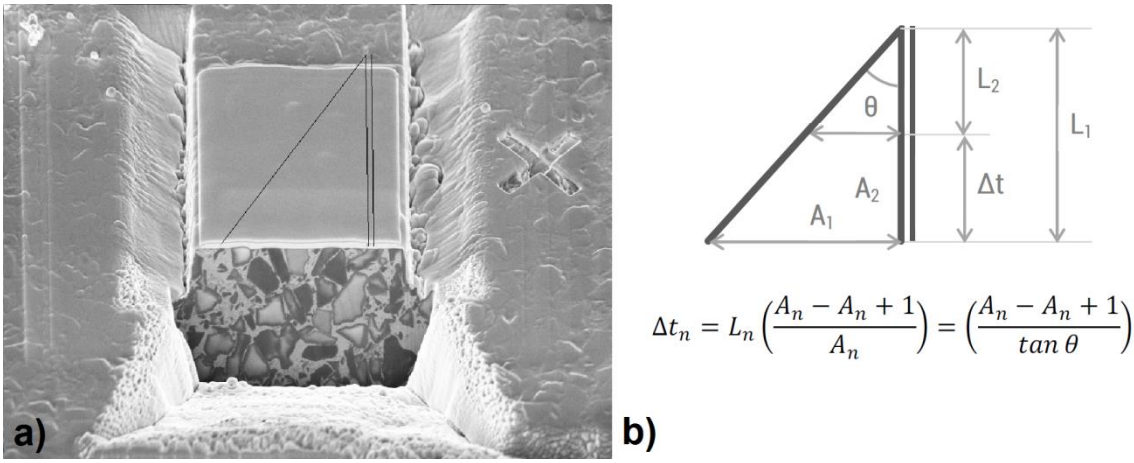

Figure 24 – a) Image taken of the VOI before the slicing showing the opened trench, geometrical guides and polished surface b) Formula that correlates slice number and position.

The sequential slicing of the material has been done with very low currents of (500pA) because of their small spot size that allows thinner slices, and because of the better visual finishing that allows a better reconstruction. The image recording was continuous observed and in this sense, a video was obtained from all the 3D-tomographic process. Having a video as the result of the slicing instead of a big batch of automatically taken FESEM micrographs allowed us to optimize which were the considered images for the tomographic reconstruction and only images with no curtain effect were considered.

This 3D-tomography technique is a time consuming process, and even more when super-hard materials with very low atom removal ratios like cBN are involved. The tomography realized for this Master's thesis took around 29h, 21 h were for the automatic image acquisition process and the rest of the time, the required hours involved to prepare the 3D-tomography.

From all the tomographic process a batch of 736 slices were obtained with an approximate thickness of around 25 nm, they were used as an in-put for the software Avizo 9.0 to do the tomographic reconstruction. The whole process (see **Figure 25**) can be mainly divided in four different steps:

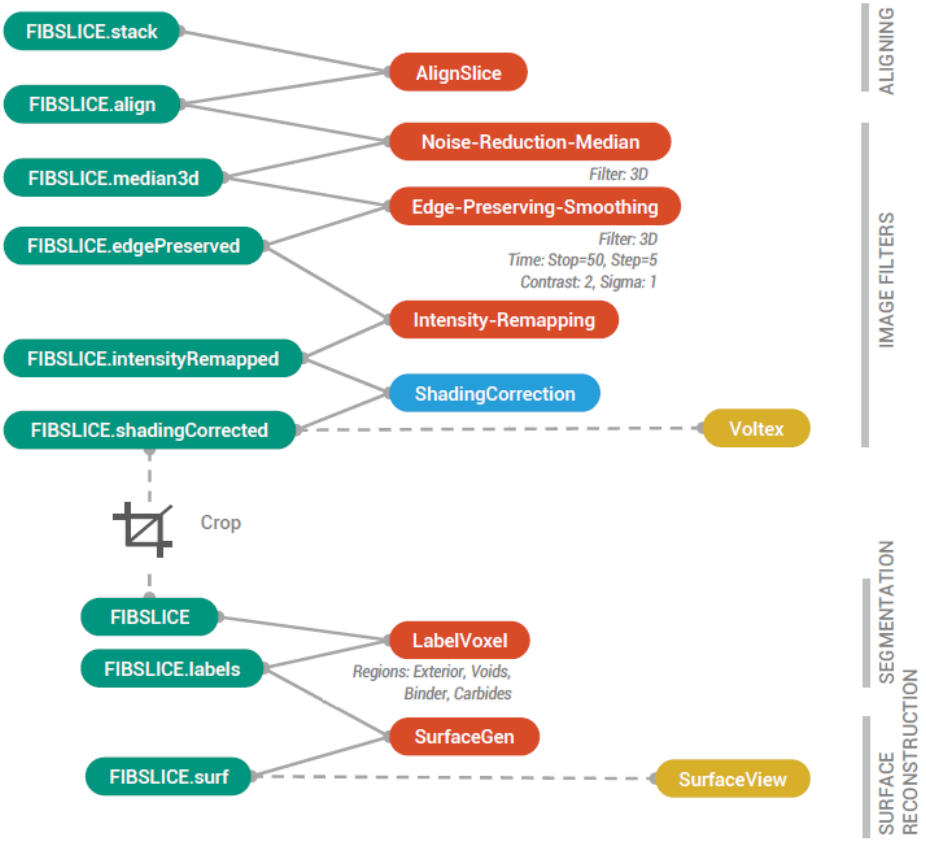

Figure 25 - Workflow as shown by software to obtain the volume reconstruction as a void surface **(43)**.

1. **Image Alignment:** The raw FESEM micrographs obtained by FIB are not perfectly positioned ones respect to the others because of the imaging perspective and stage drifting. In this Master's thesis, all the different slices were aligned manually in order to obtain the best possible 3D-alignment.
2. **Image Filtering:** The principal objectives of image filtering are improving image quality for a better visualization and to make posterior segmentation more efficient. The most important things to assure in order to achieve both goals is to avoid shadowing and differential lighting within one slice and within different slices of the volume and to optimize the contrast between different phases.

   The filters used for the process have been: *Noise Reduction Median Filter*, *Edge Preserving Smoothing Filter, Intensity remapping* and *shading correction* following the order as mentioned.
3. **Image segmentation:** With the improved (good contrast) images in greyscale is usually necessary the cropping of the region of interest before the segmentation. Segmentation process is made by the thresholding of a histogram with grey ranges from 0 (black) to 255 (white) in the X axis and Number of pixels with that value in the Y scale.

   In this case three ranges were defined as it is clearly evident in **Figure 26**:

   a. Voids from 0 to 10
   b. cBN from 10 to 156
   c. TiN from 156 to 255

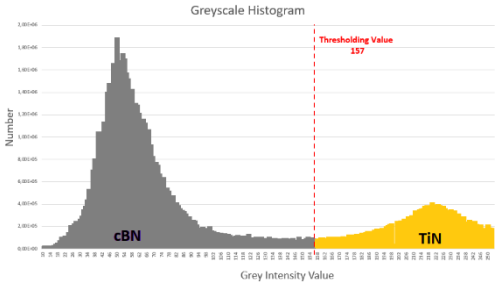

Figure 26 - Segmentation based on grey intensity.

4. **Surface reconstruction:** Avizo's SurfaceGen module computes a triangular-faced mesh of the total volume. Due to the complex geometries found in a real microstructure and because of some tomographic reconstructions artifacts (misalignments, sharp edges, etc.) the generated surface may be too detailed.

   In order to minimize the computing cost, is necessary to simplify the generated surface by resampling data before generating the surface or by limiting the number of created triangles.

After all this process, we were able to realize a 3D analysis of the material microstructure with the help of the *Material Statistics* module. It allowed us to measure: % vol. of phases, particle size, mean free path, shape etc.

Micromechanical testing

The whole micromechanical testing developed in this Master's thesis involves mainly two different stages:

1. ***Determination of mechanical properties of each constitutive phase by means of nanoindentation in order to use them as an input for Finite Element Simulation:***

The first and simplest test to be done on the micromechanical properties of the material is the analysis of the composite material properties by means of high penetration depth, around 2000 nm of maximum displacement into surface or until reach 650 mN of maximum applied load. The selected indenter geometry was Berkovich, a three-sided pyramid with a centerline-to-face angle of 65.3º, this minimizes the influence of friction on the test results. A Nanoindenter XP system from MTS was used to perform a 4x4 indentations grid in a random area of the PcBN material. The indenter was pressed into the selected sites with a constant penetration rate of 10 nm/s to a maximum penetration of 1000 nm or as mentioned before until reach a maximum applied load of around 650 mN. The penetration was held constant for 30 s at maximum penetration depth to diminish the creep effects at the onset of the unloading process and then unloading was performed at the same rate.

The calibration of the tip geometry has been done by means of the indentation of a standard material (fused silica sample) with a well-known elastic property. The reason of using this material is because it is homogeneous, it does not present pile-up mechanism and because of its mechanical properties are well characterized.

From these first 16 deep indentations the hardness and the elastic modulus of the composite material could be determined. And the study for the ISE could be developed.

From the results of the ISE study is observed that P/S^2 becomes independent of the indenter penetration as the latter gets deeper than 200 nm as it is depicted in **Figure 46**. On the other hand, lower values of penetration results are highly affected by ISE or scale effect (mainly related to the presence of the roughness effect between the TiN and the PcBN reinforcement particles). Because of this fact, penetration depth for the low-load nanoindentation has been established at a value of 200 nm due to at this penetration depth, the residual imprint can be confined inside the PcBN particles and evaluate the anisotropy effect for the reinforment particles.

For the whole grid indentation analysis of the composite material, big arrays of low-load indentation have been performed. Three arrays of 20 x 20 and one array of 10x10 indentations were programmed. The small matrix and two out of the three big arrays were done completely and the third one was interrupted due to technical problems with the equipment when only 143

imprimpts where done (see **Figure 27**). This means that finally 1043 residual indentations at a maximum penetration depth of 200 nm were done randomly in the PcBN inset (see **Table 4**).

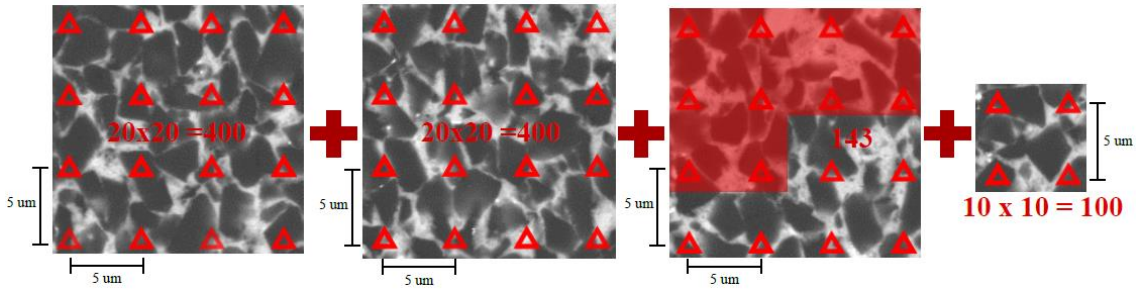

Figure 27 - Nanoindentation arrays performed for the massive nanoindentation analysis.

Table 4 - Summary of indentation experimental details.

	Nº indents	P* $_{max}$ (mN)	h_{max}(nm)	S (mN/nm)	$\tau_L/ \tau_H/ \tau_U$ (s)*
cBN + TiN	1043	32.7 ± 5.4	200	0.32 ± 0.04	60/60/10/

* $\tau_L/ \tau_H/ \tau_U$: Loading/Holding/Unloading segment

Every 200 indentations, tip shape and in particular the contact area was contrasted with a fused silica standard. The distance between imprints was kept constant and equal to 5 µm in order to avoid any overlapping effect between them. Such conditions guarantee that each individual test could be treated as an independent statistical event (44).

The statistical treatment explained in the Massive Nanoindentation section was used in order to obtain the parameters of every one of the single phase minor Gaussian distributions that define the global one. CDF scope was chosen in front of PDF one because of being considered easier to perform by analytical means. The function used to minimize the error between experimental and theoretical CDF's has been the following sigmoidal error function as:

$$CDF_{Composite-Fit} = \sum_j \frac{1}{2} f_j \, erf\left(\frac{H-\mu_j{}^H}{\sqrt{2}\,\sigma_j{}^H}\right) \qquad \textbf{Equation 16}$$

Where H is the hardness measured for each of the single indentations, f_j the volume fraction for each of the *j* phases and μ_j, σ_j the mean and standard deviation obtained for the hardness of that specific j phase. The fitting process was programed in *Origin Lab* 9.0 software to be completed when χ^2 tolerance was less than $1x10^{-15}$, with a final coefficient determination (R^2) value higher than 0.99. The massive nanoindentation study finishes supplying information about the mechanical properties (*H* and *E*) of each constitutive phase in the studied material.

2. Machining and testing of real micro-sized samples.

Four micro-pillars of 3µm diameter were machined by means of ZEISS Neon 40 FIB/FESEM equipment. The fabrication of this geometry has to be done in two different steps; one for the coarse opening of a big crater in the material with the pillar located in the center and the other for the fine polishing of the geometry walls.

For the later micro-pillar loading with a flat punch indenter tip is necessary that the pillar is sufficiently released and far from the surrounding material. If the crater in which the pillar is located is not broad enough, the tip will not be able to apply the force without touching the bulk material modifying the stress-strain curve. In order to avoid this annular milling procedure was followed. It uses a radial patterned shape generated by FIB software restoring the ion probe in the shape of an annulus. Different patterning's can be generated with bitmaps image files that are used to control the different machining conditions for every one of the treated pixels.

In the present case input for the annular milling FIB software was a bit-map obtained from a micrograph with a resolution of 125 nm/pixel. There four craters with an outer radius of 10 µm and an inner radius of 2µm were machined with the following control parameters: multipass milling[1], constant dwell time/pixel of 200 ms/pixel for every point from Refs. [2,10] and a milling current of 30KV and an intensity of around 2nA for the coarse milling while for the fine milling the intensity was changed to be around 500 pA in order to clearly distinguish the final PcBN microstructure. The whole machining process for the 4 pillars took about 20 hours of FIB erosion (17 rough machining + 3 polishing).

Annular milling is known to change the structure and composition of the samples. For example a 30 kV annular mill has been observed to create an amorphous layer of material of approximately 30 nm of thickness and implantation of significant amounts of Ga^+ up to 50 nm into the surface (45). Because of this reason, a final stage of preparation where a low energy "clean up" is performed. Normally this final polishing is done at lower voltages (5kV or less) but with PcBN this was not possible, so the final polishing parameters were: single pass milling, constant dwell time/pixel of 240 ms/pixel for every point from Refs. [1.7,3.5] and a constant milling current and intensity of around 30KV and 500pA, respectively.

[1] Multipass milling refers to the machining procedure in which the ionic beam goes over all the previous machined rings before machining a new one. This was an extremely time consuming procedure in which time increases factorial. However, this procedure was needed to achieve deep penetrations of the ion beam with high currents and acceptable machining quality.

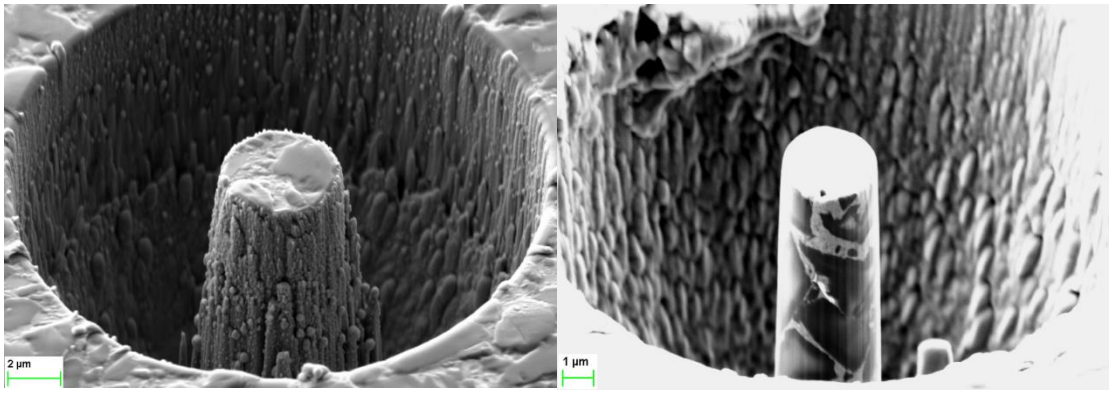

Figure 28 - FESEM images of a pillar before and after the final polishing step.

Before milling any cantilever into the material an accurate selection of which were the correct places to make them was needed. The best places to realize the cantilevers where those in which a big cBN grain was located and a cantilever could be done in a relative position so that the notch went through the interface between the big grain and the matrix. Once the place was determined, the fabrication could start.

The fabrication of cantilevers is also a process where a compromise between finishing quality and operation time had to be found. This is why depending on the desired result different cutting conditions were used:

c) Fast Milling: Used when the finishing of the surface is not so important and when is necessary to remove big amounts of material without spending a lot of time:

[30KV 2 nA 2 layers Mill for depth: 25 µm]

d) Fine milling: Specially used for the faces where a bad surface finishing could influence strongly in the measured results. Is important that these face are exactly with the desired geometry.

[30KV 500 pA 1 layer Mill for depth: 25 µm]

e) Notching conditions: no notching conditions were tested because of the impossibility separating the cantilever properly from the rest of the material.

[No DATA]

For every one of the steps involved in the fabrication of micro-cantilever the operation parameters were clearly presented in **Figure 25** and described below:

Steps 2, 3 and 4. Fast milling condition// Sample ⊥ FIB.

Steps 5 and 6. Fine milling conditions // Sample ⊥ SEM.

Step 7. Notching Conditions // Sample ⊥ FIB.

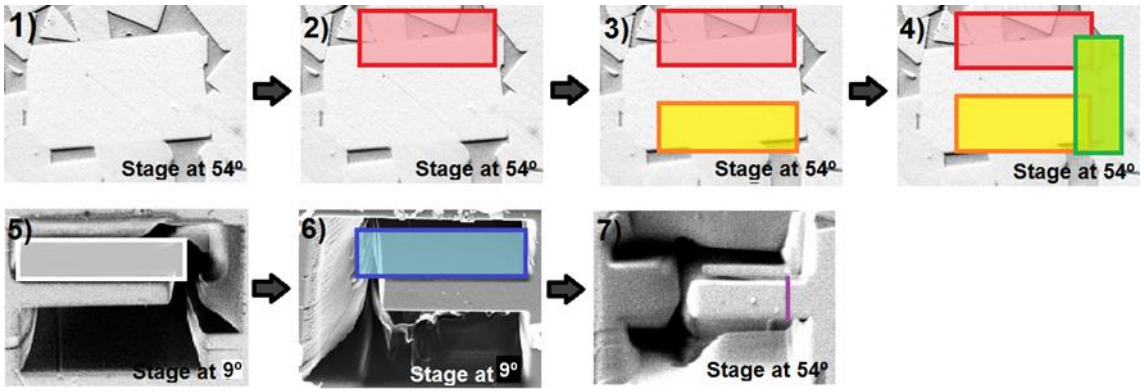

Figure 29 - Step sequence followed for the machining of cantilevers.

The desired geometry for the machined cantilevers were the one shown here below:

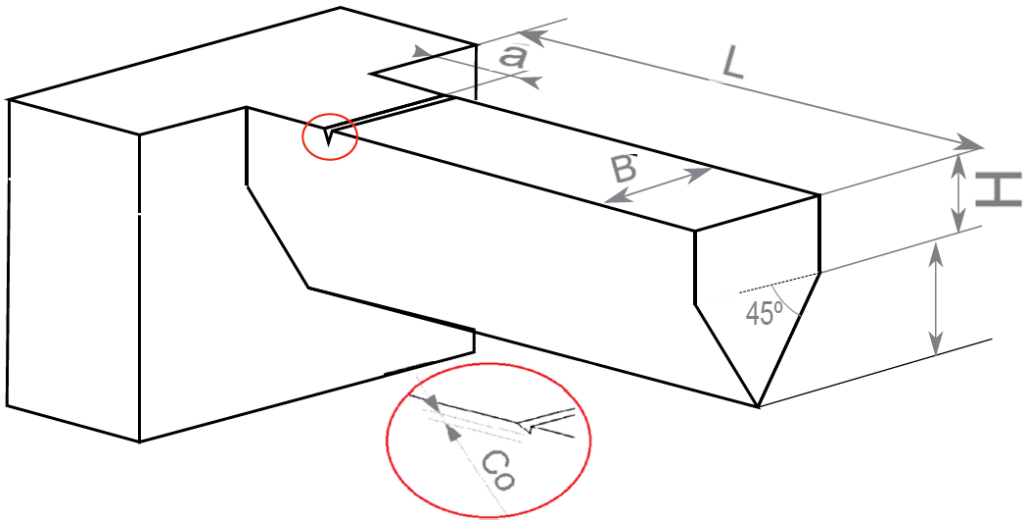

Figure 30 - Ideal geometry of the machined cantilevers.

Table 5 - Measures for an ideal cantilever. $c_o \approx 250$ nm.

Ideal Cantilever	L [µm]	B [µm]	a [µm]	H [µm]
Objective	9	3.5	Variable – 1.5	2

However, in the end Zeiss Neon 40 FIB ended to do not be enough powerful to build successfully PcBN cantilevers. Ga^+ ions do not have enough mass in order to achieve the required momentum that would permit a good machining. Steps 5 and 6 where impossible to perform within rational

timing and correct quality. A FIB with more energetic ions is required to perform PcBN cantilevers, so the micromechanical testing of these type of samples was finally dismissed. Anyways, the resulting cantilevers and the knowledge generated form this attempt of machining PcBN micro-cantilevers by means of FIB technique will be reported in the "Results and discussion" section.

FE Simulation Procedure

1.1. Search of the RVE: With the reconstructed 3D-microstructure obtained from tomography as input, an adapted and simplified method from the one described in section *Representative volume element (RVE) definition* was followed. The main objective of the whole process is to minimize the size of the simulated volume in order to minimize computation resources while maintaining enough size so that the simulated volume is representative from the macroscopic material.

Galli and Cugnoni method reported in Ref. (46) looks for the VOI with the minimum volume that ensures a constant phase vol. %. To do so, the method analyses several VOI of several sizes and in several locations until establishing the minimum size at which the Vol. % error condition in met. This VOI is denoted as the volume with size a_{ini}.

In this specific investigation the process followed to find the RVE was the following:

1. The reference Binder Volume % obtained from the whole tomographic reconstructed volume set as (100% VOI) is 28.1%.
2. From this reconstructed volume 9 volumes were created per each scale index, being the used scale index 80, 70, 60, 45 and 30 as it is depicted in**Figure 31**:

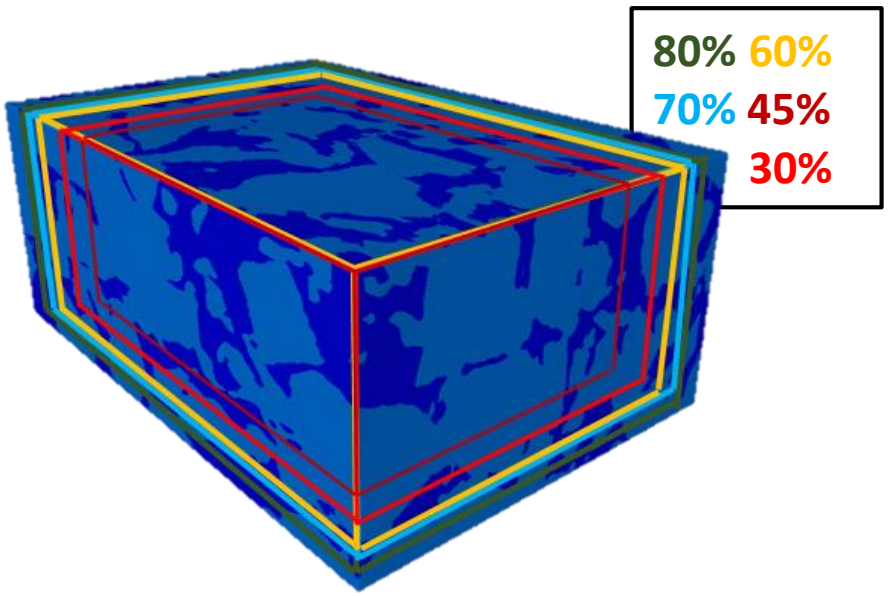

Figure 31 - Scheme showing one VOI for each of the analysed scale factor. Analysed volumes where located randomly within the volume but in this case were located all in the same corner to make size comparison easier.

3. Each of the nine volumes generated for each scale factor was places in a random position inside the tomographic reconstructed volume and its phase vol. % was analyzed through AVIZO 8.0 software tools. 45 volumes were analyzed giving as a result the data reported in **Figure 32:**

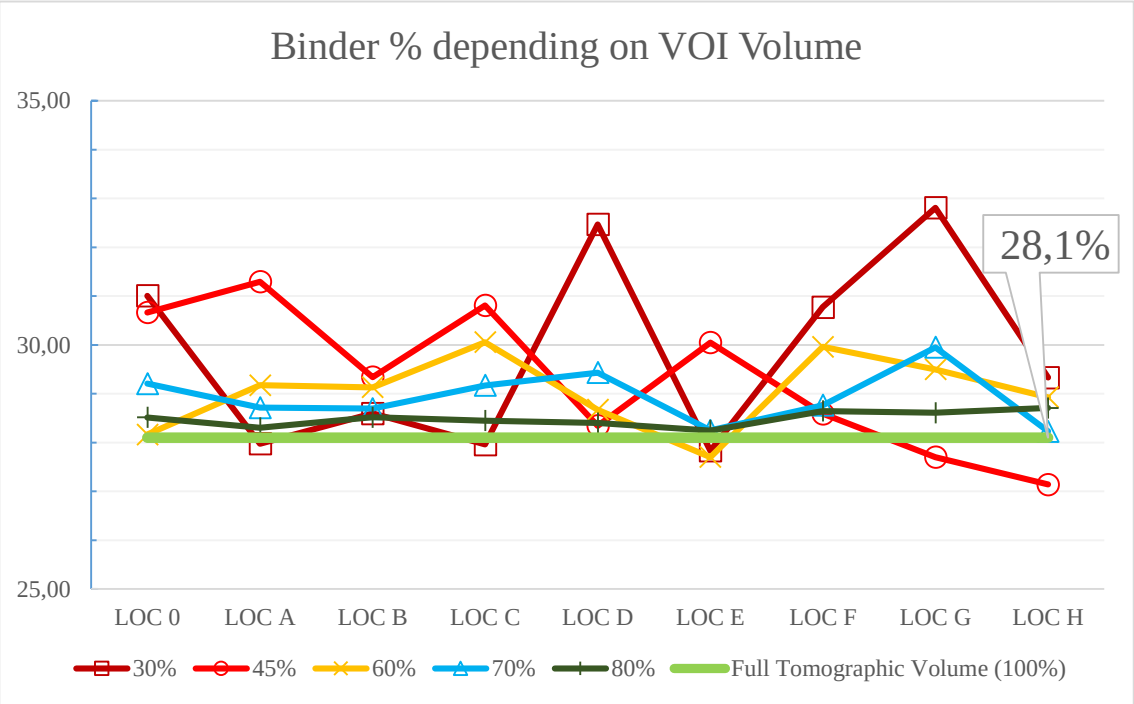

Figure 32 - Graph showing for the different VOI sizes and the different locations the Volume % of binder phase measured. The light green straight line can be considered the reference as corresponds to the bigger volume that can be analysed. It can be clearly seen how as smaller is the VOI biggest is the scattering of results.

4. Three convergence criterions where checked to decide where the binder volume fraction could be considered stable, and the most restrictive one was chosen to establish a_{ini} VOI. The minimum representative volume would be the one between the volumes that accomplish the following rule:

$$\textit{Statistical population amplitude} < 2\%$$

$$\textit{AND}$$

$$\textit{St. Dev} < 1\%$$

$$\textit{AND}$$

$$\textit{Volume \% Error} = \overline{Vol\%} - 28.1 < 1\%$$

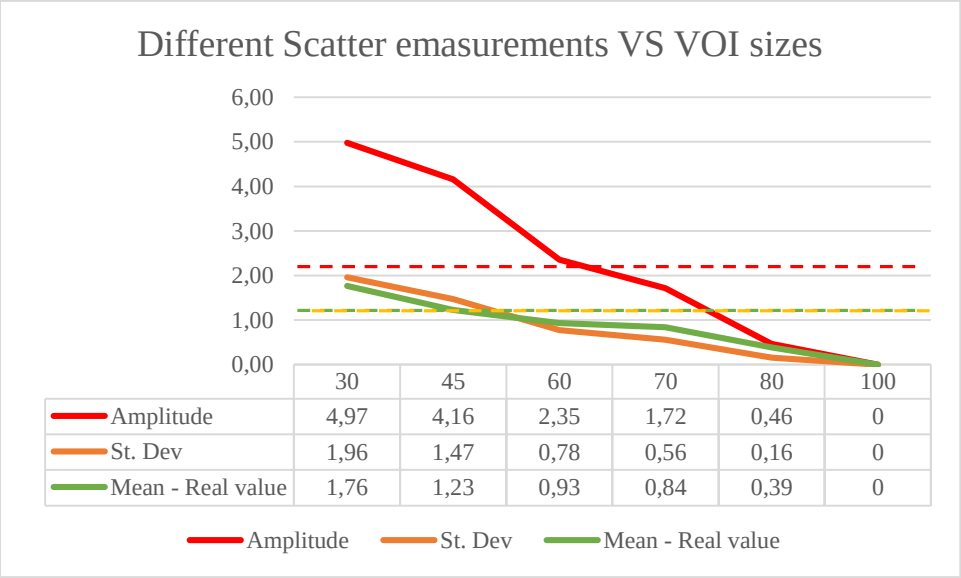

Figure 33- Graph showing the values reported by all the tested VOI for each of the stablished convergence criterions.From the graph it can be observed how the smallest tested volume that meets all of the "must have" criterions is the one with a 70% size of the original extracted volume.

5. All the following steps in order to perform the FES were held with a VOI 30% smaller than the original reconstructed tomographic volume.

1.2. <u>Generating the mesh:</u> Most of the times extracting a geometric model from 3D images can be complex, but in the other hand it may be used for :

- Visualizing boundaries of relevant features,
- Measuring with high precision the generated geometry, and
- Simulating physical properties on the reconstructed model.

The objective of this Master's thesis is to mechanically simulate a real microstructural volume of a PcBN composite material and to do so the generation of a geometric volume (a mesh in this case) is necessary. The traditional pipeline followed for mesh generation for volumetric data is shown below in **Figure 34**.

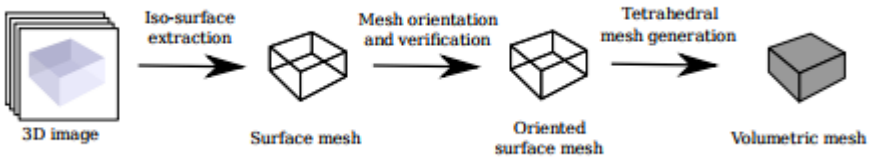

Figure 34 - The traditional pipeline for tetrahedral mesh generation from volumetric data (disregarding the volume and image pre-processing). Adapted from **(47)**.

As explained in Chemical and microstructural characterisation:**,** Avizo 9.0 software uses the labeled data as an in-put to create a surface, which can be later analyzed and used to obtain microstructural information of the material.

In order to generate the surface Avizo 9.0 performs a mesh of triangular elements over the outer voxels of each label. As in 2D imaging happens with pixels, in the generation of the mesh, as more triangles are included in the surface and smaller they are more detail and definition is achieved. In the first approach of generating a surface from the labeled reconstructed data Avizo 9.0 tries to replicate all of the complex geometries present in the real microstructure and all of the geometry inaccuracies introduced by the image processing and the tomographic reconstruction process, because of this the initial resulting surface contains over 6 million of triangles. Working with such a detailed surface would be computationally impossible in terms of data processing and of visualizations so the first step has to be the simplification of the surface.

In **Figure 35,** the difference between two simplification levels in the surface reconstruction for the cBN phase can be observed:

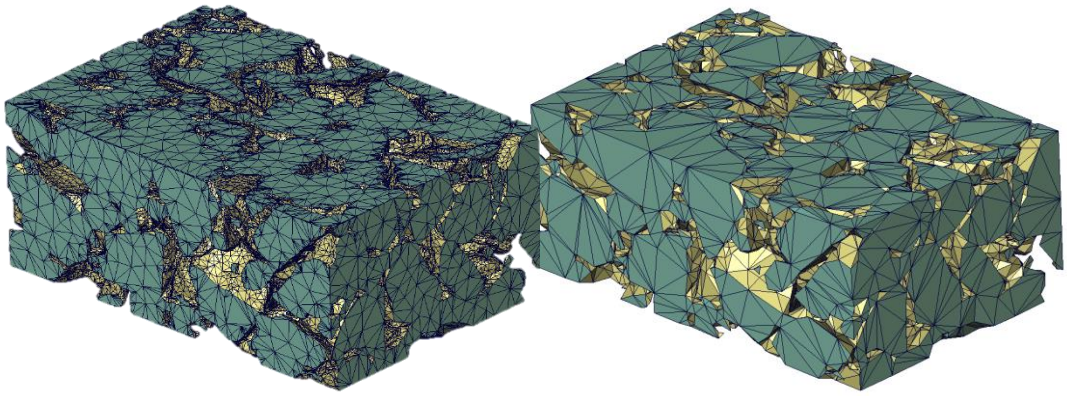

Figure 35 - Reconstructed surface simplifications the original generated mesh with more than 6M triangles is consecutively simplified and the quality of the generated surface in comparison to the original volume is checked. The surface in the right contains around 250k elements and still represents correctly the original surface, in the left side there is the example of an over-simplified surface (25k elements) where the triangles used are too big too keep a proper reconstruction of the original volume.

For the current simulation process, the surface used as the initial tetrahedral grid generator had 200k triangles. This resulted to be the best agreement between computation demands and geometrical quality of the surface.

Once the surface is created, the mechanical simulation cannot be performed yet, the surface is only a 2D geometry displayed in a 3D shape so it cannot be treated as a volumetric object with volumetric physical properties. A 3D mesh have to be generated from the generated surface filling the empty spaces inside the cBN grains or the TiN binder surface through mathematical algorithms that turn the triangles into tetrahedrons and fill the voids by iterative calculations.

However, the passing from surface to volumetric mesh is not always direct and is most of the times one of the most intricate problems in modelling and simulation process. The reason of this is that the mathematical process held for the transformation is highly sensitive to badly shaped elements, wrongly oriented, etc. Some considerations and verifications had to be done in order to obtain the desired 3D mesh:

- The surface mesh has to be always a **closed surface**. The polyhedral surface mesh bounds the simulation domain and an error of this type would lead to infinite volumes.
- **Orientation check**, microstructure of materials may have very complex surfaces with big orientation charges. When this happens the step from 2D to 3D-structures may be difficult, automatic and manual corrections must be done in the mesh so that critical errors do not appear.
- **Aspect ratio** of a triangle relates the length of its 3 segments, being one for an equilateral triangle and infinite for a isosceles triangle with its short side being 0. As smaller is the aspect ratio of the initial surface triangles more accurate will be the 3D mesh reconstruction and better quality will have the later simulation.

  In this Master's thesis, the higher aspect ratio allowed for the surface triangles was of around 24.92.

The checking processed was held manually and with the support of automatic verifications of AVIZO 9.0 until the tetrahedral grid generation was possible without reporting any error in aspect ratio, triangle orientation, etc.

The obtained mesh uses tetrahedral elements of the type (C3D4) with only 4 integration points per tetrahedron, located in each of the four vertex. This type of element is very stiff for structural simulations but it's simplicity makes it's calculation easier and a higher number of elements can be then included in the model. The final 3D tetrahedral mesh has around 800k tetrahedral elements, 550k corresponding to PcBN grains and 250k corresponding to TiN binder, giving as a result a binder volume percentage of 32% which is in good agreement with the previous microstructural analysis. The following grid shows the different steps from the 3D image data set until the 3D tetrahedral volumetric mesh as it is presented in the following table:

	3D image stack (AVIZO)	Labelled microstructural information (AVIZO)	FES Mesh (ABAQUS)
Isometrical		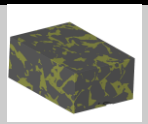	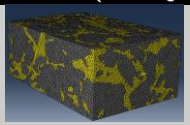
XY Plane	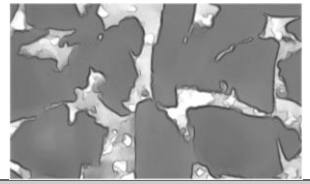	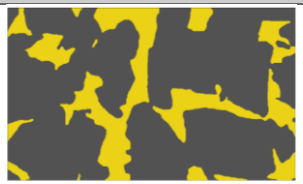	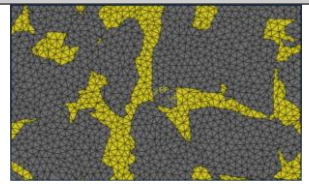
XZ Plane	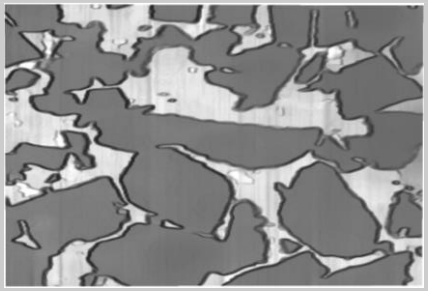		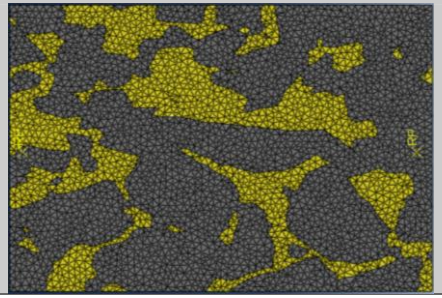
YZ Plane	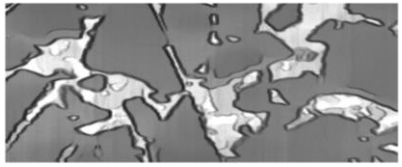		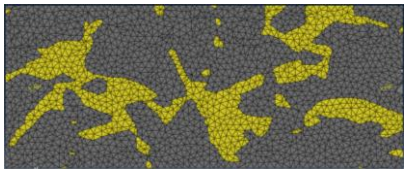

1.3. Mechanical simulation: Once the tetrahedral mesh is obtained it can be imported to ABAQUS software as a model and defined as an Orphan Mesh. The process followed in the ABAQUS workbench will be now explained following the same workflow that ABAQUS software suggests for developing a complete simulation.

1. The geometry that we are going to work with is the above mentioned tetrahedral mesh extracted from the centre of the tomographic reconstructed volume with a volumetric size of 70% of the initial reconstructed volume having final measures of (9.5x5.7x13.9 µm).

   The ABAQUS model is comprised by two different parts, the cBN grains and the TiN meshes and have been assembled considering a perfect interaction between them. Perfect interaction between particles and matrix does not allow slip between phases nor decohesion. Such condition was imposed through the *Merge/Cut* tool present in the *Assembly* module in ABAQUS . This instance forces the nodes in the interface to be common to both constitutive phases.

2. Every one of the orphan meshes imported in ABAQUS needs to have it's mechanical properties well determined. Both material have been modelled to follow an elastic + linear plastic mechanical behaviour. Elastic properties and yield strength were obtained from published press and for the plastic regime a nearly ideally plastic behaviour was stablished as:

Table 6 - Material properties set as simulation inputs.

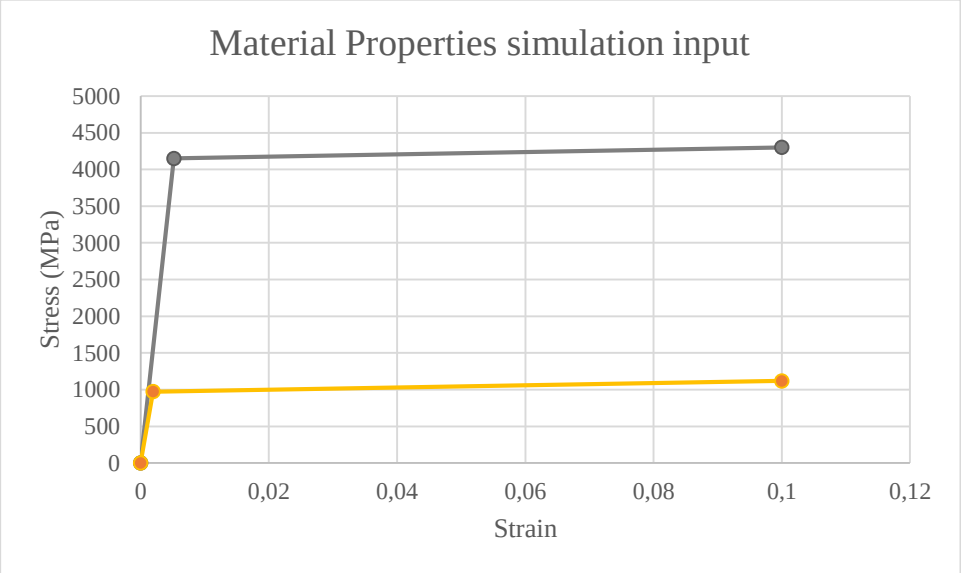

Phase	Young Modulus (GPa)	Poisson Ratio, υ (-)	Yield strength, σ_{yC} (MPa)	$\sigma_{10\%\ Plasticity}$ (MPa)
TiN	500 (48)	0.24 (49)	972.4 (50)	1118.3
cBN	798.4 (51)	0.12 (49)	4150 (16)	4300

Although this type of materials does not present such an ideally plastic behaviour, the solution of the mechanical system would not converge if it was not defined this way.

3. The simulation was run as a mechanical test that is held in time. And considers Step 0 as the initial conditions of testing and Step 1 as the final conditions. In this case, the applied boundary conditions were clearly depicted in **Figure 36**:
   a. One of the faces BC simulates the static plate of a compression test machine. All rotations (URX,URY,URZ) and the displacement in the axis of force application (UZ) are restricted to 0 from the beginning of the testing until the end (From step 0→1), as:

      $$UZ = URY = URX = URZ = 0$$

   b. The other face simulates the moving plate that applies the load, and is moving against the sample to compress it. A displacement in the force application axis (UZ) corresponding to the desired effective strain is imposed into the surface in order to study the mechanical response of the volume element.

In both cases, the displacement restrictions where indirectly applied to the faces of the tested parallelepiped through an intermediary reference point. To do so, each reference point was cinematically coupled to its correspondent face by restricting the displacement in the axis of strain application (z) and the rotations around the other two axis (Rot-x, Rot-y).

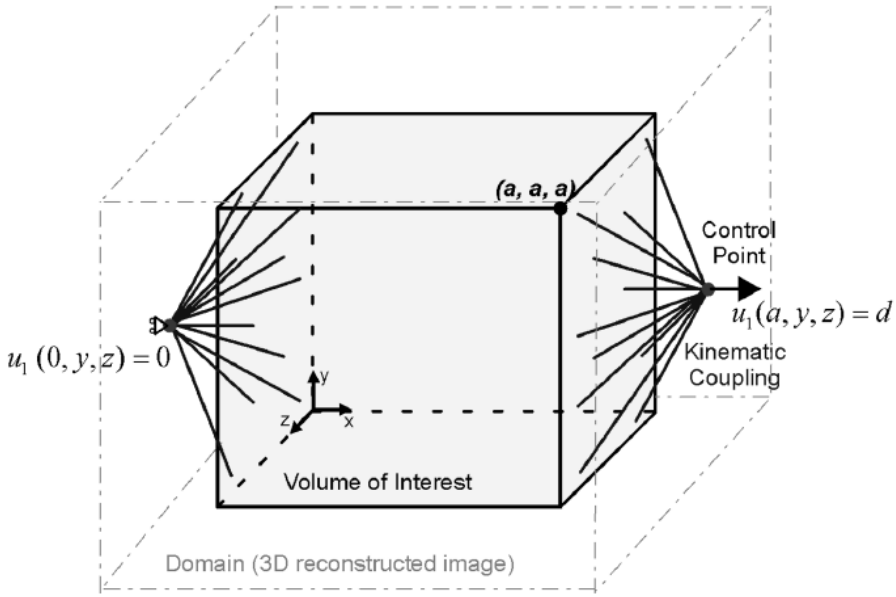

Figure 36 - Scheme of the BC imposed over the reconstructed volume. Observe how the BC are not directly applied into the parallelepiped faces but they are into control points cinematically coupled with the faces **(46)**.

Once all the boundary conditions are set and all the parts in the model are well defined the simulation is ready to be solved.

Results and discussion

Chemical and microstructural characterisation

Energy-dispersive X-ray spectroscopy (EDS)

Figure 37 show the EDS spectre for wide scanning area (General Spectre – See **Figure 22**) .

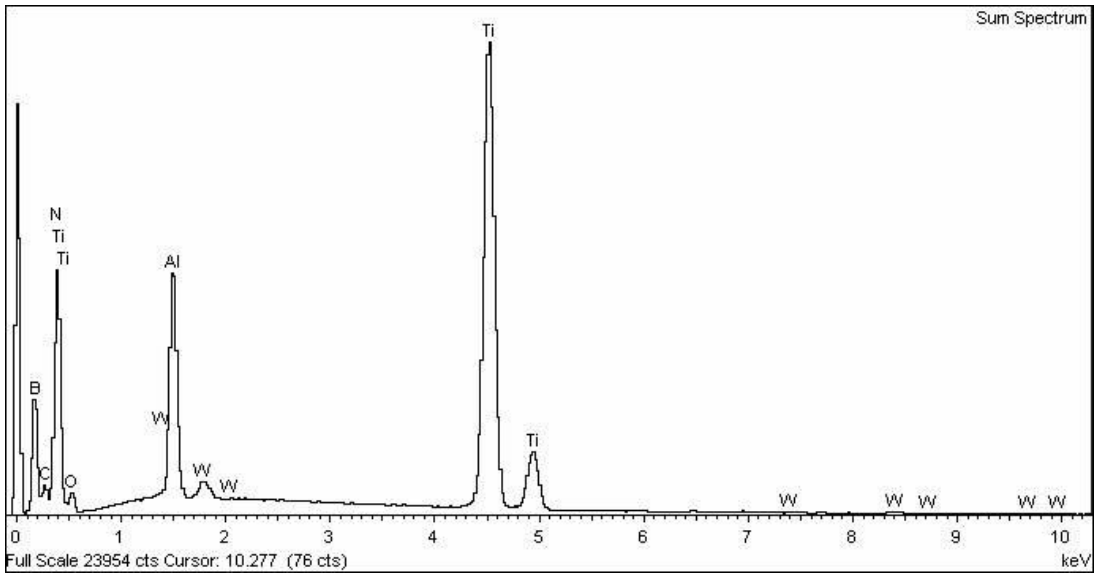

Figure 37. EDS spectrum taken from a wide scanning area of 20x30 µm.

The main elements that can be found are: Boron, Nitrogen, Titanium, Aluminium and Tungsten. These elements are in good concordance with the expected composition and with the commercial information supplied by Sumitomo Carbide. As a first approach, the existence of these elements in the spectres is justified from:

- B and N, from the cBN from the ceramic reinforcement particles.

- Ti from the ceramic binder, which is supposed to be TiN (according to commercial information).

- Al and O, are appearing nearly as residual elements in the composition and are assumed to be artefacts from the last polishing step. From further local EDS measurements, it can be seen that most of the Al and O appear in binder spots where OPAN may have remained in the dimples caused by differential polishing. Furthermore, Al and O appear in weight % of around ≈ 50% O close to Al_2O_3 weight ratio, which is around 47% O.

Aluminium in low quantities in the composition of the binder is also found because of the addition of aluminium in the sintering moment in order to enhance interface adhesion and wettability between cBN and TiN. Al cannot be added in high weight % because its excess is detrimental to the mechanical strength of the composite due to the poor hardness and is easy to cleave (52).

- W and C, are shown in the spectra with very low intensity because they may appear from the impurities of WC, of the base where the PcBN insert is assembled.

The more specific EDS analysis for spectrums (from 1 to 5) showed in **Table 7**, follows semi-quantitative composition results with a technique precision of 0.5 in weight percentage.

Table 7 - Chemical composition resulting from EDS analysis in the different studied localizations**.**

Weight %	B	C	N	O	Al	Ti	W
cBN dot (Spect. 1)	46.8	-	48.8	-	1.3	3.04	-
Binder dot (2)	-	-	25.3	-	-	74.7	-
Binder dot (3)	20.7	9.9	35.9	-	2.7	20.2	1.62
Binder 4	15.’	7.9	24.8	9.6	7.6	34.2	0.91
Binder 5	25.3	6.8	27.0	5.6	5.5	30.8	-

The obtained results are in good agreement with the existence of cBN and TiN as main constituents of the studied material. And the obtained spectrums are clear enough (**Figure 38** and **Figure 39**) to consider the results as reliable.

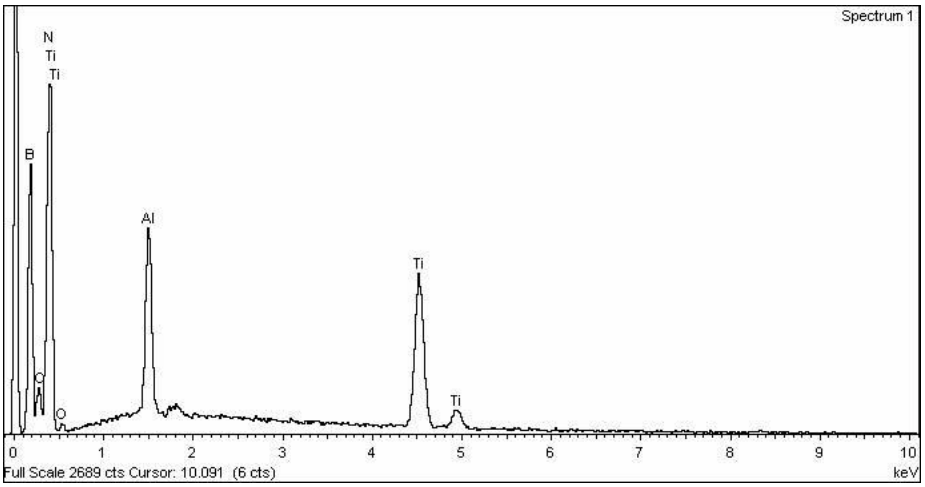

Figure 38. EDS spectrum of a boron nitride position showing a high signal for the elements of B and N.

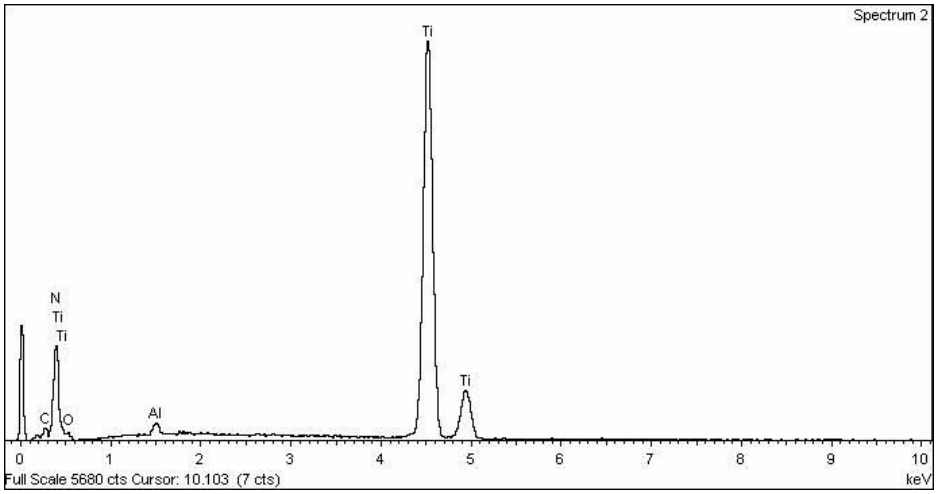

Figure 39. EDS spectrum of a titanium nitride point showing signals of Ti and N.

2D microstructural characterization

Three different methodologies have been followed to determine microstructural parameters of the material;

Table 8 compares all the results of the different characterization processes.

	Grain size ($\overline{d_{cBN}}$)		**Vol.% Binder**		**Mean free path (λ)**		**Contiguity (C)**	
	Grain ($\overline{d_{cBN}}$)	**size**	**Vol.% Binder**		**Mean free path (λ)**		**Contiguity (C)**	
	Mean (µm)	St. Dev.	Mean	St. Dev.	Mean (µm)	St. Dev.	Mean	St. Dev.
Linear intercept	1.62	±0.19	40.92	5.43 ± 5.43	1.22	± 0.16	0.40	± 0 03
Method	2.71	±0.18	31 05	0.73	2.04*	± 0.11*	-	-
2D particle analysis	2.71	±0.18	31 05	± 0.73	2.04*	± 0.11*	-	-
3D tomography	-	-	28.10	-	0.87 µm	0.62		

Table 8 - Comparative table of the main microstructural results for the three followed methods**.**

*2D particle analysis method is not able to determine by itself a value of "Mean free path". The showed result is obtained by means of using equation $\lambda = \frac{v_{TiN}}{v_{cBN}} \bar{d}_{cBN} \frac{1}{1-C}$ with contiguity value obtained by linear intercept method and all the other values from 2D particle analysis method.

Big differences have been found between the results shown by the three methodologies. The precision of each methodology is supposed to be higher as higher is the number of dimensions used. For example in the case of linear intercept methods situations as the one showed in **Figure 40** may lead to underestimation of the grain size and over estimation of the Vol. % Binder. This is in goo agreement with the obtained results because linear intercept method is the technique that shows smaller particle size and higher binder content. Moreover, methodologies based in the analysis of 2D images are highly dependent on the way that particles appear in the surface and is possible that very big particles appear to be small in the surface.

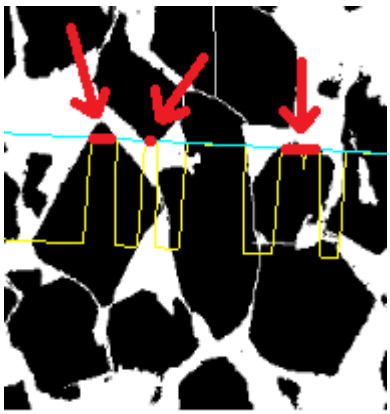

Figure 40 - Possible artefacts origin in linear intercept method.

3D microstructural characterization

Because of these drawbacks and to avoid other problems related to the partial analysis of 2D-dimensional micrographs, the results obtained from the 3D characterizations are the ones that are considered for all the following processes.

In the following paragraphs all the microstructural information that could be extracted from the treatment of the 3D reconstructed volume is going to be detailed.

The first and most obvious result from tomographic reconstruction analysis is the qualitative observation of the real microstructure in a digital format that you can observe from any point of view. **Figure 41** and **Figure 42** show the obtained reconstruction:

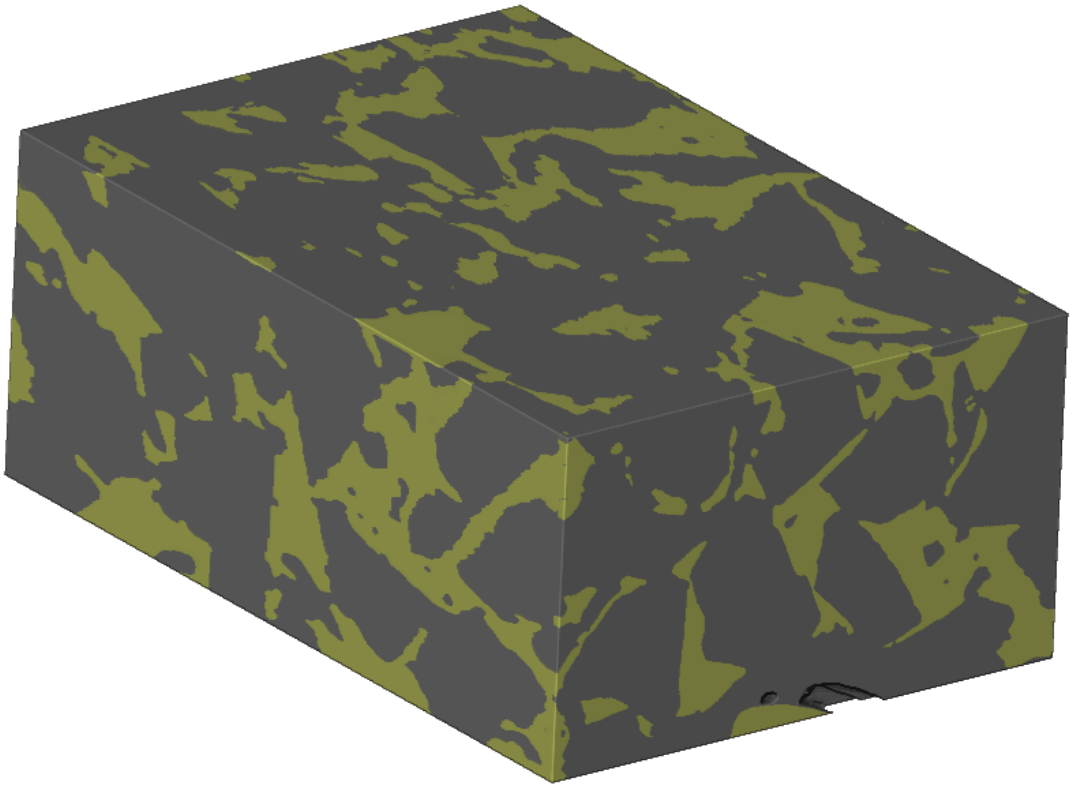

Figure 41 - Reconstruction by FIB tomography of BN2020 PcBN composite material.

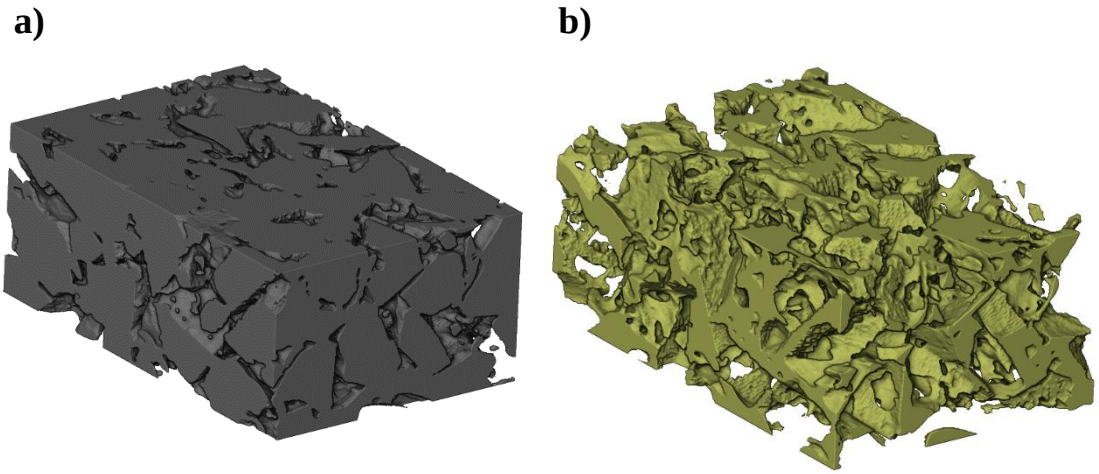

Figure 42 - Reconstruction by FIB tomography of BN2020 a) cubic boron nitride phase b) binder phase.

As can be observed in the reconstructions, there is a complex network of TiN through all the empty space between the cBN grains. TiN matrix forms a fully connected network that perfectly surrounds the cBN grains. This microstructure morphology enhances direct loading transference

from matrix to reinforcement and allows the composite material to reach mechanical properties that take advantage of good features from both of the phases mechanical performance.

Volume fraction of each of the phases existing in PcBN can be measured directly attaching a *materials statistics* module to the thresholded labels data in AVIZO 9.0. This module counts how many voxels are assigned to each o the labelled regions obtaining very accurate measurement of the volume fraction, see Table 9.

Table 9 - Summary of phase content results from the 3D microstructural analysis

		Volume (%)	Weight (%)
υ_{TiN}	Binder	28.10	37.16
υ_{cBN}	Reinforcement	71.89	62.84
υ_{Voids}	Voids	0.02	-

The volume of the reconstructed tomographic volume is approximately 10.6x6.4x15.6 µm = 1058.3 μm^3. Assuming that PcBN particles present a spherical shape with a diameter of around 2.71µm (measured by 2D particle analysis), it is obtained that the reconstruction volume contains approximately 100 cBN grains.

Because of raw data was acquired from FIB, which is a technique that supplies a big stack of hundreds of images, an easy measure of sample homogeneity can be done by measuring the volume of binder for every slice by doing a 2D image analysis. This indicates how the vol. % varies along *z*-axis in the tomographic volume.

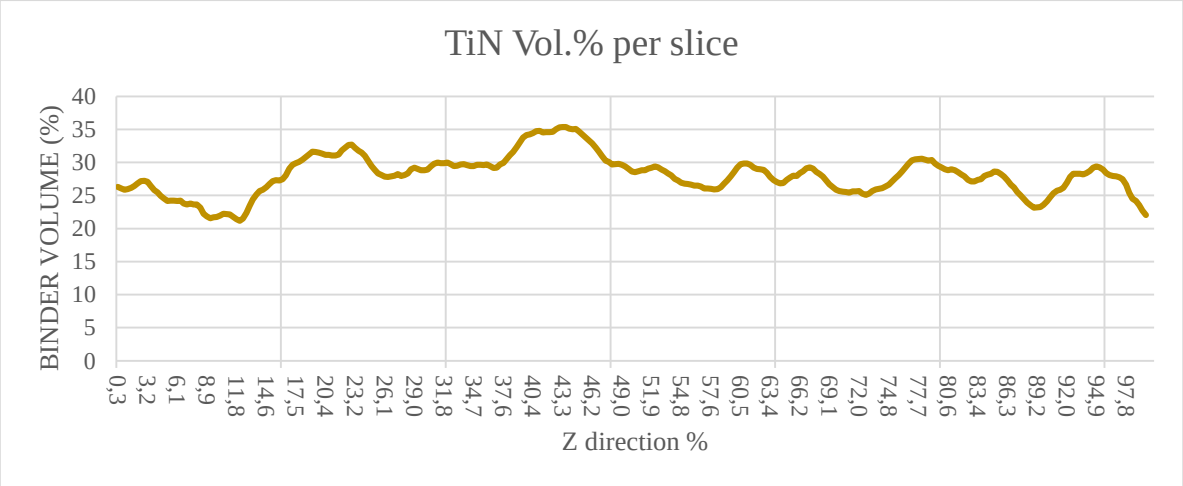

Figure 43 - Variation of binder volume percentage through Z direction.

Binder distribution can be considered quite homogeneous, having a mean value of 28.18 % and a standard deviation of around 3%. This distribution along Z axis is depicted Figure 43.

Anyways, the best way to analyse how is the binder organized in the composite material and which is exactly its morphology is through the skeletonization process. Skeletonization is an image processing technique that gives information from the geometry and topology of a complex shape by means of a shape simplification. Skeletonization simulates an erosion-like process into a shape deleting iteratively points from the shape boundary until obtaining a one-point thick curve. In **Figure 44** the obtained skeleton for binder topology is shown:

AVIZO 9.0 software offers direct measures from mean free path of the binder phase when an

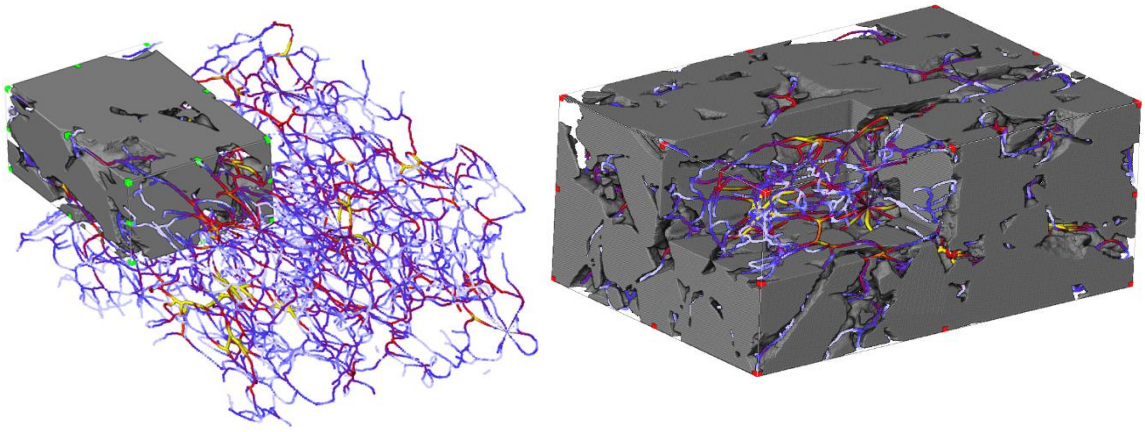

Figure 44 - Skeletonization of the binder shape**.**

skeletonization is performed. Mean free path could correspond intuitively to the mean length of the straight lines that could be gone over through a binder section without hitting any reinforcement grain. Imagining for example a pultruded composite rod, the binder direction that goes parallel to reinforcements could be defined as a maximum mean free path, while the one that goes perpendicular to the reinforcement would be the minimum mean free path. When the skeletonization is performed, both measures are related to skeleton length and skeleton thickness respectively. These are one of the most precise measures that can be made from binder mean free path in a composite material as they are three dimensional measurements. As 2D measurements does not differentiate between maximum or minimum mean free path. An average mean free path has to be calculated to compare 2D and 3D mean free path values as it is depicted in **Figure 45.**

λ_{Max}	λ_{Min}	λ_{Mean}
0.87 µm (St Dev.: 0.62 µm)	0.087 µm (St Dev.: 0.06 µm)	0.48 µm (St Dev.: 0.59 µm)

Figure **45** shows a summary of the results obtained from the whole microstructural study previously explained.

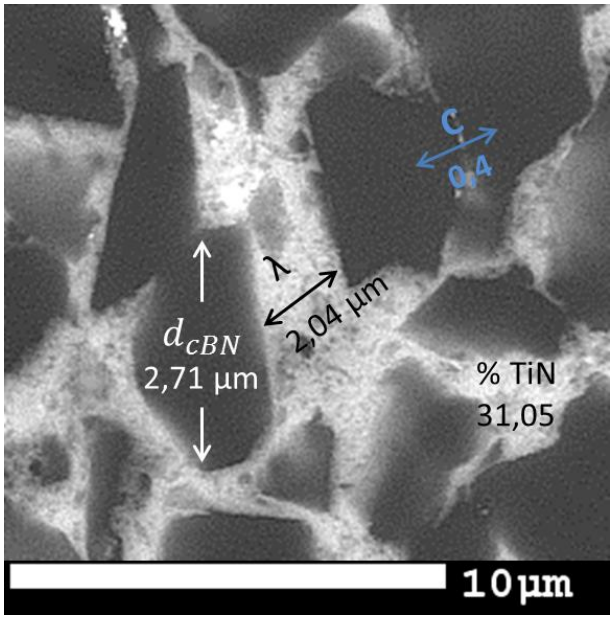

Figure 45 - Resume of the microstructural parameters determined by 2D particle analysis method.

For the case that we are studying the most important influence of microstructural parameters is not in mechanical properties, as long as different grades are not being compared mechanically from this point of view. The main influence of microstructure in this Master's thesis is:

- The RVE size that will have to be used in order to consider the FE simulation representative of the macroscopic behavior of the material.
- The massive nanoindentation testing conditions necessary to distinguish between each constitutive property of each phase separately (without influence of the other phases).

Mechanical characterisation

Indentation size effect (ISE) study

The realisation of deep indentations with continuous monitored stiffness and load has allowed to perform a study of the ISE that permits a better discussion and validation of the parameters obtained by the nanoindentation technique.

The ISE study is justified because of the fact that mechanical properties, such as flow stress or hardness in several mechanical tests are size dependants (53). This dependency becomes more obvious when the size and scales becomes significantly small. The observed tendency in the

mechanical properties of materials when going into smaller scale is an inverse relationship, showing stronger mechanical properties as smaller is the region of interest (ROI). In reference to indentation testing, the phenomenon where the indentation hardness increases with decreasing size is called ISE.

One of the most accepted focuses for explaining ISE is the one that relates deformation mechanisms with their specific activation volumes (V*). This point of view, allows relating the different mechanical properties measurements with physical changes that may happen in the material. This is obviously in contradiction to the classical continuum mechanics theory in which material properties are the same for every differential of volume of the material. So, although continuum mechanics are useful in some contexts when going into complex materials systems or smaller scales they are not enough.

The correct understanding of the ISE in the material that wants to be studied is critical if reliable mechanical properties measurements are wanted to be obtained. The complete comprehension of ISE could lead to the possibility of comparing mechanical testing at different scales that nowadays cannot be successfully understood. The extrapolation between nano and macro-mechanical properties is still not solved, and improvements in this field could help in the work with multi-scale materials design. In contrast, nowadays is common to find commercial documents that compare nanoindentation hardness results with macro-Vickers hardness results when the difference of hardness for the same material tested at these different conditions can be of more than 100% (54).

In the case of the studied material and the followed experimental procedure, the most important question that the ISE study has to answer is: at which penetration depth the nanoindentation technique is able to differentiate the mechanical behaviour in terms of hardness for each constitutive phase?

In order to answer this question, 15 instrumented indentations were held up in the Nanoindenter XP equipment from MTS, up to a penetration depth of 1000 nm or until reaching a maximum applied load of around 650 mN. In this way, possible ISE or tip defect interactions were evaluated by plotting the ratio between applied load and stiffness squared (P/S^2) as a function of the displacement into surface as it is depicted in **Figure 46**.

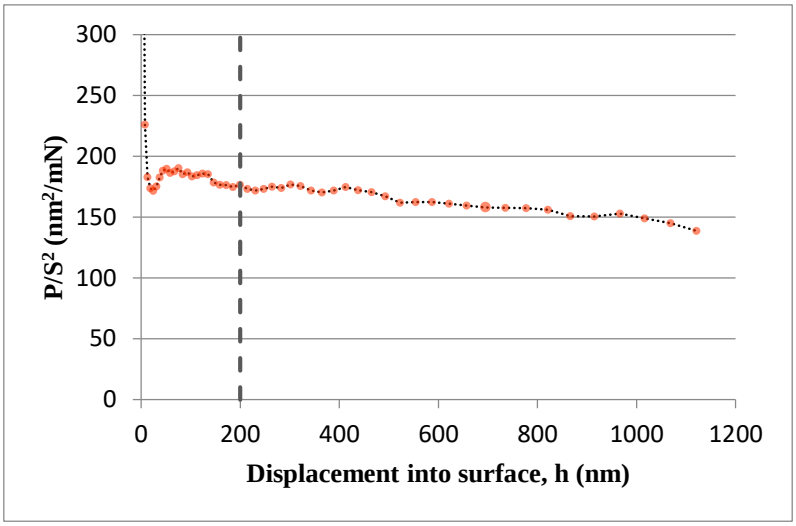

Figure 46 - P/S^2 ratio against displacement into surface for the imprints performed at 1000nm of maximum displacement into surface.

By studying this parameter, the results are independent from the contact area, the tip calibration as well as the surface effects (mainly related to the roughness generated during the polishing process). And as it may be seen from the resulting graph, P/S^2 data starts to be independent of indenter penetration as the latter gets deeper than 200 nm. On the other hand, indents with smaller penetration depths show very big affectation by indentation size effect and scale artefacts.

Another consideration that must be discussed is the fact that the ISE study is being done for the properties of the composite material. The indentation experiments for the ISE study have indentation depths that lead to consider the heterogeneous material as a material with homogenised properties.

The scale effects and artefacts that may affect indentation results are different for every one of the different phases present in the material. It can be said that soft materials are relatively more influenced by ISE than hard materials, showing a proportionally wider range of hardness from micro testing to nano testing (53). This fact makes the TiN matrix to be the most restrictive material in the sample, if reliable hardness measurements are needed the testing must be held under the conditions imposed by the most restrictive phase. A penetration depth of 200 nm was considered to be the penetration depth that met the compromise between: obtaining deep indents free of size effect artefacts and shallow indents representative of every one of the single phases.

Nanoindentation – Composite Hardness

The main results extracted from the deep indentations tests concern the mechanical behaviour of the material as a composite, and the contribution of all its phases is observed at the same time. Table 10 summarizes the two main determined parameters.

Table 10 - Mechanical results for deep nanoindentations (h = 1000nm).

Deep indentations results → Composite Material porperties	
Composite Hardness (GPa)	**Composite Elastic Modulus (GPa)**
52.93 (St. Dev: 7.35)	850.2 (St. Dev.: 160.7).

From the first array of 16 deep indentations performed at 1000 nm of maximum displacement into surface, the hardness and elastic modulus of the material as a composite system were obtained. The following figures show the results obtained from this first nanoindentation batch performed at the micrometric length scale:

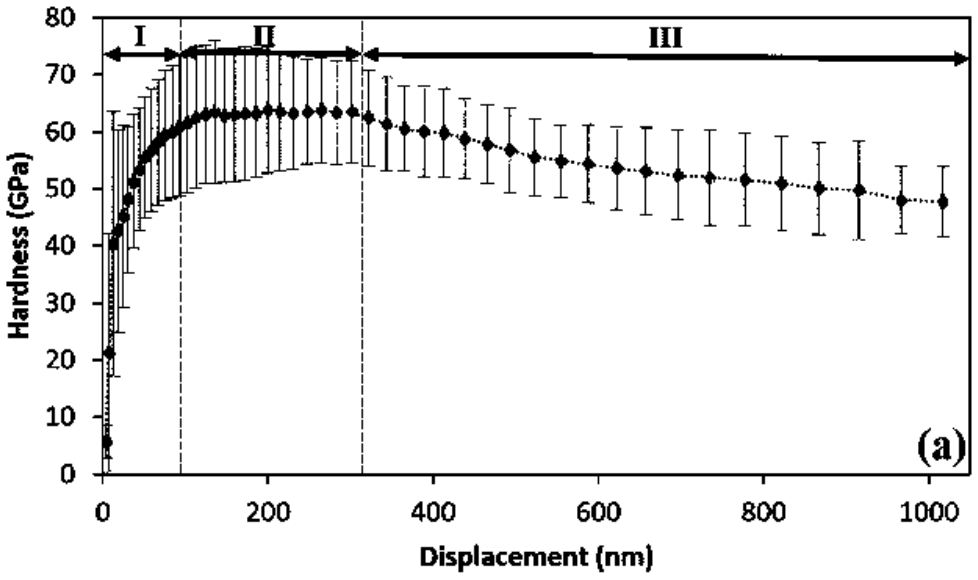

Figure 47 - Micromechanical properties evolution versus displacement into the surface: Hardness. (Composite material curve).

The presence of a stabilization regime in the case of hardness determination can be discussed; even at penetration depths of more than 750 nm the hardness measurement seems to decrease as the penetration increases. This behaviour can be due to the interaction between elastic strain field with the cBN hard particles and also with the TiN ceramic matrix, making difficult the hardness measurement to stabilize.

The observed behaviour for the deep indentations, the hardneess vs. displacement curves allowed us to discriminate three different regions. In region I, during the first nanometres of contact, the hardness values are not precise being overestimated (reaching values of 60 GPa) and showing big scatter. The behaviour in this first region could be attributed to scale effects, mainly related to superficial roughness between the ceramic binder and the reinforcement particles as well as the tip defect. Region II could be described as a plateau between 100 and 300 nm of penetration depth where the hardness stabilizes around a value of 64 ± 1 GPa. In this range, the plastic flow generated during the indentation process is approximately 7 times the maximum penetration depth, for the penetrations involved within the plateau, all the plastic flow could be considered to be confined inside either the cBN grains or TiN binder showing specific features in the test curves. The high hardness value shown in this stage can be related to cBN particles. Finally, in stage III plastic flow is bigger than particle size and it starts to interact with the ceramic TiN binder, accordingly the curve decreased moderately.

So, as it can be observed in this region, the composite hardness does not present an homogeneous value that could be considered exactly the composite hardness. However, a progressive decrease in the hardness scatter at the highest depths allows to approximate mean hardness values for the composite with acceptable precision. The average hardness of the PcBN composite is of 52.9 ± 7.35 GPa with averaging distance from 500 and 900 nm of maximum penetration depth.

No published articles that reported nano-hardness for PcBN composite materials of the same characteristics of the current material have been found. All the reported hardness are not tested in 70% cBN/30% TiN material and moreover, they correspond to Vickers “macro” indentations (showing lower hardness values).That is why the discussion of the obtained value of around 53 GPa has to be done in a different way than direct comparison with bibliography results.

In this sense, just as a qualitative measure, and an indicative comparison, the result will be compared with the value approximated by the nano-hardness of each phase applied to the rule of mixtures as it is presented below:

$$H_{Composite} = f_{TiN} \cdot H_{TiN} + f_{cBN} \cdot H_{cBN}$$

$$H_{Composite} = 0.3 \cdot 21^{*} + 0.7 \cdot 70^{**} = 55.3 \text{ GPa}$$

* (55): Reported values for micro hardness of TiN

** (56): Thick film nanoindentation measurement without contribution of the substrate

By comparing this first approach with the composite material, the hardness obtained from the deep nanoindentation tests (up to 1000 nm penetration depth), is obvious that the obtained value is assumable to be correct, and is within the expected limits.

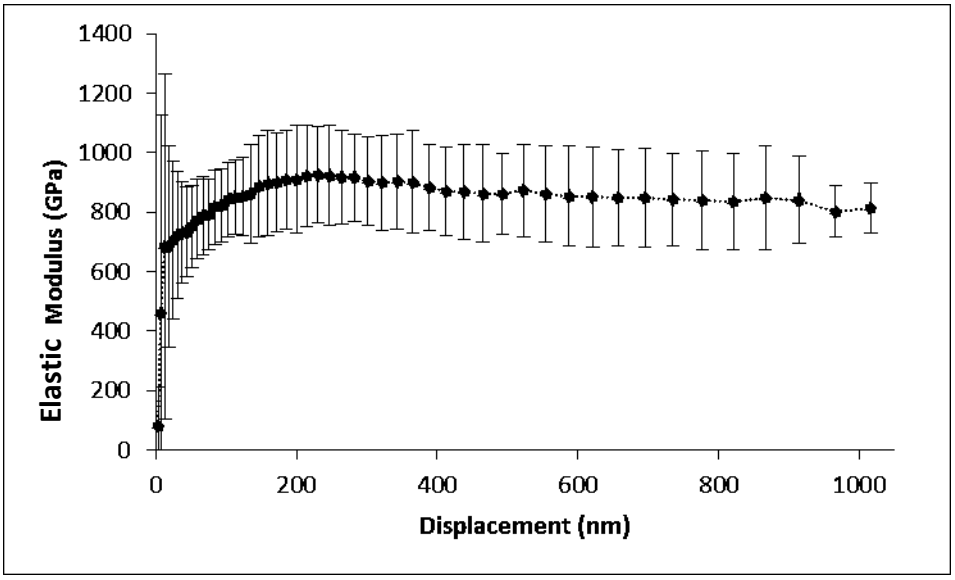

Figure 48 - Micromechanical properties evolution (elastic modulus) vs. displacement into the surface for the composite material.

In the case of the elastic modulus there is a stabilization of the mechanical property with the increase of displacement into surface. Moreover, there is a big difference in the scatter of measurements after a penetration depth of around 900 nm, showing how at deeper indentation depths the property may be stable around the value of 850 ± 161 GPa. Because of the same reasons explained for hardness, direct comparison with bibliography cannot be done so a first qualitative approach will be done by means of the rule of mixtures for the elastic modulus as reported below:

$$E_{Composite} = f_{TiN} \cdot E_{TiN} + f_{cBN} \cdot E_{cBN}$$

$$E_{Composite} = 0.3 \cdot 500^{*} + 0.7 \cdot 850^{**} = 745\ GPa \text{ (St. Dev.: 110 GPa)}$$

* (48): determined by means of spherical nanoindentation.

** (57): Determined by means of berkovitch tip nanoindentation in bulk polycrystalline, and translucent *c*BN, manufactured by Sumitomo, Inc.

Due to the high dispersion in the elastic modulus results, the results from the experimental analysis and from the mixture rule approach are overlapped, and cannot be considered statistically different. However, the mean value of both measurements is of about 100 GPa, this can be caused by the experimental difficulties of determining elastic parameters of the material by means of

nanoindentation with sharp tips or because of the use of different techniques in the materials property approximation.

Massive nanoindentation results – Intrinsic Hardness of each constitutive phase

1043 nanoindentations where performed on the material following the method described in

Micromechanical testing **section** , with a maximum penetration depth of around 200 nm with the intention to determine the hardness for each constitutive phase. In order to check the ability to confine each nanoindentation test as a representative measure of the properties of each of the phases separately, FESEM direct observation was performed. **Figure 49** shows a representative indentation where the whole measure is taken inside a cBN grain (from a surface/2D scope). From the observation of the micrograph is possible to notice the fracture mechanisms induced by nanoindentation in the ceramic brittle particles, some cracks are generated in the surrounding area of the imprint (Marked by red arrows in **Figure 49**).

However, FESEM technique does not allow us to see how is each cBN grain under the visualization surface due to a 2D-image is directly obtained, see **Figure 49.** Furthermore, it is not possible to ensure that the whole stress field induced by the single test is completely contained in cBN grain, this noise factor is reduced by the performance a high number (>1000) of individual tests.

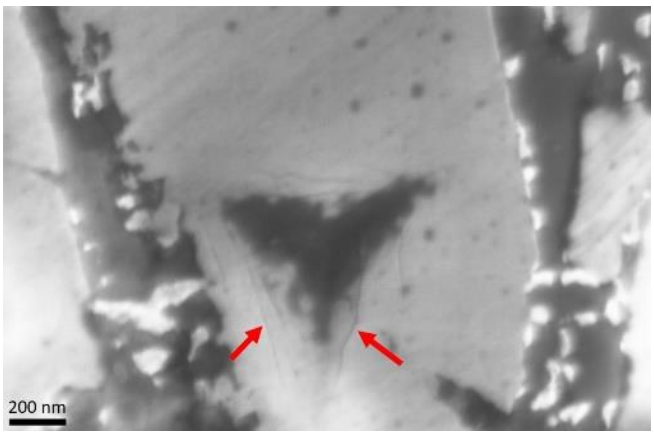

Figure 49 - Residual imprint at 200nm depth confined in cBN particles.

When all the instrumented indentations are performed, the hardness of each of the tested points can be extracted by analysing all the P-h (–load vs. displacement) curves data using the Oliver and Pharr method (28) (30) can directly be obtained. From the hardness obtained by using these equations, the hardness histogram can be represented as it is depicted in **Figure 50**.

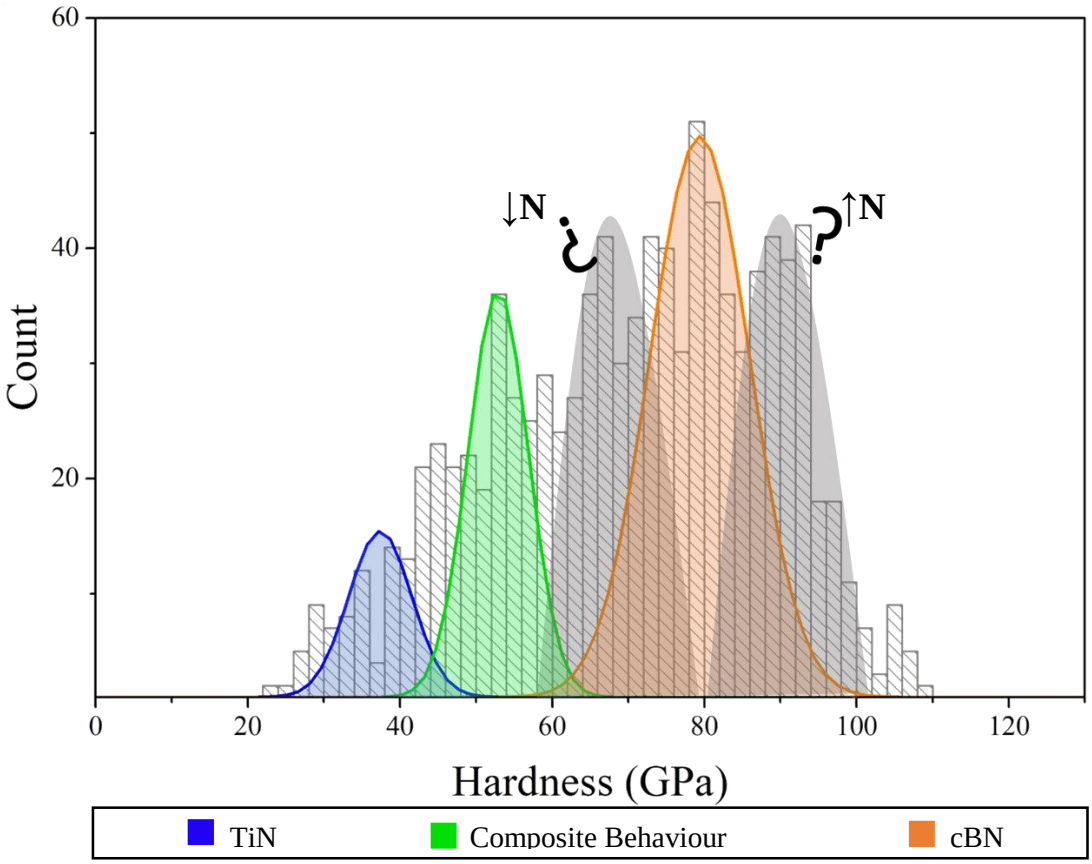

Figure 50 - Histogram of hardness values (bin size of around 2 GPa) determined from 1043 indents performed at 200 nm of maximum penetration depth. The simulated hardness distributions using the statistical fitting parameters are overlapped.

Figure 50 shows the hardness histogram with a constant bin size of 2 GPa, determined from 1043 indents. Following the method described in the theoretical frame of massive nanoindentation, fitting the experimental CDF curve through the correct statistical methods, three peaks centred at different hardness mean values can be considered the most representative for the different constitutive phases present in the composite material. The lowest peak which value is around 38 GPa corresponds to TiN binder, while the highest peak around 82 GPa corresponds to cBN reinforcement particles. Finally, the intermediate peak around 55 GPa can be related to those imprints located in TiN/cBN interfaces, cBN grains with very this thickness from the free surface, highly constrained TiN binder, etc. Indentations performed in such locations were not able to distinct single-phase mechanical performance due to the contribution of binder and particles in their response. The hardness value for the middle peak is in good agreement with the hardness value obtained from deep indentations (1000 nm penetration depth), even shallow nanoindentations at composite locations or deep indentations would report the mechanical properties of the interaction of both phases working together, reporting a hardness value of 55

GPa. Furthermore, **Table 11** summarizes the main hardness values directly obtained from the statistical method employed in this section for each constitutive phase.

Table 11 - Summary of the hardness of each phase obtained by the massive nanoindentation method.

Phase	Hardness (GPa)
TiN	38 ± 6
Composite	55 ± 7
cBN	82 ± 12

All of the hardness reported are higher than most of the hardness reported in literature [(51), (56), (58), (59)] in the case of cBN this could be explained by the size effect related to shallow indents and to the difficulty of indenting harder materials. Following, three nanoindentation hardness trend (each one representing one of the three differentiated hardness groups shown by the massive nanoindentation method) will be analysed to check that there are no artefacts or vagueness in the nanoindentation single tests as it is depicted in **Figure 51.**

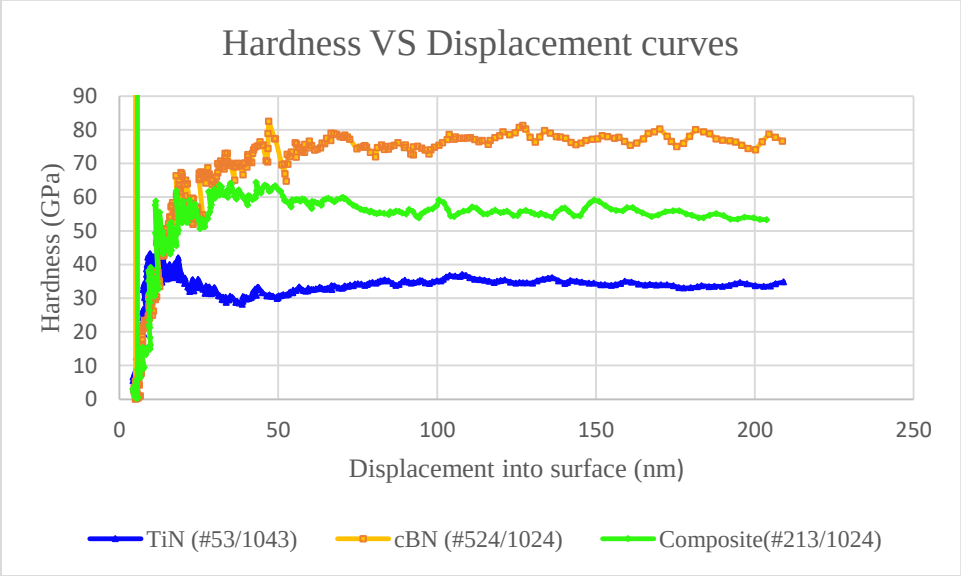

Figure 51 - H-h curves for single nanoindentations performed respectively in TiN binder locations, composite and PcBN grains.

The main conclusion that can be done from the direct observation of the H-h curves is that the nanoindentation testing conditions ensure that the hardness determined from each of the single tests is measuring the mechanical properties of the precise phase that is being indented without the contribution of the other phases in the surrounding volume. Once the first instabilities due to the tip/substrate interaction are over (h>50nm) the curve shows a flat shape that corresponds to a single-phase confined stress field. For example in the case of a deeper indentation in a cBN grain,

as the stress field became bigger with the displacement, the hardness would experience a drop because of the interaction of the stress field used by the indentation with softer surrounding materials.

From direct observation of the obtained histogram seems like two minor populations could be highlighted. Because of this, an attempt of fitting the experimental CDF curve with 5 populations in the fitting parameters was also held, obtaining worst correlation and less physical interpretation than the model for 3 peaks. However some possible explanations to this peaks centred at 66 and 92 GPa (see **Figure 50**) will be discussed in order to explain some possible mechanical differences between cBN grains and to propose possible future investigations on PcBN materials. The two considered hypothesis to explain those possible extra populations in PcBN composites are:

a. Different content of B/N cBN grains: H. Sachdev reports in Ref. (60) the influence of several impurities in the morphology of cubic boron nitride. According to this study, since boron displays a huge variety of structural features and heteroatoms some specific planes as {1 1 1} can be prone to form B clusters. As a consequence of this octahedral/irregular shaped grains can be considered as B rich materials and find their crystallographic packaging distorted. In case of assuming this, the topic of discussion would be if the mechanical difference from rich-B grains and poor-B grains are mechanically different enough so that massive nanoindentation technique differentiates both populations. In order to try to bring light to this hypothesis Raman and electron microprobe analysis (EPMA) were performed is different areas of the material, obtaining better and more interpretable results with the second technique.

EPMA allowed us to obtain the different chemical composition of an area as shown in **Figure 52**.

Even B or N are both small atoms that are difficult to analyse through EPMA technique, and no relevant results were obtained from B compositional maps. In the

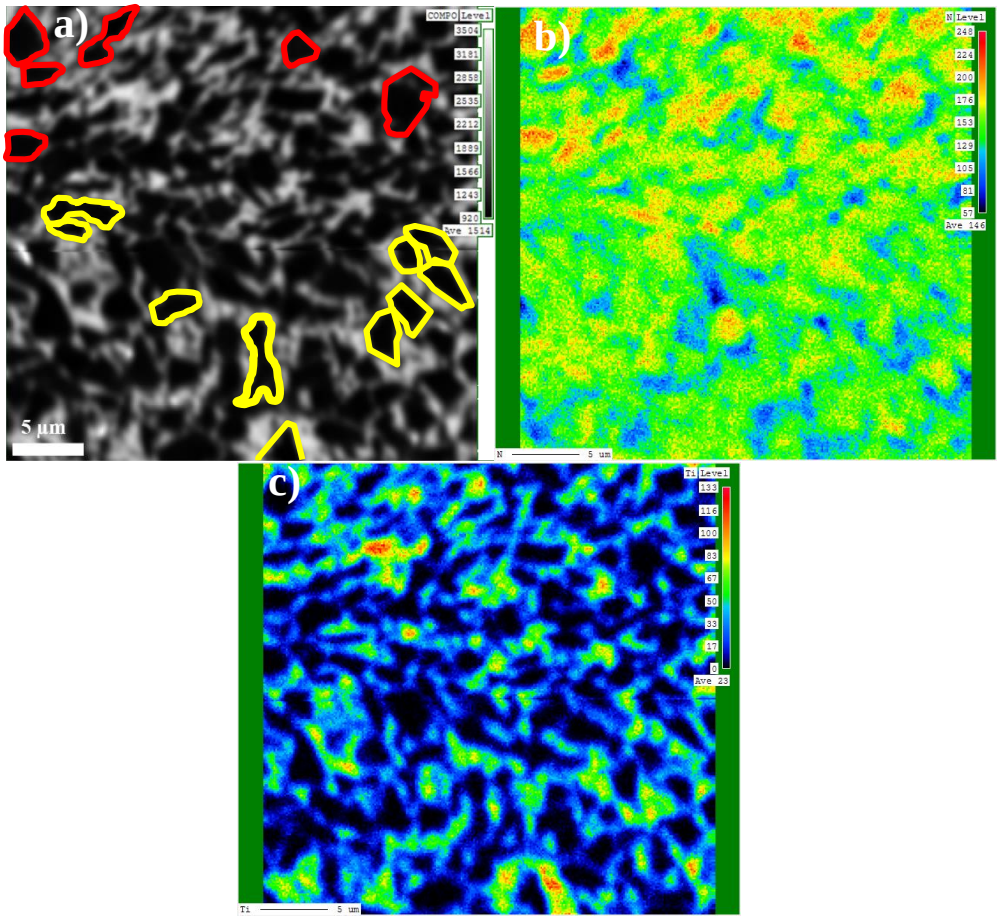

Figure 52 - SEM image of the studied region and EPMA atomical composition maps for N and Ti.

other hand two populations of cBN grains could be distinguished by this technique observing the compositional maps for N element. Comparing **Figure 52 a)** and **b)** is clear how grains highlighted in red in Figure 52 **a**) have a higher content of N than those highlighted in yellow. Articles as the one published by M. Dios (61) explain how during the processing of hard materials diffusive process from the matrix to the particles could explain this N enrichment of cBN particles.

A more detailed research where EPMA and massive nanoindentation were carried at exactly the same well characterized area where single nanoindentations could be compared in mechanical properties knowing their N amount is required to exactly answer if there are mechanical differences between rich and poor cBN populations, and if massive nanoindentation has enough resolution to do so.

b. Anisotropic mechanical behaviour due to crystallographic orientation: Another of the possible explanations for the two peaks surrounding cBN peak in hardness histogram could be crystallographic orientation anisotropy. FCC structures give as a result isotropic mechanical properties on materials; however, the distortion of this lattice due to impurities (described above) or the presence of cleavage planes could give as a result mechanical behaviour differences between cBN indented grains.

   A more detailed research where EBSD and massive nanoindentation were carried at exactly the same well-characterized area should be carried in order to dismiss all possible mechanical differences between crystallographic orientations of cBN grains.

Micropillar compression

The resulting geometries for the micromachined pillars have been the following:

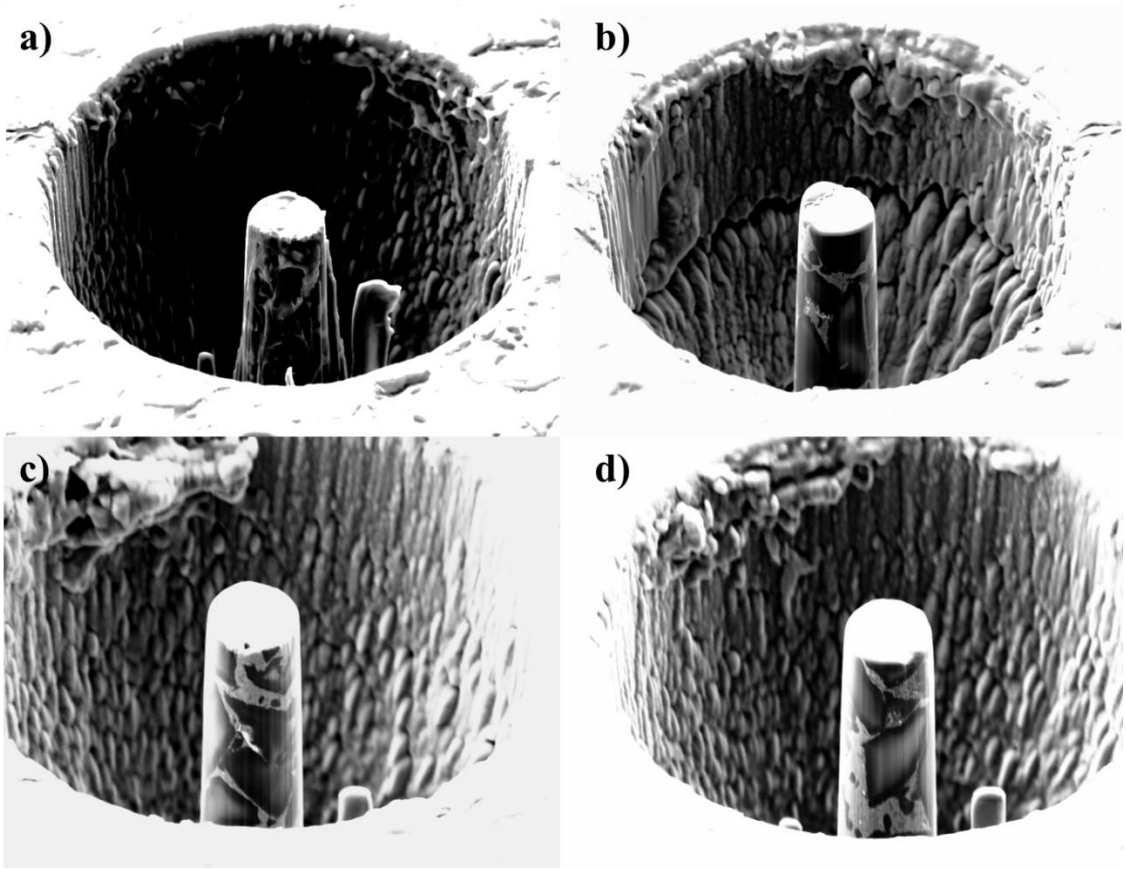

Figure 53 - Resulting micropillars from the followed machining method.

Table 12 - Geometric characteristics of all the machined pillars and established quality factors for compression testing of micro-sized pillars.

Pillar	Diameter (µm)	Height (µm)	Aspect ratio (2<D/L<3)	Tapper angle (<3º)
A	3.2	7.3	2.3	2.4
B	3.0	7.7	2.6	1.7
C	3.0	≈8.1	2.7	2.1
D	3.0	7.7	2.6	2.4

The machined pillars meet the desired size, tapering angle and aspect ratio enough to ensure a correct micro-mechanical testing (see

Table 12). Therefore, the sample has been supplied to the Dr. Warren C. Oliver from the Nanomechanics Inc. (Oak Ridge, EEUU) to perform the in-situ micromechanical testing at room temperature (these experiments will be conducted along the 2017 October month).

In-situ compression of the micropillars inside a SEM chamber will be performed obtaining analytical data from the resulting stress-strain curves and qualitative information from the observation of the failure modes during the compression.

Notched cantilever flexion

As explained in the "Materials and methods" section in page 54, a suitable methodology for machining PcBN micro-cantilevers through Ga^+ FIB technique was not achieved. However, it is considered of interest the "Know-how" acquired during the whole developing process. Because of this, the final obtained geometries will be reported, and an analysis of the possible causes and possible solutions for the problematic will be developed.

After trying all the possible machining solutions in the available facilities and arriving to the conclusion that the intended experiment could not be done, the geometries that were nearer to the desired shape are depicted in Figure 54**.**

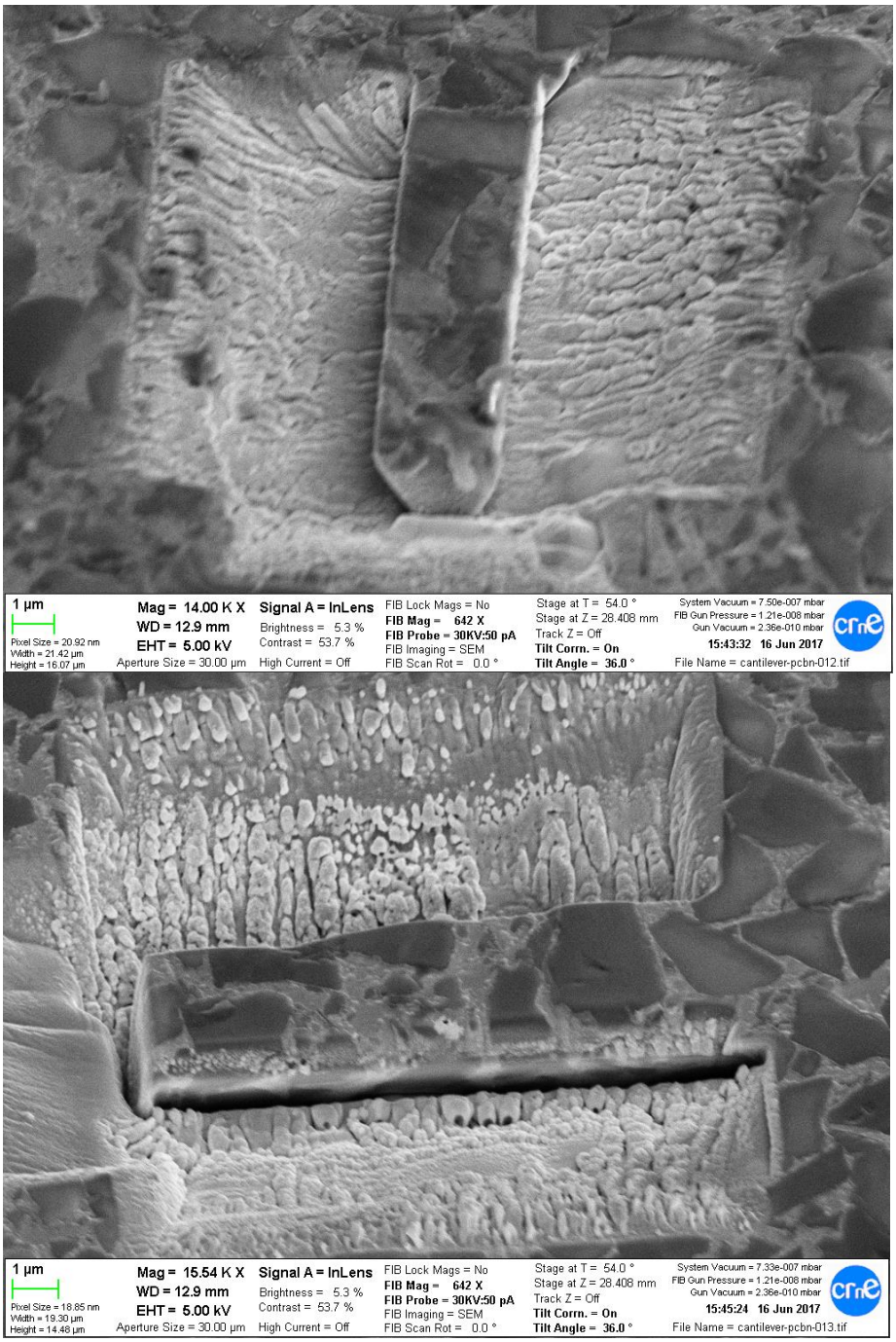

Figure 54 - Failed geometries for FIB micromachined PcBN notched micro-cantilevers.

In both images showed in **Figure 54** is observed that even after the steps of fine milling of the lateral faces, the whole cantilever is not detached from the rest of the material. As it is obvious, the micromechanical testing of the sample not possible if the beams are not able to deflect.

The energetic covalent bonding and the high packing of FCC crystal structure from cBN makes that the Ga^{+} ions, no matter which is the induced energy, are unable to penetrate efficiently into the material. This fact added to the loss of machining efficiency when cutting the sample with a

relative angle of 45º to the ion beam leads us to the main conclusion of the whole process. cantilever machining in PcBN is highly complex to machine by means of Ga^+ FIB technique.

The possible solutions for the reported problem could be:

a) ***Machine the cantilevers in the border of a sample.*** Having the cantilevers in the border may allow there searcher to keep the machined surface always perpendicular to the ion beam enhancing the machining efficiency and being able to achieve deeper trenches. This procedure could also machine constant section beams.
b) Using a FIB with more energetic ions such as Xe FIB equipment.

ABAQUS Simulation

Several outputs can be obtained from FE simulation, the outputs to required to be calculated and reported from the compression tests simulations were:

S: Stress components and invariants

Mises: Mises equivalent stresses

PE: Plastic Strain components

PEEQ: Equivalent plastic strains

U: Translations and rotations

RF: Reaction forces and moments

ELEDEN: All energy density components

Each of these results were asked to be computed foreach of the nodes present in the model. In the other hand, a *Field History output* was created and attached to the Reference Point where the displacement was imposed. This way much less calculation is needed to obtain displacement/reaction force data in the stressed surface.

The Output - Compressive σ- ε curves

The main result obtained from the whole simulation is the prediction of the material behaviour in a compression test. The obtained stress strain curve for the deformation controlled test is depicted in **Figure 55:**

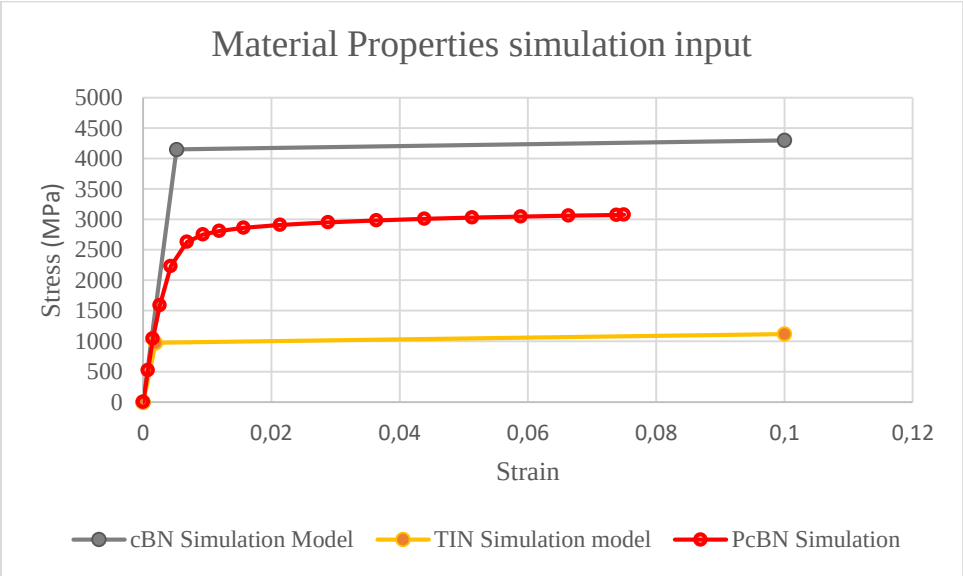

Figure 55 - Stress strain curve obtained from the simulation of a compression test with an applied deformation of 7.5% of the original length.

Table 13 - Discussion of predicted elastic properties of the material.

Material	E Rule of mixtures		Simulation E (GPa)
	Low boundary $\frac{1}{E_{co}} = \frac{f_b}{E_b} + \frac{(1-f_b)}{E_r}$	High boundary $E_{co} = f_b E_b + E_r f_r$	
TiN	-	-	500
cBN	-	-	798,4
PcBN 28/72	684,1	714,85	697,4

From the obtained curve, it can be studied both, elastic and plastic behaviour of the material:

- Elastic properties. Simulation reports an elastic modulus of 697 GPa for the composite material. As it can be seen in **Table 13** this value is in good agreement with the limits that set rule of mixtures for composite materials Young Modulus. The reported value corresponds to a very stiff material, that exceeds in rigidity other materials that are typically used precisely by their stiffness as SiC (486 GPa) or hard metals (600-500 GPa typically).

In comparison to deep nanoindentation results (850 ± 161 GPa) although simulation result is overlayed with the systematic error that nanoindentation reports, it seems that instrumented indentation technique shows higher values. As it has been discussed before nanoindentation gives appropriate results for Hardness characterization, while for Young modulus the error and noise introduced makes the the technique not suitable for this purpose.

We can consider the approximation of the elastic modulus by means of the simulation to be accurate because of two main reasons. In one hand, the analysed volume is a virtual reconstruction that exactly replicates real microstructure of the material, making the geometrical interactions, geometrical stress intensity factors and morphology very close to reality. In the other hand, the main approximation assumed in the simulation that could affect mechanical properties is nearly not observed in the elastic regime. The assumption of perfect interfaces doesn't affect quite much (E_{error}<2%) the elastic behaviour of materials during FE simulations.

- Plastic properties. The reported compressive yield point value from simulation corresponds to ($\varepsilon_{y\ III}$, $\sigma_{y\ III}$) = (0.7%, 2.63 GPa). This corresponds to the typical mechanical behaviour shown by most ceramic materials, the bared deformation is low but the stress resistance is high. Anyways, mechanical design and performance on ceramic materials is not ruled by yield point and plasticity, and normally the most determinant property for integrity of the ceramic components is fracture toughness (K_{Ic}). Only in the cases where there is an hydrostatic compressive stress into materials where no cracks or defects can be developed there is a point on considering yield stress as a design parameter. In this concrete case, stress triaxiality (with positive stress components) can be generated specially in the binder-particle interface (See *Qualitative analysis of the stress distribution within the material* section). Interphase regions are the most critical for composite materials and in possible that the material fails through interfaces even before reaching its yield point because of stress concentration.

  Is in the studied plastic region where the assumption of perfect interfaces arises worst results in comparison to reality. Assuming that there is no critical damage able to break the component until the yield point is surpassed (while working inelastic region); after it, the mechanical behaviour very probably would not be characterized by such an ideally plastic behaviour as the stress-strain curve from simulation shows. Once the yield stress point is exceeded cracking, debonding or decohesion would start in the material interface and other micro-mechanisms as crack deflection, crack bridging etc. would be more determinant for the mechanical behaviour of the composite material than the scarce plasticity provided by the ceramic matrix.

Although based on some assumption, obtaining the stress-strain curve of a material from FE simulation gives a well-based approximation on several parameters (especially in the elastic regime) that would be very difficult to test by other means. Mechanical behaviour of bulk materials is completely determined by micro-mechanisms that have to be tested and simulated in the scale in which they act. For the moment, the only way to do so is through systematic micro-mechanical characterization of materials.

Qualitative analysis of the stress distribution within the material

One of the main advantages of FE simulation is the possibility of manipulate, visualize and customize virtually microstructures or elements that couldn't be treated in the same way in physical world. In the same way, results arose by FE simulations are typically characterized for being visual and graphical.

Through the observation of the finite element, results it can be observed where are the exact places where the main stresses are developed and concentrated.

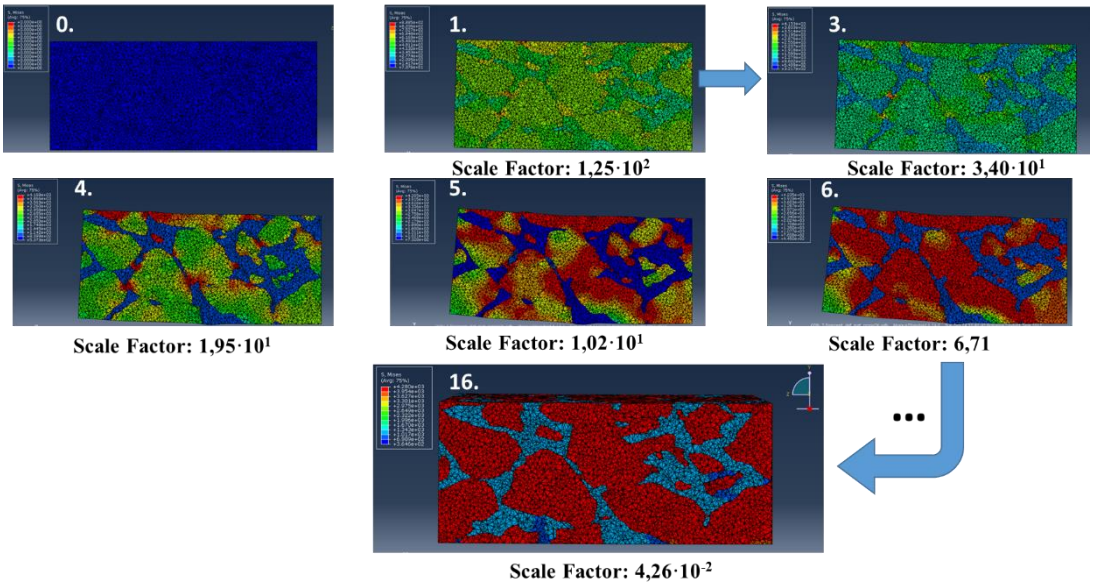

Figure 56 - Von Misses stress distribution for different points of the stress strain curve.

Figure 56 shows how the stress is being distributed along the microstructure as the mechanical solicitation is applied. **Figure 57** shows how FE simulation allows to analyse local interactions and behaviours of materials. In the right image of the figure is concluded that the principal stress concentration in the first loading steps is given in the contact points between cBN grains. In the other side is shown how the binder located near the cBN grains surrounding them are the ones that support higher load in the matrix, this is because these material is the one responsiblefor the loading transference from the "softer" binder to the high resistant grains.

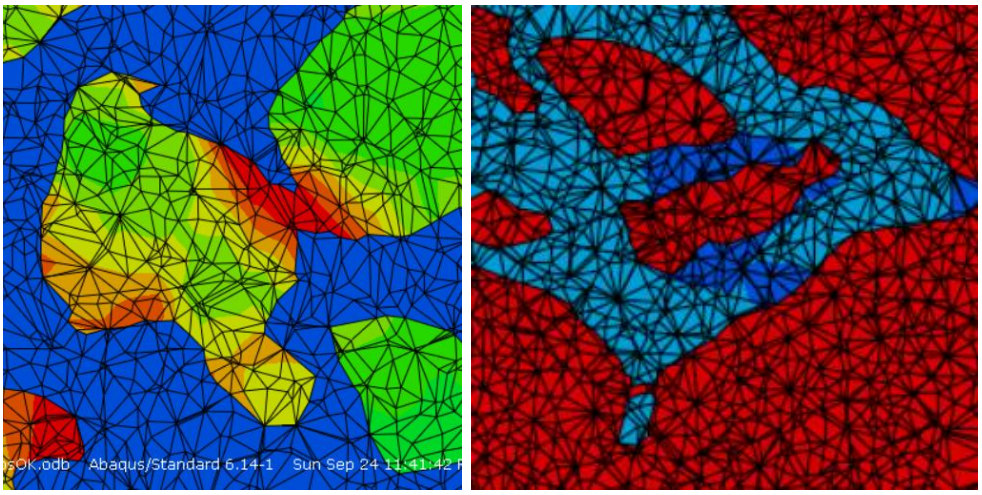

Figure 57 - Detail view of an "yz" section showing the points with higher stress concentration is arisen.

By analysing the equivalent von misses stress distribution, it can be concluded that the main phase bearing stress are the cBN grains as expected. When the sample reaches mechanical equilibrium cBN phase is supporting a von misses equivalent stress of 4.28 GPa while TiN is only in the range of 1.1 GPa.

However, although TiN matrix bears less stress while the sample is on service, from an energetic point of view is the phase that absorbs most of the applied solicitation. **Figure 58** clearly shows how most of the energy introduced into the system is concentrated in the matrix phase; this is because of having a lower yield compression point and therefore being able to absorb a higher amount of energy through plastic deformation.

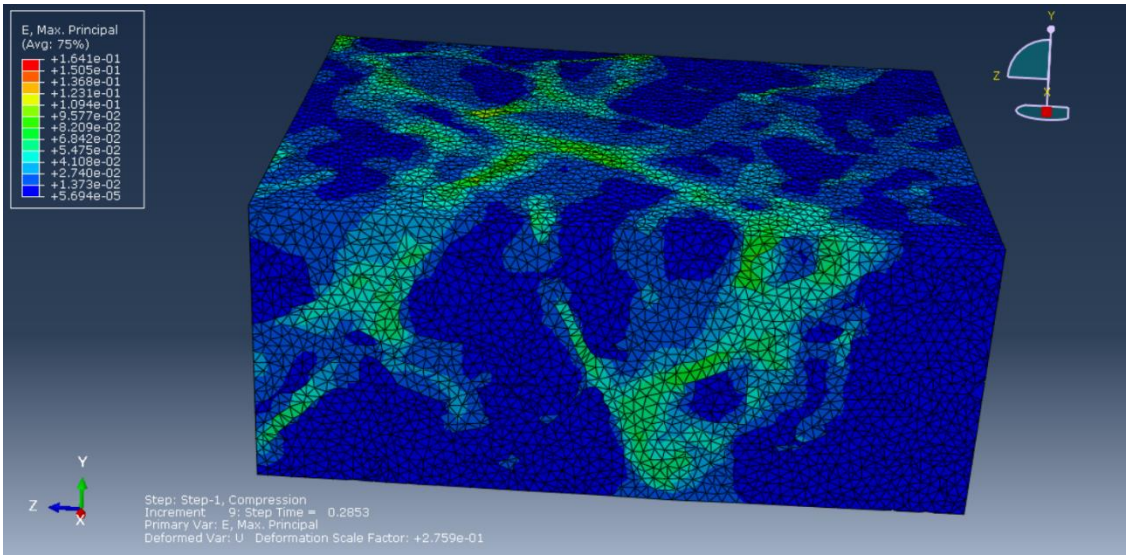

Figure 58 - Energy density absorption diagram.

Conclusion and Summary

A complete micro-mechanical analysis was held on a PcBN sample embedded in a machining chip-breaker cutting insert. The first step for this integral study was a deep microstructural characterization that described the studied sample as a composite material with a 28% in volume of TiN binder and a 72% of cBN reinforcing particles with a mean average diameter of 2.71 ± 0.18 µm. The shape and morphology of all the phases present in the material has been graphically depicted through 3D image analysis.

The Master's thesis has been useful to characterize the mechanical behaviour of the material at the micrometric length scale as a composite and to evaluate the intrinsic hardness for each constitutive phase. Massive nanoindentation technique has reported hardness values of 82, 32 and 55 GPa, for cBN grains, TiN matrix and the cBN/TiN interface. Such a high values for the material hardness makes it a perfect choice for the applications for which is currently being used. This micromechanical testing methodology has also been useful to raise new questions in the matter of mechanical properties of PcBN materials. Therefore, the influence of boron diffusion and compositional gradients inside the microstructure has to be studied deeply in following projects.

Information obtained from Finite Element Analysis (FEA) complemented this data by showing how the load was being distributed between phases. Qualitatively, PcBN material showed a mechanical behaviour typical from ceramic materials with high hardness and an elevated stiffness with a reported compressive young modulus of 697 GPa. Under a compressive strain enough to surpass the reported yield point of ($\varepsilon_{y\ III}$, $\sigma_{y\ III}$) = (0.7%, 2.63 GPa) cBN grains bear much more stress under compression solicitations than the matrix, while TiN is the phase that absorbs a higher fraction of the energy introduced into the material while testing.

The followed methodology has been validated as a well packed testing route that permits to study the material through empirical testing in order to obtain the needed input for FE simulation techniques and from it obtain information from the mechanical performance of the material in the physical world. The combination of experimental testing and FE simulation works in a synergic way and gives results with a higher added value than those that could be obtained from both, testing methodologies used separately.

Further work and improvements

The generated knowledge on PcBN mechanical properties has given as a result a batch of questions that could be answered through some of the following actions:

- Perform the comparison of the FEA results with the real behavior of PcBN micro-pillars being compressed. This work will be done in collaboration with the Nanomechanical Inc. company located in USA, where they in-situ compress the micro pillars.
- Minimize the number of assumptions and simplifications that are needed in the FE simulations.
    - Use as an input for materials models in FE simulation the output supplied by the micromechanical testing of micro pillars machined exclusively in each of the composite material phases separately.
    - Re-machine PcBN notched cantilevers with a Xe FIB, in order to characterize cBN-TiN interface and avoid to use perfect interface approach.
- Develop the interface characterization in composite materials through notched cantilevers in materials easier to machine through FIB.
- Study by means of the same methodology other PcBN materials with different matrix composition and content, different grain sizes, processing routes, etc. In order to be able to relate microstructure and mechanical behavior.
- Study the influence of factors as orientation of cBN grains or Boron content within grains with the measured hardness in massive nanoindentation methodology. Perform EBSD and EMPA exactly in the same region that will be later tested.

Financial Analysis

Before developing this section any further, is important to highlight the fact that this master thesis is not an engineering project which objective is the economical benefits of any company o institution. This project looks over anything else the achievement of technical knowledge and the deep characterisation of the material. However, it has already been debated in the introduction how these type of research gives good externalities and savings to third parties.

Anyways, an approximated cost for all the activities developed to perform the work is going to be discussed. In the following cash flow we can observe how there are only costs and not incomes that is why concepts as profitability does not make sense for this project.

All the detailed costs have been calculated from real market prices, and are disaggregated in **Table 14**:

Table 14 - Summary of all the expenses that would carry this master thesis.

		Units	Unitary Cost (€/unit)	Cost (€)
CONSUMABLES	PcBN sample	-	-	
	Clarofast resin	0,005	35 €/kg	0,175
	Diamond polishing dispersion	0,3 L	300 €/L	90
	Polishing mats	1	200 €/L	200
			COSTS FOR RAW MATERIALS AND CONSUMABLES =	290.2 €
INSTRUMENTATION	Mechanical polisher	5	10 €/h	50
	FIB	33	106 €/h	3498
	EMPA	3	50 €/kg	150
	SEM	6	29.55 €/kg	177.3
	Nanoindenteder	72	40 €/h	2880
	Raman	4	25 €/h	100
			COSTS FOR INSTRUMENTATION =	6.855,3 €
OTHERS	ABAQUS license	1	0 €	0
	AVIZO license	1	0€	0
	Documentation	-	0 €	0
			OTHER EXPENSES =	0€
HUMAN RESOURCES	Specialist Technician	7	42.47 €/h	297.29
	Tutor and associated	45	15 €/h	675
	Projectist	900	9.25 €/h	8325.0
			LABOUR COSTS=	9297.3 €
			SUB. TOTAL:	**16442.6 €**

Is important to underline some considerations in order to understand some of the figures shown in **Table 14:**

- PcBN samples, we supplied to the university department by an external company without any charge.

- AVIZO license corresponds to the student version, which is free.

-ABAQUS simulations were held on remote through a borrowed License, which charge is not under UPC possession.

- The access to bibliography, specialised press and other information sources have been supplied by the correct library services that offer UPC. UPC students have free access to the main knowledge portals on the internet.

- This Master thesis was enlarged to be formed by 30 ECTS credits (European credit transfer and accumulation system), and the hours that a student is supposed to be dedicating to this amount of credits is around 900.For the projector salary the current labour agreement for engineers in Spain (62).

- The tutor cost corresponds to the salary established by the Spanish public university system in ref. (63).

References

1. *Grid indentation analysis of composite microstructure and mechanics: Principles and validation.* **al., G. Constantinides et.** 189-202, Cambridge : Materials Science & Engineering A, 2006, Vol. 430.

2. *Ultraviolet light-emitting diode of a cubic boron nitride pn junction made at high pressure.* **Osamu Mishima, Koh Era, Junzo Tanaka, and Shinobu Yamaoka.** 962, Tsukuba-shi : Applyed Phisics Letter, 1988, Vol. 53.

3. **Bhushan, Bharat.** *Tribology Issues and Opportunities in MEMS.* Columbus : Springer Science & Business Media, 1997. ISBN 978-94-010-6121-6.

4. *Mechanical and tribological properties of cBN films on silicon and tungsten carbide substrates.* **M. Keunecke, K. Yamamoto, K. Bewilogua.** 142-149, Braunschweig : Thin Solid Films, 2001, Vols. 398-399.

5. *Machining of high performance workpiece materials with CBN coated cutting tools.* **E. Uhlmann, J.A. Oyanedel Fuentes, M.Keunecke.** 1451-1454, Berlin : Thin Solid Films, 2009, Vol. 518.

6. *Experimental and finite element simulation based investigations on micro-milling Ti-6Al-4V titanium alloy: Effects of cBN coating on tool wear.* **Thanongsak Thepsonthi, Tuğrul Özel.** 4, Piscataway : Journal of Materials Processing Technology, 2013, Vol. 213. 532-542.

7. *Nanoindentation of ultra-hard cBN films: A molecular dynamics study.* **al., ChengHuang et.** 215-224, Chongqing : Applied Surface Science, 2017, Vol. 392.

8. *Analysis of residual stress in cubic boron nitride thin films using micromachined cantilever beams.* **al., G.F.Cardinale et.** 11, Davis : Diamond and related materials, 1996, Vol. 5. 1295-1302.

9. *Tool wear and machining performance of cBN–TiN coated carbide inserts and PCBN compact inserts in turning AISI 4340 hardened steel.* **Abhijeet S. Morea, Wenping Jianga, W.D. Brownb, Ajay P. Malshea,.** 1-3, Fayetteville : Journal of materials processing, 2006, Vol. 180. 253-262.

10. *Effect of PCBN tool grade on joint strength and tool life in friction stir spot welded DP 980 steel.* **T. Hartman, M.P. Miles, S.T. Hong, R. Steel, S. Kelly.** 531-536, Provo : WEAR, 2015, Vols. 328-329.

11. *Comparison of tool life between ceramic and cubic boron nitride (CBN) cutting tools when machining hardened steels.* **Sahin, Y.** 7, Ankara : Journals of MAterials Processing TEchnology, 2009, Vol. 209. 3478-3489.

12. *Cubic boron nitride competing with diamond as a superhard engineering material – an overview.* **al., S. Neves Montero et.** 68-74, Rio de Janeiro : Journal of Materials Research and Technology, 2013, Vol. 2(1).

13. *Indenter materials for high temperature nanoindentation.* **Wheeler JM, Michler J.** 101301, Thun : Rev Sci Instrum , 2013, Vol. 10.

14. **Callister, W.D.** *ntroducción a la Ciencia e Ingeniería de los Materiales.* . Barcelona : Reverté, S.A. , 1997. 84-291-7253X..

15. **Sarin, Vinod K.** *Comprehensive Hard Materials Volume 3: Super Hard Materials.* Oxford : Elsevier, 2014. ISBN 978-0-444-63383-5.

16. *Cubic boron nitride: synthesis, physicochemical properties and applications.* **Laurence Vel, Gerard Demazeau, Jean Etourneau.** 149-164, Talence : Materials Science and Engineering , 1991, Vol. B10.

17. **Kanyanta, Valentine.** *Microstructure-Property Correlations for Hard, Superhard, and Ultrahard Materials.* Switzerland : Springer Nature, 2016. ISBN 978-3-319-29289-2.

18. *The study of the CBN grain shape on its microcutting performance based on finite element method.* **al., Geng Zhi et.** 340-343, Beijing : Advanced Materials Research, 2014, Vol. 1027.

19. *The influence of microstructure on the fracture properties of polycrystalline cubic boron nitride.* **al., P. Alveen et.** 115-123, Dublin : Computational Materials Science, 2015, Vol. 109.

20. *The measurement of grain contiguity in two-phase alloys.* **Gurland, J.** 452-455, s.l. : Transactions of the Metallurgical Society of AIME, 1958, Vol. 212.

21. *Deformation and fracture processes and the physical metallurgy of WC-Co hardmetals.* **Almond, B. Roebuck and E. A.** 2, s.l. : International Materials Reviews, 1988, Vol. 33. 90-122.

22. **Torres, Y.** *Comportamiento a fractura y fatiga de carburos cementados WC-Co,.* Barcelona : Ph.D. thesis. UPC, 2002.

23. *Structure of sintered tungsten carbide-cobalt alloys.* **H. E. Exner and H. F. Fischmeister.** 417-426, Munich : Archiv für das Eisenhüttenwesen, 1966, Vol. 37.

24. *The application of focused ion beam microscopy in the materials sciences.* **Munroe, P.R.** 2009, Materials Caracterization, Vol.60, pp. 2-13.

25. **Yao, N.** *Focused Ion Beam Systems: Basics and Applications. Cambridge: Cambridge University Press.* Cambridge : Cambridge University Press, 2007.

26. *Three-dimensional characterization of 'as-cast' and solution-treated AlSi12(Sr) alloys by high-resolution FIB tomography.* **al., F. Lasagni et.** 3875-3882, Vienna : Acta Materialia , 2007, Vol. 55.

27. *Hardness measurement at penetration depthas small as 20 nm.* **J. B. Pethica, R. Hutchings, W. C. Oliver.** 593-596, Cambridge : Phil. Mag, 1983, Vol. A 48.

28. *An improved technique for determining hardness and elastic modulus using load and displacement sensing indentation experiments.* **W.C. Oliver, G.M. Pharr.** 1564-1583, Oak Ridge : J. Mater. Res., 1992, Vol. 7 No. 6.

29. **Piqué, Emilio Jimenez.** Introduction to Nanoindentation. *Docency Slides.* Barcelona : UPC, 2016.

30. *Measurement of hardness and elastic modulus by instrumented indentation: Advances in understanding and refinements to methodology.* **W.C. Oliver, G.M. Pharr.** 1, Knoxville : Journal of Materials Research, 2004, Vol. 19.

31. **H. Buckle, J.W. Westbrook, H. Conrad.** *The science of hardness testing and its applications.* Ohaio : American Society for metals, 1973. 453-459.

32. *Statistical indentation techniques for hydrated Nanocomposites: Concrete, Bone and Shale.* **F.J. Ulm, M. Vandamme, C. Bobko and J.A. Ortega.** 9, Cambridge (MA) : Jpurnal of American Ceramic Society, 2007, Vol. 90. 2677-2692.

33. **Llanes, Luis.** Materials Science Issues on MICROMECHANICAL DESIGN, NANOMECHANICS AND COATINGS. *Apuntes de clase.* Barcelona : UPC-CMEM, 2016.

34. *Multi-scale modeling of elasto-plastic response of SnAgCu lead-free solder alloys at different ageing conditions:Effect of microstructure evolution,particle size effects and interfacial failure.* **al., M. Maleki et.** 132-144., Lausanne : Materials Science & Engineering A , 2016, Vol. 661.

35. *The influence of particle size and particle fracture on the elastic/plastic deformation of metal matrix composites.* **C.-W. Nan, D.R. Clarke.** 9, Santa Barbara : Acta Materialia, 1996, Vol. 44. 3801-3811.

36. *Dislocation shielding and flaw tolerance in titanium nitride.* **S. Kumar, D.E. Wolfe, M.A. Haque.** 739-747, Pennsylvania : International Journal of Plasticity, 2011, Vol. 27.

37. *Three-dimensional visualization and microstructure-based modeling of deformation in particle-reinforced composites.* **N. Chawla, R.S. Sidhu, V.V. Ganesh.** 1541-1548, Tempe : Acta Materialia , 2006, Vol. 54.

38. **Maleki, Milad.** Deformation And Damage In Lead-Free Solder Joints: Microstructure-Based Modeling And Experimental Characterization. *Doctoral Thesis.* s.l. : École Polythechnique Fédérale de Lausanne, 2012.

39. *A micromechanics-based nonlocal constitutive equation and estimates of representative volume element size for elastic composites.* **W.J. Drugan, J.R. Willis.** 4, Cambridge : Journal of the Mechanics and Physics of Solids, 1996, Vol. 44. 497-524.

40. *Numericla and statistical estimates of the representative volume element of elastoplastic random composites.* . **Matteo Galli, Joël Cugnoni, John Botsis.** 31-38, Laussane : European Journal of Mechanics A/solids, 2012, Vol. 33.

41. *Coated SUMIBORON BNC2010/BNC2020 for Hardened Steel Machining Realizing Long and Stable tool life.* **al., Yasuke Matsuda et.** 85-90, s.l. : SEI TECHNICAL REVIEW , April 2015, Vol. 80.

42. *The Measurement of Grain Contiguity in Two-Phase Alloys.* **Gurland, J.** 452-455, Providence : Trans. Metall. Soc. AIME , 1958, Vol. 212.

43. **Viñas, Miquel Turón.** *FIB tomography of WC-Co Composites.* Barcelona : UPC - Master Thesis, 2012.

44. *Hall-Petch strengthening of the constrained metallic binder in WC–Co cemented carbides: Experimental assessment by means of massive nanoindentation and statistical analysis.* **al, J.J. Roa et.** 487-491, BArcelona : Materials Science & Engineering A, 2016, Vol. 676.

45. **W.R. McKenzie, E.A. Marquis and P.R. Munroe.** *Focused ion beam sample preparation for atom probe tomography.* New South Wales : Formatex, 2010.

46. *Representative Volume Element Size of Elastoplastic and Elastoviscoplastic Particle-Reinforced Composites with Random microstructure.* **J. Cugnoni, M.Galli,.** 165-185, Lausanne : CMES-Comput.ModelEng., 2010, Vol. 66.

47. *Comparing techniques for tetrahedral mesh generation.* **al., M. A. S. Lizier et.** Sao Paulo : s.n., 2007.

48. *Contact damage and fracture micromechanisms of multilayered TiN/CrN coatings at micro- and nano-length scales.* **al., J.J. Roa et.** 308-315, Barcelona : Thin Solid Films, 2014, Vol. 571.

49. *Charting the complete elastic properties of inorganic cristalline compounds.* **al., Maarten de Jong et.** Berkeley : Nature Scientific Data, 2015.

50. **James F.Shackelford, William Alexander.** *CRC MAterials Science and Engineering Handbook. 3rd Edition.* Page 419 : CRC Press, 2000. ISBN 9780849326967.

51. *Elasticity of cubic boron nitride under ambient conditions.* **al, Jin S. Zhang et.** 063521, Urbana : Journal of applyed physics, 2011, Vol. 109.

52. *Reactive sintering cBN-Ti-Al composites by spark plasma sintering.* **al., Yungang Yuan et.** 138-143, Qinhuangdao : Diamond and related Materials , 2016, Vol. 69.

53. *Indentation size effect in policristalline F.C.C. metals.* **A.A. Elmustafa, D.S. Stone.** 3641-3650, Hampton : Acta Materialia, 2002, Vol. 50.

54. *Indentation Size Effect in nanohardness.* **Yu.V. Milman, A.A. Golubenko, S.N. Dub.** 7480-7487, Kiev : Acta Materialia, 2011, Vol. 59.

55. *Bulk titanium nitride ceramics – Significant enhancement of hardness by silicon nitride addition, nanostructuring and high pressure sintering.* **al., U.W. Bläß et.** 10 2733-2744, Freiberg : Journal of the European Ceramic Society, 2015, Vol. 35.

56. *A nanoindentation study of thick cBNfilms prepared by chemical vapour deposition.* **al., C.Y. Chan et.** 438-444, Hon Kong : Journal of crystal growth, 2003, Vol. 247.

57. *The synthesis, characterization, and mechanical properties of thick, ultrahard cubic boron nitride films deposited by ion-assisted sputtering.* **P. B. Mirkarimi, D. L. Medlin, K. F. McCarty, D. C. Dibble, W. M. Clift, J. A. Knapp, and J. C. Barbour.** 1617-1625, Livermore : Journal of Applied Physics, 1998, Vol. 82 (4).

58. *An international round-robin experiment to evaluate the consistency of nanoindentation hardness measurements of thin films.* **Lee, Kitty W.** 57-61, Evanston : Surface and coatings TEchnology, 2003, Vol. 168.

59. *Hardness and elastic modulus of TiN based on continuous indentation technique and new correlation.* **D. S. Stone, K.B. Yoder, W.D. Sproul.** 2543, MAdison : Journal of Vacuum Science & Technology A: Vacuum, Surfaces, and Films, 1991, Vol. 9.

60. *Influence of impurities on the morphologies on the morphology and Raman spectra ofcubic boron nitride.* **Sachdev, H.** 12, Saarbruecken : Diamond and related materials, 2003, Vol. 2003. 1275-1286.

61. *Chemical precipitation of nickel nanoparticles on Ti(C,N) suspensions focused on cermet processing.* **al., M. Dios et.** 2-8, Madrid : Int. Journal of Refractory Metals and Hard materials, 2016, Vol. 63.

62. *Orden ESS/86/2015, de 30 de enero, por la que se desarrollan las normas legales de cotización a la Seguridad Social, desempleo, protección por cese de actividad, Fondo de Garantía Salarial y formación profesional, contenidas en la Ley 36/2014, de 26 de di.*

63. *Resolución de 30 de enero de 2015, de la Dirección General de Empleo, por la que se registran y publican las tablas salariales correspondientes a los años 2013, 2014 y 2015 del Convenio colectivo de ámbito estatal para los centros de educación universitar.*

64. Cubero, Victor Lamelas. Determinación de la tenacidad a fractura del WC mediante la nanoindentación de microvigas pre-entallados. *Proyecto Final de Grado.* Barcelona : UPC, 2015.

65. *Intrinsic hardness of constitutive phases in WC–Co composites: Nanoindentation testing,statistical analysis,WC crystal orientation effects and flow stress for the constrained metallic binder.* **al, J.J. Roa et**. 3419-3425, Barcelona : Journal of the European CeramicSociety, 2015, Vol. 35.

66. *On the hardness ofcoated systems.* **al., Korsunski et.** 171-83, Oxford : Surface and Coatings technology, 1998, Vol. 99.

67. *On the computation of the absolute hardness of thin solid films.* **Puchi-Cabrera E.S., Berrios J.A., Teer D.G.** 2-3, Caracas : Surface andcoatings technology, 2002, Vol. 157. 185-196.

68. *Three dimensional (3D) microstructure-based modeling of interfacial decohesion in particle reinforced metal matrix composites.* **J.J. Williams, J. Segurado, J. LLorca, N. Chawla**. 113-118, Madrid : Materials Science and Engineering A, 2012., Vol. 557.